博士論文

過剰発現によりストレス環境への耐性を向上させる酵母遺伝子集団の性質に関する研究

2023 年 3 月

佐伯　望

岡山大学大学院

環境生命科学研究科

Abstract

Gene expression, the process by which gene information is used to produce proteins and other molecules, is carefully regulated in living organisms in response to changes in their internal and external environments. This regulation is crucial for the survival and growth of the organism. Therefore, overexpression of genes, in which there is an abnormal increase in the production of proteins or other molecules, can be detrimental to the organism. On the other hand, gene overexpression has been observed in drug-resistant bacteria and cancer cells, suggesting that it may be beneficial for the survival and growth of the organism under certain conditions. Despite this, the mechanisms underlying the adaptive nature of gene overexpression still need to be fully understood.

In this study, I first discovered mutations that can be overexpressed or adaptively overexpressed in certain genetic backgrounds. Extreme overproduction of gratuitous proteins can lead to growth defects. Genetic screening in the budding yeast *Saccharomyces cerevisiae* has isolated several dubious ORFs whose deletions mitigated the protein burden effect, but individual characterization has yet to be delineated. I found that deletion of the *YJL175W* ORF yielded an N-terminal deletion of Swi3, a subunit of the SWI/SNF chromatin remodeling complex, and partial loss of function of Swi3. The deletion mutant showed a reduction in transcription of genes encoding highly expressed, secreted proteins and an overall reduction in translation. Mutations in the chromatin remodeling complex could thus mitigate the protein burden effect, likely by reallocating residual cellular resources used to overproduce proteins.

I then developed an "overexpression profiling" method to identify genes whose overexpression is functionally adaptive (GOFA) in the budding yeast *Saccharomyces cerevisiae*. This method involved cultivating a cell population that overexpressed each gene in the yeast genome and using high-throughput sequencing to identify the overexpressed genes in the enriched population. We applied this method to identify GOFAs under heat, salt (NaCl), and oxidative stress conditions. The identified GOFAs differed from stress-responsive genes and indicated factors such as calcium and copper necessary for cells to survive under the conditions. Recent studies showed that differences in genetic backgrounds could significantly influence the effects of mutations. In this study, we also used overexpression profiling to investigate the impact of adaptive gene overexpression on strains with different genetic backgrounds under salt stress conditions. I found that strains with different genetic backgrounds had distinct GOFAs under the same stress conditions. These differences reflected calcium and potassium requirements for salt-stress tolerance among the strains. This suggests that genetic background plays an essential role in determining GOFAs.

This study systematically identified genes whose overexpression is functionally adaptive by developing an “overexpression profiling method.” These gene groups shed light on the relationship between environmental and genetic backgrounds, which is not yet fully understood. Overexpression profiling is also helpful in identifying essential but missing factors in specific environments and genetic backgrounds.

Contents

Chapter 1: General introduction

Cells are the basic units of life and serve as a building block of animals, plants microorganisms. Cells are enclosed by a membrane and resemble small rooms, “Cells.” Robert Hook first discovered cells in 1665, while Schleiden and Schwann theorized that cells were the minimal unit of life in 1838 and 1839, now known as Cell theory. Cells can self-renew and replicate the processes that require resources from the outside world. However, because external resources are limited, cells must have evolved systems for strategically allocating these limited resources. The regulation of gene expression in cells is a highly orchestrated system crucial in allocating limited resources. Gene expression synthesizes a functional product, such as proteins, from the genetic information (Beadle and Tatum 1941). The regulation of gene expression allows cells to adjust gene expression in response to environmental changes, (Jacob and Monod, 1961). As a result, cells can survive and proliferate under stressful environments.

Perturbation to the sophisticated intercellular system can have negative consequences, such as excessive gene expression caused by mutations, known as overexpression (Prelich 2012). Overexpressed, caused by mutations, can disturb cellular systems, causeing harm to the cell (Moriya 2015). Even when unnecessary and no function, known as “gratuitous” proteins, are overexpressed, they consume cellular resources and ultimately reduce the cell’s overall function, such as its ability to reproduce (Kafri et al. 2016). Researchers have suggested that understanding how cells respond to these perturbations can be approached by applying the concept of robustness in the engineering field (Kitano 2004).

While overexpression can negatively affect the cell, it can also lead to adaptation to new environments. However, it is still not fully understood why and how overexpression can be

adaptive, despite the presence of well-established stress response systems. Some studies have shown that overexpression of specific genes may have beneficial effects, such as increasing the efficiency of cellular metabolism or, in some cases, even leading to the development of new traits (Zhong et al. 1999; L. C. Kim and Simon 2022; Peter et al. 2018). Several studies also have shown that differences in genetic background strongly affect the phenotype of mutations. For instance, the gene deletion phenotypes such as gene essentiality and the tolerance to gene overexpression due to gene amplification, also depend on genetic background and environments (Galardini et al. 2019; D. Robinson et al. 2021). Similarly, adaptive mutations also depend on environments and genetic backgrounds, referred to as the context-dependency (Brettner et al. 2022; Eguchi, Bilolikar, and Geiler-Samerotte 2019). The adaptive effects of overexpression may vary depending on genetic background.

In this theme, I aimed to get at the relationship between overexpression and cellular adaptation, focusing on the effects of overexpression on cells, especially the positive results. In Chapter 2, I studied mutants that mitigated stress due to ultimate overexpression and revealed that redistribution of cellular resources is effective in the ultimate overexpression stress. In Chapter 3, I developed a new method to study adaptive overexpression named overexpression profiling. I used a genetic tug-of-war library, whose original purpose was studying cellular robustness, to study the adaptive overexpression (Moriya, Shimizu-Yoshida, and Kitano 2006). This study revealed adaptive overexpression indicated factors such as calcium and copper necessary for cells to survive under the given conditions.

Chapter 2: Analysis of mutants that mitigate stress due to ultimate overexpression.

2.1 Introduction

Expression levels of intracellular proteins are tightly controlled to maintain an organism's capacity for proliferation and survival, and an excess of proteins can cause cellular dysfunction (Sopko et al. 2006; Makanae et al. 2013; Moriya 2015). Potentially, any harmless protein inhibits cell growth when it is hugely overexpressed because it depletes cellular protein production resources. This phenomenon is known as the protein burden/cost effect (Moriya 2015; Kafri et al. 2016; Snoep et al. 1995). The protein burden effect was initially observed as growth defects of bacterial cells overexpressing gratuitous proteins (Kurland and Dong 1996), and later analyzed in yeast as well (Makanae et al. 2013; Kafri et al. 2016; Eguchi et al. 2018; Farkas et al. 2018). The protein burden effect is triggered by the cost of gene expression upon overexpression of gratuitous proteins; the overexpression overloads cellular transcription and translation resources (Kafri et al. 2016; Farkas et al. 2018). Because the protein burden effect is triggered by the massive overexpression of unneeded proteins, cancer cells, where an increase in the chromosome numbers is common (Ben-David and Amon 2020; Kintaka, Makanae, and Moriya 2016), should be under the condition of the protein burden effect. While the protein burden effect initially appears to be a simple phenomenon, little is known about the physiological conditions and cellular responses triggered by the protein burden effect.

Extreme overexpression of fluorescent proteins such as GFP and RFP are thought to trigger this effect (Kafri et al. 2016; Eguchi et al. 2018; Farkas et al. 2018; Kintaka, Makanae, and Moriya 2016). To clarify the physiology of cells suffering from the protein burden effect, Kintaka et al recently conducted genetic profiling (Kintaka et al. 2020). Upon isolating a series of deletion and

temperature-sensitive mutants harboring genetic interactions affecting the overexpression of GFP (GFP-op) in the budding yeast *Saccharomyces cerevisiae*, I found that the deletion of specific uncharacterized ORFs mitigated growth defects triggered by GFP-op. However, the molecular details underpinning the alleviation of the protein burden effect in these mutants remained unclear.

The SWI/SNF complex is a chromatin remodeling complex that remodels nucleosomes and changes chromatin structure by using the hydrolysis energy of ATP (Kassabov et al. 2003). The SWI/SNF complex is evolutionarily conserved in eukaryotes (Phelan et al. 1999). In humans, the complex is also known as BAF or PBAF complex (Phelan et al. 1999). The SWI/SNF complex is composed of 12 subunits in budding yeast and 11–15 subunits in human (Dutta et al. 2017; Helming, Wang, and Roberts 2014). The SWI/SNF complex has Swi2/Snf2 as the ATPase component, Swi3 and Snf5 as the core subunits, and several other accessory subunits. 20% of all human cancers have mutations in the SWI/SNF complex subunits (Kadoch et al. 2013). For instance, 98% of Rhabdoid tumors and 20–40% of Familial schwannomatosis have a homozygous deletion or truncating mutation in SNF5 (Wilson and Roberts 2011). However, the underlying mechanism relating to the mutations in the SWI/SNF complex and cancer physiology is still unclear.

In this study, I characterized the yeast deletion mutants in which the growth defects triggered by GFP-op are mitigated and revealed that one of the deletion mutants unexpectedly created an N-terminal deletion of *SWI3*, a component of the SWI/SNF complex, and a reduction in transcription levels of certain genes. I thereby suggest that transcriptional alterations may free up ribosomes to accept ectopically expressed mRNA for translation and mitigate the protein burden effect.

2.2 Results

2.2.1 Deletion of *YJL175W* ORF mitigates GFP-op-triggered growth defects

Overexpression of GFP (yEGFP3) under the control of a strong *TDH3* promoter from a multicopy plasmid pTOW40836 causes growth defects, probably due to the protein burden effect (Eguchi et al. 2018). Kintaka et al. recently performed a systematic screening of deletion mutants and temperature-sensitive mutants in which GFP-op-triggered growth defects were aggravated or mitigated (Kintaka et al. 2020). They also performed the synthetic genetic array analysis to obtain genetic interaction scores between GFP-op and the mutants. The genetic interaction score indicates how much the growth of GFP-op in a mutant differs from what is expected from each of the growth of GFP-op in the wild type and the growth of the vector control in the mutant. If the score is negative (namely the mutant negatively interacts with GFP-op), the growth defect triggered by GFP-op is aggravated. While if the score is positive (namely the mutant positively interacts with GFP-op), the growth defect is mitigated.

The screening isolated 100 mutants positively interacted with GFP-op (Kintaka et al. 2020), and the mutants contained the deletions of four dubious ORFs; *YGL024W*, *YGL218W*, *YJL175W*, and *YKL053W*. These ORFs overlap with and are located on opposite strands from the verified genes *PGD1*, *MDM34*, *SWI3*, and *ASK1* and are thus unlikely to encode functional proteins (*Saccharomyces* Genome Database, Fig. 1A). Figure 1B shows the genetic interaction scores between GFP-op and the indicated mutants. All *ykl053wΔ* and TS mutants of *ASK1* (*ask1-2* and *ask1-3*) demonstrated positive interactions, suggesting that *ykl053wΔ* disrupts the function of the *ASK1* gene. Conversely, although *ygl218wΔ* and *yjl175wΔ* yielded positive interactions, *mdm34Δ* and *swi3Δ* did not. This suggests that the deletions

of *YGL218W* and *YJL175W* result in different consequences due to the loss of function of *MDM34* and *SWI3*.

I then analyzed growth rates and GFP levels in liquid media to confirm the positive interactions between GFP-op and deletion mutants of three dubious ORFs. Among the three deletion mutants, only *yjl175wΔ* showed a significantly higher growth rate ($p = 0.002$; Fig. 2A); *yjl175wΔ* also presented with higher GFP levels than wild-type (WT) cells ($p = 0.0001$; Fig. 2A). This phenotype was not observed in *swi3Δ* cells wherein GFP levels were lower than those in WT cells ($p = 0.01$; Fig. 2B), indicating that *yjl175wΔ* does not cause loss of function by *SWI3*. Figures 2C and D show the growth curves and GFP expression levels of *yjl175wΔ* and WT cells, and the dramatic decrease in growth rate triggered by GFP-op in WT was not observed in these cells. I thus focused on *YJL175W-SWI3* for subsequent analysis.

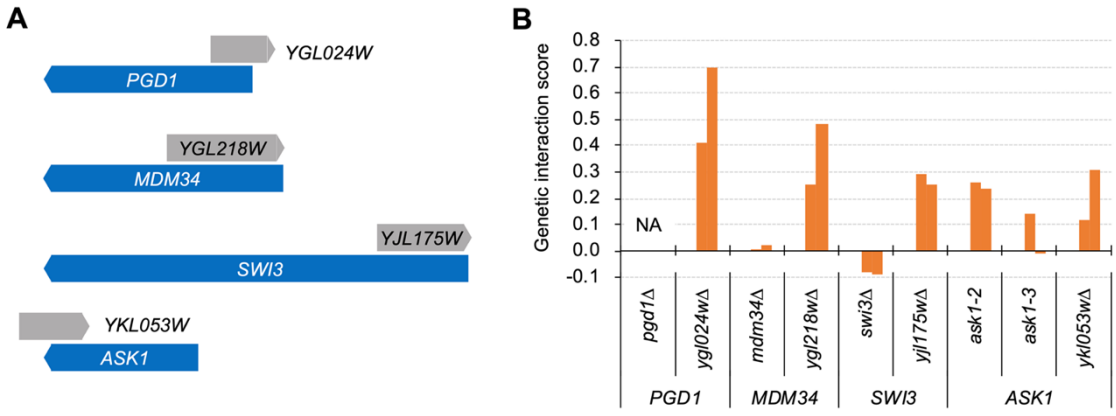

Figure 1. Dubious ORFs of whose deletions showed positive interactions with GFP-op overlapping other ORFs. A) Genetic interaction score of the dubious ORFs and overlapping other ORFs. Gray and blue arrows show dubious ORFs, and the verified ORFs overlapped, respectively. B) Genetic interaction scores of indicated mutants with GFP-op. For each mutant, the scores from two independent experiments are shown. Data were obtained from Kintaka et al.

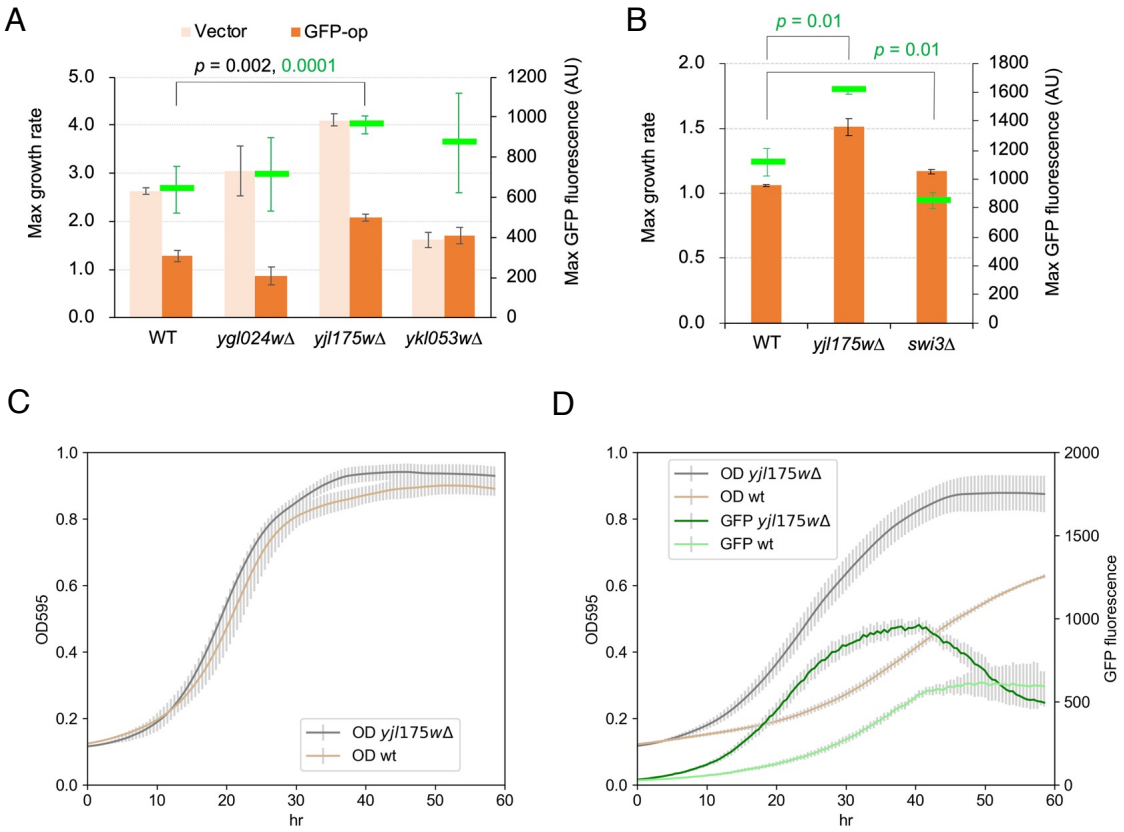

Figure 2. Deletion of YJL175W mitigates GFP-op-triggered growth defects. A and B) Max growth rates (orange bars) and max GFP fluorescence levels (green boxes) of wild type (WT) and indicated mutants grown in the synthetic medium (−Leu/Ura). (A) The max growth rate and max GFP fluorescence p-values. (B) The max GFP fluorescence p-values. C) Growth curves of WT and the *YJL175W* deletion mutant with empty vector in synthetic medium (−Leu/Ura). D) Growth curves and GFP fluorescence of WT and the *YJL175W* deletion mutant upon GFP-op in synthetic medium (−Leu/Ura).

2.2.2 Deletion of *YJL175W* leads to a partial loss of function of Swi3

I then performed transcriptome (RNA-seq) analyses to elucidate the consequences of *YJL175W* deletion. I first analyzed the transcripts expressed at the *YJL175W-SWI3* locus (Fig. 3A). Although the deletion of *YJL175W* removes the 5′ region of *SWI3* (Fig. 3C and 3D), partial *SWI3* transcripts were still expressed, with an estimated expression level at about 63% of WT. The end of the transcript (dotted line, Fig. 3A) suggests that the deletion of *YJL175W* produced a truncated Swi3 lacking its N-terminal 193 amino acid (Fig. 3D). Swi3 is a subunit of the SWI/SNF chromatin remodeling complex (Peterson and Herskowitz 1992), and known functional domains of Swi3 are located at the C-terminus (Boyer et al. 2002; Da et al. 2006); the truncated Swi3 contains all three domains, SWIRM, SANT, and LZ (Fig. 3A), suggesting that a truncated Swi3 retains some function. Western blot analysis validated the expression of truncated Swi3 in *yjl175wΔ* cells (Fig. 3B).

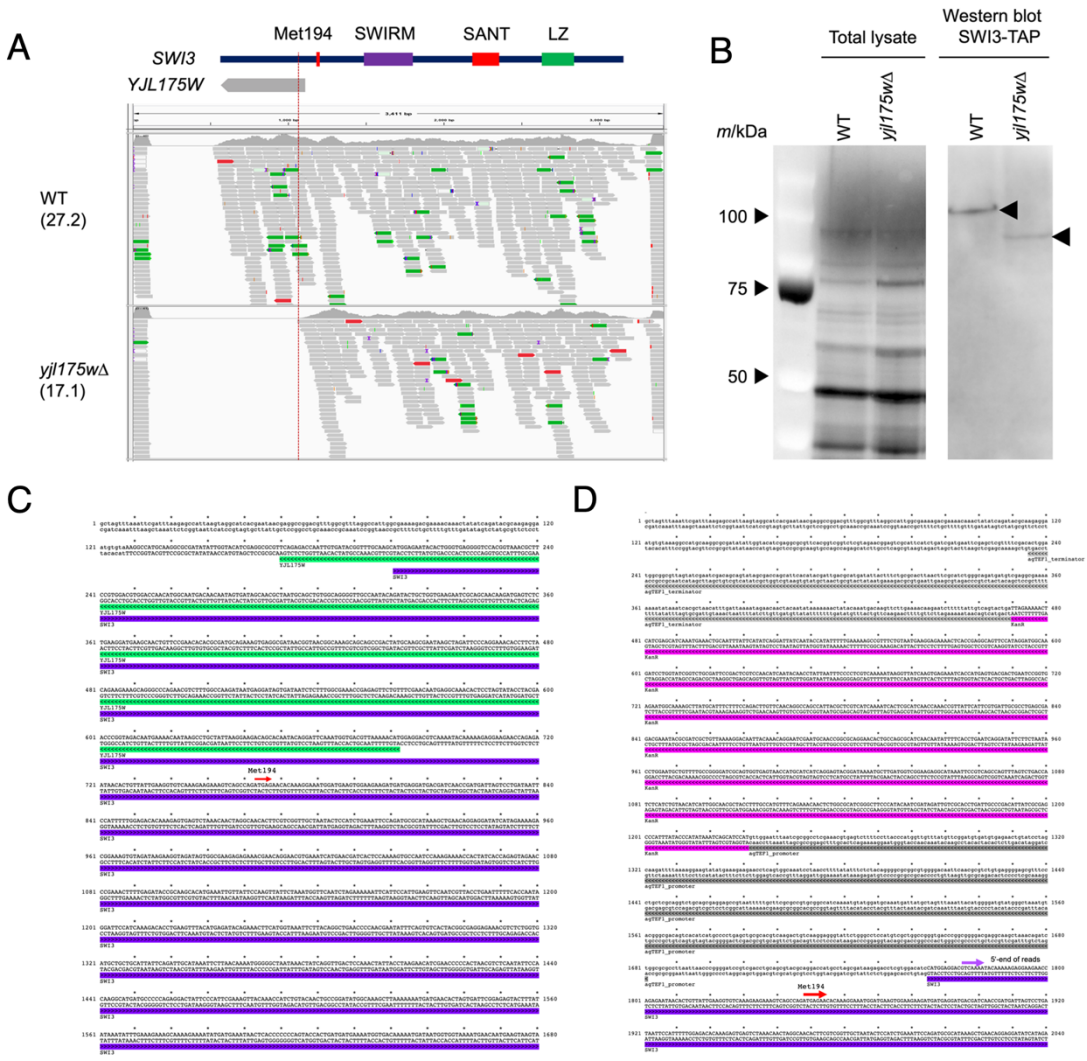

Figure 3. Deletion of *YJL175W* creates a partial loss of function of Swi3. A) RNA-seq reads mapped to the *YJL175W-SWI3* locus in the wild type (WT) and *yjl175w*Δ transcripts displayed using IGV (2.4.9). Corresponding locations of Swi3 domains and *YJL175W* are also shown. The dotted line represents the predicted transcript end of truncated *SWI3* in *yjl175w*Δ. Expression levels of the SWI3 transcripts (TPM) in each cell are also shown. B) A truncated form of Swi3 expressed in *yjl175w*Δ cells. The TAP-tag was fused to the C-terminus of *SWI3* in WT and *yjl175w*Δ, and Swi3-TAP was then detected by Western blot. C) The DNA sequence of *YJL175W-SWI3* locus of the wild-type strain from 200 bp upstream of the *SWI3* start codon. Corresponding positions of *YJL175W* and *SWI3* (N-terminal region) are colored. The predicted start codon of *swi3ΔN* is shown as Met194. D) The DNA sequence of *YJL175W-SWI3* locus of the *YJL175W* deletion strain from 200 bp upstream of the *SWI3* start codon.

To further assess the effects of *YJL175W* deletion, I compared the transcriptional profiles of *swi3Δ* (Dutta et al. 2017) and *yjl175Δ*. Complete transcriptional changes associated with *SWI3* and *YJL175W* deletions were weakly correlated ($r = 0.37$) (dots, Fig. 4A), a correlation that increased ($r = 0.68$) when transcripts with expressions significantly changed by *yjl175wΔ* were compared (red dots, Fig. 4A). The previous study demonstrated that the expression levels of mRNAs encoding transcription factors were significantly altered in *swi3*Δ cells16, and indeed, the *YJL175W* deletion presented with expression changes in transcription factors similar to those associated with *SWI3* deletion ($r = 0.61$; Fig. 4B and C). These results suggest that the *YJL175W* deletion resulted in a similar transcriptional change as the deletion of *SWI3*. However, the transcriptional change range was much wider in *swi3Δ* cells (standard deviation (SD) = 0.86) than that in *yjl175wΔ* cells (SD = 0.63; Fig. 4D), indicating that the deletion of *YJL175W* resulted in less pronounced transcriptional changes than the deletion of *SWI3*. This difference in transcriptional changes was also observed for the expression of transcription factors; although changes in the transcription factors were equally distributed in *swi3*Δ cells, the transcriptional decrease was far greater than the increase in *yjl175*Δ cells (Fig. 4C).

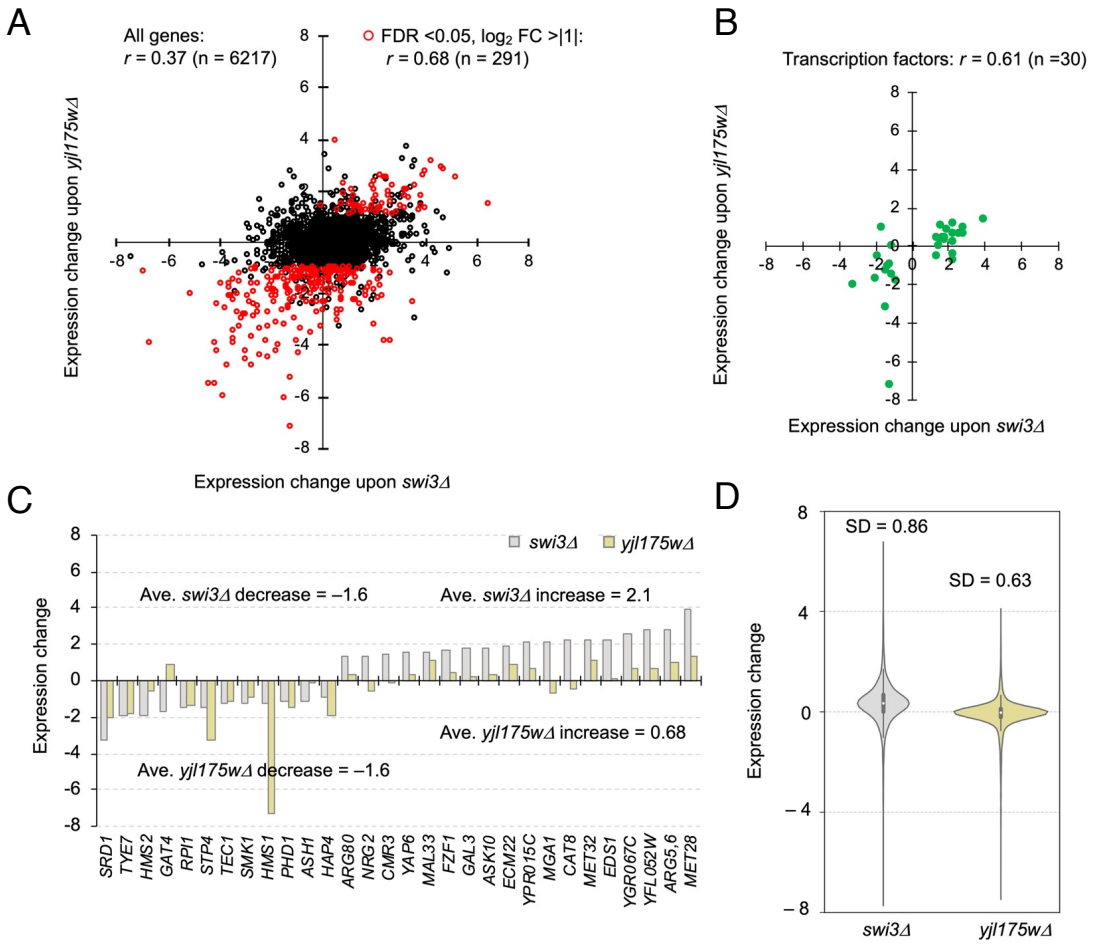

Figure 4. The effect of *swi3*Δ and *yjl175w*Δ on gene expression levels. A) Relationship between expression changes of transcripts upon *SWI3* and *YJL175W* deletion. Red dots show transcripts with a false discovery rate (FDR) ≤ 0.05 and $\log_2$ FC ≥ |1|. B and C) Expression changes of transcripts of transcription factors under *swi3*Δ and *yjl175w*Δ. Only transcription factors known to be affected by the *SWI3* deletion are shown. In E, average $\log_2$expression changes of increased and decreased genes under *swi3*Δ and *yjl175w*Δ are shown. D) Distributions of expression changes of transcripts in *swi3*Δ and *yjl175w*Δ. The sample number is represented by *n* and the Pearson correlation coefficiency by *r*. Expression change is shown as $\log_2$FC over WT.

I thereby concluded that the *YJL175W* deletion caused partial loss of function of *SWI3*, particularly related to the activation of transcription of Swi3 targets, as the underlying cause of the difference between the phenotypes of *swi3*Δ and *yjl175w*Δ shown in Fig. 1.

2.2.3 Transcriptional consequences of N-terminal deletion of Swi3

I then analyzed the transcriptional profile of *yjl175wΔ* in more detail to further delineate the transcriptional consequences of the N-terminal deletion of Swi3 (*swi3ΔN*) created by the deletion of *YJL175W*. Figure 5A shows variations in transcripts between WT and *yjl175w*Δ cells. The number of decreased genes (230) was about 3.4 times higher than that of increased genes (67). Overall alterations of expression levels of these transcripts upon *yjl175w*Δ are shown in Fig. 5B. The decreased 230 genes constituted 4.58% of the total transcripts in WT cells and were decreased to 1.18% in *yjl175w*Δ. The increased 67 transcripts constituted only 0.14% of total WT transcripts and were increased to only 0.45% in *yjl175w*Δ (Fig. 5B). This asymmetrical distribution, showing more decreased transcripts than increased ones (Fig. 5C), suggests an overall reduction of transcription in *yjl175w*Δ cells compared with that in WT cells. Of note, however, these ratios do not necessarily reflect intracellular mRNA ratios, as the number of each transcript is normalized to the number of total transcripts.

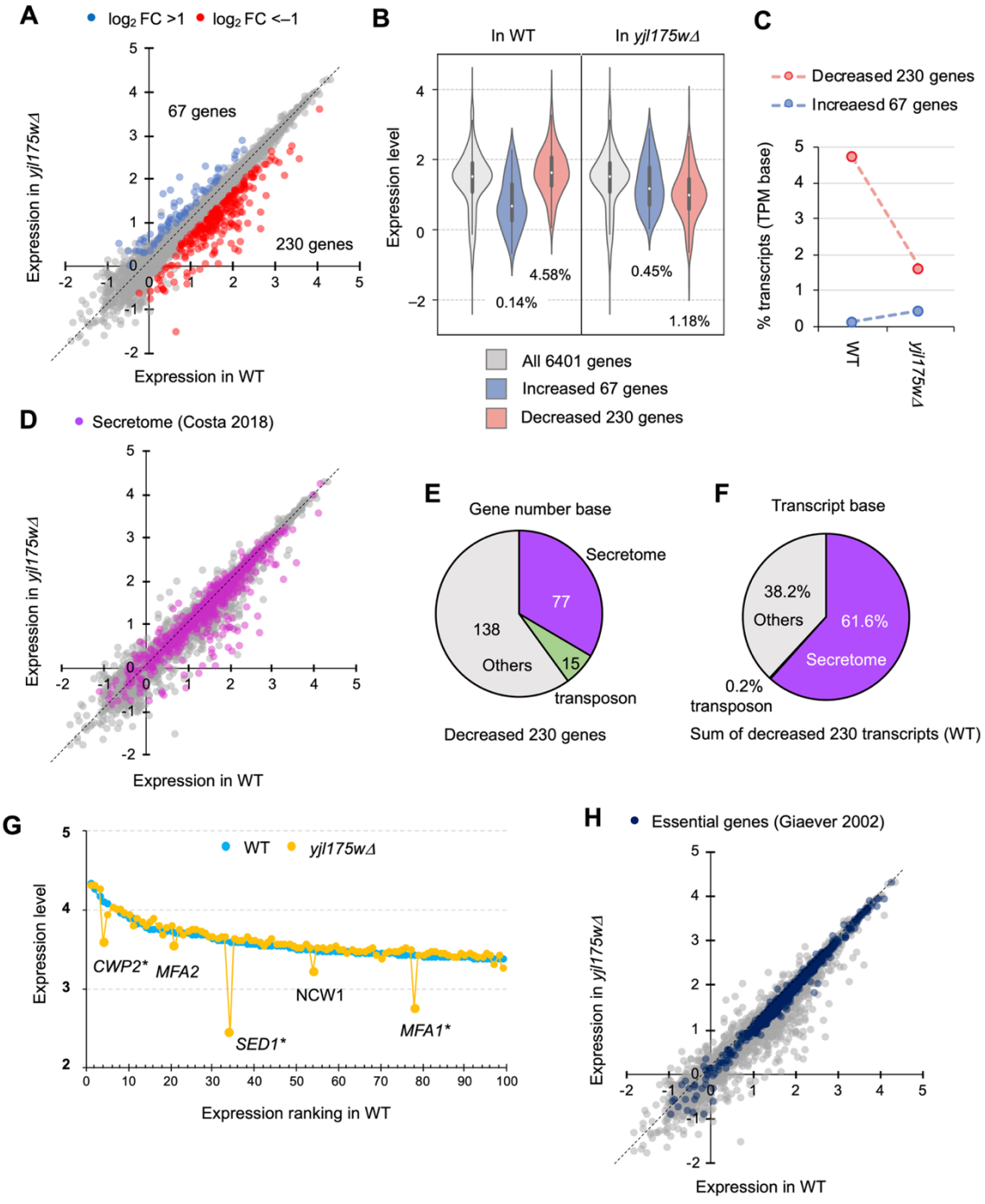
A
log2 FC >1
log2 FC <–1
67 genes
230 genes
Expression in yjl175wΔ
Expression in WT
B
In WT
In yjl175wΔ
Expression level
0.14%
4.58%
0.45%
1.18%
All 6401 genes
Increased 67 genes
Decreased 230 genes
C
Decreased 230 genes
Increaesd 67 genes
% transcripts (TPM base)
WT
yjl175wΔ
D
Secretome (Costa 2018)
Expression in yjl175wΔ
Expression in WT
E
Gene number base
Secretome
77
138
Others
15
transposon
Decreased 230 genes
F
Transcript base
38.2%
Others
61.6%
Secretome
0.2%
transposon
Sum of decreased 230 transcripts (WT)
G
WT
yjl175wΔ
Expression level
CWP2*
MFA2
NCW1
SED1*
MFA1*
Expression ranking in WT
H
Essential genes (Giaever 2002)
Expression in yjl175wΔ
Expression in WT

Figure 5. Transcriptional consequences of deletion of *YJL175W*. A) Comparison of transcript levels between WT and *yjl175w*Δ. Blue and red dots indicate significantly increased transcripts (FDR ≤ 0.05 and $\log_2$ FC ≥ 1) and decreased transcripts (FDR ≤ 0.05 and $\log_2$ FC ≤ − 1), respectively. Numbers of increased and decreased genes are also shown. B) Distributions of all, 67 increased, and 230 decreased transcripts upon *YJL175W* deletion; their proportions in WT and in *yjl175w*Δ transcripts are also shown as the percentage. The percentage was calculated as follows: (the sum of TPMs of 67 increased or 230 decreased transcripts)/(the sum of TPMs of all 6401 genes) × 100. C) Alteration of transcripts upon deletion of *YJL175W*. The transcript percentage was calculated as in (B). D) Expression levels of transcripts coding for secreted proteins (secretome) in WT and *yjl175w*Δ. Purple dots show transcripts of secretome proteins. The secretome protein list (1088 proteins) was obtained from Costa *et al.* (Costa et al. 2018). E and F) Proportions of the numbers of genes (E) and sums of transcripts (F) of secretome proteins in the 230 genes significantly decreased upon *YJL175W* deletion. The sum of the TPMs of contained transcripts calculates transcript sum. G) Expression levels of the top 100 highly expressed genes in WT and *yjl175w*Δ. Five representative genes with expression levels significantly reduced upon *YJL175W* deletion are shown. Genes with asterisks showed a greater than twofold decrease upon *YJL175W* deletion. The adjusted *p*-values of the expression changes of indicated genes were ≤2.1E-30 (Table S3) H). Expression levels of transcripts of essential genes in WT and *yjl175w*Δ. Dark blue dots represent transcripts of essential genes. Essential gene list (1274 genes) was obtained from Giaever *et al*.(Giaever et al. 2002). Expression change is shown as $\log_{10}$ TPM.

I then performed gene ontology (GO) enrichment analysis to reveal processes and genes affected in the *yjl175wΔ* cells (Tables 1 and 2). The set of 67 increased genes was enriched with GOs related to methionine biosynthetic processes, likely associated with an increase in the transcription factors *MET28* and *MET32* (Fig. 4C) (Kuras et al. 1996; Blaiseau et al. 1997). The set of 230 decreased genes was enriched with GOs related to transposon activity, which is likely associated with a decrease in the transcription factors *TYE7* and *TEC1* (Fig. 4C) (Servant et al. 2012; Laloux et al. 1990). Decreased genes were significantly enriched with GO genes for secreted proteins (Costa et al. 2018) (Table 2, GO0071944: cell periphery); in fact, 77 out of the 230 decreased genes encoded secretory proteins (Fig. 5D and E), a level that was significantly higher than expected ($p = 1.62E{-}26$). Transcripts of secreted proteins accounted for more than 60% of the decreased transcripts, whereas transposon-related transcripts accounted for only 0.2% (Fig. 5F), suggesting that those secreted proteins were highly expressed. Figure 6G shows the expression levels of the top 100 highly expressed genes in WT. Specific reductions in *yjl175wΔ* transcripts encoding secretory proteins, such as *CWP2*, *MFA2*, *SED1*, *NCW1*, and *MFA1*, were observed, and no transcript increased more than twofold. The decreased secretory genes were not essential for viability (Giaever et al. 2002), and the *yjl175wΔ* cells did not present with reductions in growth under normal growth conditions (Fig. 2C). I thereby speculated that the *YJL175W* deletion might only affect the transcription of non-essential genes. In fact, essential genes made up just 5% (15 genes) of the 297 genes with expression levels altered by more than twofold (Fig. 5H), which was far fewer than expected ($p = 1.82E{-}15$). I thus concluded that the *swi3ΔN* mutant generated by the deletion of *YJL175W* caused a selective transcriptional reduction of genes encoding highly expressed, non-essential secreted proteins.

Table 1 GO analysis of 67 genes increased upon deletion of *YJL175W*.

GO term	*p*-value	GO ID	Matches
Biological process			
cysteine biosynthetic process*	1.94E-09	0019344	7
sulfur amino acid metabolic process*	7.71E-09	0000096	10
methionine biosynthetic process*	1.08E-08	0009086	9
Molecular function			
sulfur compound transmembrane transporter activity*	3.60E-03	1901682	4
anion transmembrane transporter activity*	6.94E-03	0008509	7
sulfite reductase (NADPH) activity*	8.35E-03	0004783	2
Cellular component			
sulfite reductase complex (NADPH)*	5.00E-03	0009337	2

Table 2 GO analysis of 230 genes decreased upon deletion of *YJL175W*.

GO term	*p*-value	GO ID	Matches
Biological process			
DNA integration*	3.01E-07	0015074	14
generation of precursor metabolites and energy	8.06E-06	0006091	25
transposition, RNA-mediated*	3.72E-05	0032197	17
Molecular function			
aspartic-type endopeptidase activity*	2.31E-08	0004190	15
aspartic-type peptidase activity*	2.31E-08	0070001	15
RNA-DNA hybrid ribonuclease activity*	6.75E-08	0004523	14
Cellular component			
cell periphery#	6.43E-11	0071944	66
fungal-type cell wall#	5.56E-09	0009277	23
cell wall#	1.38E-08	0005618	23

*GO related to transposon activity. #GO containing genes encoding secreted proteins.

2.2.4 N-terminal deletion of Swi3 leads to change in translation status

Given that *swi3ΔN* (*yjl175w*Δ) was shown to mitigate the protein burden effect, I speculated that translation status in the mutant cells affected the ectopic expression of proteins therein. I thus analyzed the polysome profiles of WT and *yjl175w*Δ (Fig. 6A) by calculating polysome/monosome ratios (Fig. 6B) to represent cell translation efficacy. In the vector control, the polysome/monosome ratio was significantly lower in *yjl175w*Δ than in WT; that is, the number of translating ribosomes was lower in *yjl175w*Δ. This result suggests that the reduction in transcription of some genes in *yjl175w*Δ might lead to a reduction in overall translation, freeing up ribosomes to produce foreign proteins. Interestingly, the difference in polysome/monosome ratio between WT and *yjl175w*Δ cells did not occur under GFP-op conditions (Fig. 6B), suggesting that under such conditions, the same number of ribosomes is engaged in translation in *yjl175w*Δ as that in WT, leading to the higher GFP levels observed in the mutant.

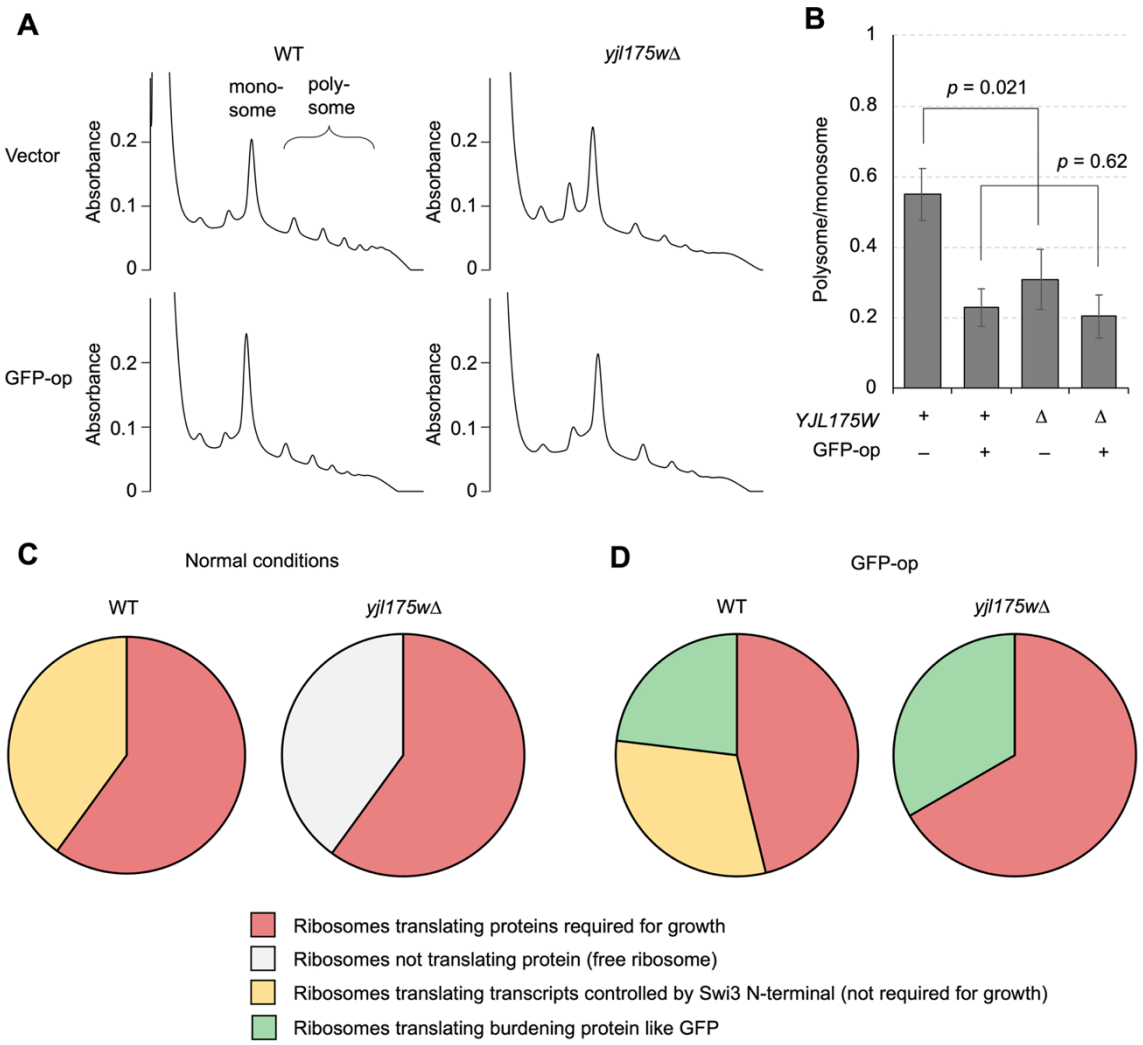

Figure 6. Translational consequence upon deletion of *YJL175W*. **A**) Polysome profiling of WT and *yjl175w*Δ cells under normal (vector) and GFP-op conditions. Predicted monosome and polysome peaks are shown. **B**) Ratios of polysome to monosome in indicated conditions. **C** and **D**) Conceptual pie chart models interpreting how translational changes observed in *yjl175w*Δ mitigated growth defects upon GFP-op. These charts show the hypothetical allocations of ribosomes in indicated conditions, but their percentages are not based on real data. See the main text for a detailed explanation of these charts.

2.3 Discussion

In this study, I showed that the deletion of *YJL175W* unexpectedly led to a partial loss of function of Swi3 (*swi3*Δ*N*) and mitigated growth defects triggered by GFP-op, a condition implicated in the protein burden effect. *YJL175W* is a misannotated ORF because there is no homologous protein even in closely related *Saccharomyces* species. Therefore, the phenotype of the *YJL175W* deletion should be solely created by the truncation of Swi3 accidentally created by the *YJL175W* deletion. A substantial portion of transcription was reduced upon *swi3*Δ*N* via the selective reduction of transcripts encoding highly expressed, secreted proteins (Fig. 5). This transcriptional reduction also led to a reduction in total protein translation (Fig. 6A and B). Cellular conditions created by the *YJL175W* deletion were speculated in accordance with these results. Figures 6C and D show conceptual pie chart models explaining such conditions. In normal conditions, ribosomes are used to translate both proteins that are and are not required for growth (Fig. 6C, WT). In *yjl175w*Δ cells, the number of transcripts encoding proteins not required for growth was lower, and consequently, ribosomes tasked with translating those transcripts were freed up to perform other translations (Fig. 6C, *yjl175w*Δ). In GFP-op, ribosomes are used to translate GFP, leading to a reduction in the number of ribosomes translating proteins required for growth followed by growth defects (Fig. 6D, WT). Free ribosomes created by *yjl175w*Δ reinstates extra ribosomes for GFP translation, avoiding a reduction in the translation of proteins required for growth (Fig. 6D, *yjl175w*Δ) and mitigating growth defects.

Although *yjl175w*Δ cells have an increased capacity to produce exogenic proteins, this phenomenon is associated with an apparent trade-off. These cells are sensitive to stressors, such as high temperature, alkaline pH, and many chemicals (*Saccharomyces* Genome Database), perhaps due to a transcriptional reduction of stress tolerance-related genes. The selective

reduction of transcription not required for normal growth but required for stress responses, likely affords additional resources for producing exogenic proteins. In *yjl175w*Δ cells, total resources for protein production were unchanged compared with those in WT cells; however, the allocation of these resources was found to be altered.

Swi3 is a subunit of the SWI/SNF chromatin remodeling complex that regulates transcription by remodeling chromosomes. The deletion of this subunit thereby causes significant changes in the transcriptional profiles of many genes (Dutta et al. 2017) (Fig. 4). The N-terminal deletion of Swi3 created by *yjl175w*Δ leaves three important domains associated with Swi3 function, and transcriptional change via *yjl175w*Δ is less pronounced than that via *swi3*Δ (Fig. 4A). Interestingly, the N-terminal deletion does not result in milder transcriptional change but instead yields a different transcriptional profile from that of *swi3*Δ, such as opposing directional changes observed in the transcripts of ribosomal proteins. This finding indicates that the N-terminus of Swi3 might influence a specific set of genes.

A hallmark of cancer cells is an increase in chromosome number that triggers a massive overexpression of proteins (Tang and Amon 2013). Cancer cells must thereby evolve to overcome the protein burden effect. At least 20% of all human cancers contain mutations in the SWI/SNF complex including Swi3 homolog BAF155/SMARCC1 and BAF170/SMARCC2(Kadoch et al. 2013; Helming, Wang, and Roberts 2014; Shain and Pollack 2013). Loss of expression or the C-terminal truncation of BAF155 is associated with the proliferation of human cancer cell lines (DelBove et al. 2011). While mutations of Swi3 homologs found in cancer cells are not entirely the same as the N-terminal deletion of Swi3 described here in yeast, it might create a similar situation to that of evolved cancer cells, that is, mutations in the SWI/SNF complex associated with an extensive transcriptional reduction and mitigation of the protein burden effect, facilitating rapid growth.

2.4 Materials and Method

Strains used in this chapter

The strains used in this study are listed in Table 3. The yjl175wΔ deletion cassette was generated by PCR using the genome of yjl175wΔ strain in the yeast knockout collection (Horizon) as a template with the primers 5′-CGGCCGCTCTAGAACTAGTGGATCCGATGGAATTTCTTTGTAAACGCA-3′ and 5′-ATTGGGTACCGGGCCCCCCCTCGAGGCCCAAAAACGTATCTCTGCTTA. The cassette was cloned into the pRS413 vector via gap-repair cloning method in yeast. The C-terminal coding region of truncated SWI3 in the plasmid was fused in-frame to the TAP tag generated by PCR using a TAP collection strain as a template (Dharmacon) and gap-repair cloning in yeast. PCR reactions for yjl175wΔ-TAP cassette were performed with the primers 5′-GATGGAATTTCTTTGTAAACGCATT-3′ and 5′-GCCCAAAAACGTATCTCTGCTTAAA-3′. BY4741 was transformed with the yjl175wΔ-TAP cassette by homologous recombination and selected on yeast extract/peptone/dextrose (YPD) plates containing 200 μg/mL G418. Insertion of the cassette was verified by genomic PCR with primers external to the integration locus, 5′-GACCGTTCCCAGTTAAGGTCGA-3′ and 5′-CGCTGCCAATGCTGAAGTATGT-3′.

Table 3 Strains used in this study.

Strain	Genotype	Reference
BY4741	*MATa his3Δ1 leu2Δ0 met15Δ0 ura3Δ0*	Brachman et al.
ygl024wΔ	*MATa ygl024wΔ::KanMX his3Δ1 leu2Δ0 met15Δ0 ura3Δ0*	Winzeler et al.
yjl175wΔ	*MATa yjl175wΔ::KanMX his3Δ1 leu2Δ0 met15Δ0 ura3Δ0*	Winzeler et al.
swi3Δ	*MATa yjl176cΔ::KanMX his3Δ1 leu2Δ0 met15Δ0 ura3Δ0*	Winzeler et al.
ykl053wΔ	*MATa ykl053wΔ::KanMX his3Δ1 leu2Δ0 met15Δ0 ura3Δ0*	Winzeler et al.
SWI3-TAP	*MATa SWI3-TAP::HIS3MX6 leu2Δ0 met15Δ0 ura3Δ0*	Ghaemmaghami et al.
yjl175wΔ-TAP	*MATa yj175wΔ-TAP::KanMX his3Δ1 leu2Δ0 met15Δ0 ura3Δ0*	This study

Growth conditions and yeast transformation

Yeast culture and transformation were performed as previously described. (Amberg, Burke, and Strathern 2005). YPD medium was used for yeast culture. Synthetic complete (SC) medium lacking uracil (–Ura) or leucine and uracil (−Leu/Ura) was used to culture yeast cells harboring plasmids. The strains used in this study are listed in Table 3. BY4741 was used as WT control. GFP is overexpressed under the control of the TDH3 promoter on the 2-μm plasmid pTOW40836 (Moriya, Shimizu-Yoshida, and Kitano 2006). pTOW40836 was used as empty vector control.

RNA−seq analysis

Sample preparation for RNA-seq was performed as described in Takasaki et al. (Takasaki et al. 2013). BY4741 and *yjl175w*Δ were grown in YPD at 30 °C and sampled during the logarithmic growth phase. Cells were collected by centrifugation at 10,000 g for 10 min. Total RNA from 0.5 g of collected yeast cell samples was extracted using a FastRNA Pro Soil-Direct Kit (Qbiogene) according to the manufacturer's instructions. Samples were treated with DNase to remove genomic DNA from total RNA with Recombinant DNaseI (RNase-free) (TaKaRa). After ethanol precipitation, the purified total RNA was stored at −80 °C until use in subsequent experiments. RNA purity and concentrations were estimated with a NanoDrop spectrophotometer (Thermo Fisher Scientific). RNA quality and quantity were estimated with a Bioanalyzer (Agilent, Tokyo, Japan). cDNA from purified mRNA was synthesized using a cDNA Synthesis Kit

(TaKaRa) according to defined protocols. Briefly, first, poly(A) RNA was reverse-transcribed with an oligo (dT)-T7 primer containing a T7 promoter sequence; this was used to synthesize double-stranded cDNA. cDNA templates were then transcribed in vitro with T7 RNA polymerase (TaKaRa), yielding large amounts of antisense RNA (aRNA). Finally, aRNA was further reverse transcribed to cDNA with a biotinylated oligo (dT) primer for next-generation sequencing. Sequencing of the synthesized cDNA was performed by paired-end sequencing on an Illumina Hiseq2000 sequencing system provided by the Hokkaido System Science Co., Ltd. We analyzed three biological replicates for each strain.

Transcriptome data analysis

RNA-seq data of Swi3 knockout and WT strains (GEO, ID: 302174480, 302174481, 30174486, and 302174487) (Dutta et al. 2017) were downloaded from the SRA database. Our RNA-seq data of deletion of YJL175W and WT are available from the SRA database (SRA, ID: SRR10848971 and SRR10848972). All RNA-seq data, including ours and Dutta's, were aligned to the Ensembl R64-1-1 genome using HISAT2 version 2.1.0 with gene annotations from Ensembl R64-1-1. HISAT2 options were -p 8 –dta. Ensembl R64-1-1 was obtained from iGenomes by Illumina, Inc. Visualizations of mapped fragments were conducted with an Integrative Genome Viewer (2.4.9). Assembly and estimation of transcript abundances were performed with HTSeq version 0.11.1. Downstream analysis was conducted using Python (3.6.8). Transcripts per kilobase millions (TPMs) were calculated according to a previously described method (B. Li et al. 2010).

TAP–tag western blot

Detection of TAP-tag protein by Western blot was performed as described in Ishikawa et al. (Ishikawa et al. 2017). Yeast strains were aerobically cultured at 30 °C in 2 mL of YPD medium. Optical density at 660 nm (OD_{660}) was measured, and units of 1 OD_{660} were harvested during the log phase. Cells were treated with 1 mL of 0.2 N NaOH for 5 min at room temperature and then suspended in 2× NuPAGE LDS sample buffer (Invitrogen) and heated to 70 °C for 10 min. Protein lysate in the supernatant was labeled with EzLabel FluoroNeo (ATTO) and subjected to polyacrylamide gel electrophoresis with lithium dodecyl sulfate (SDS-PAGE), followed by Western blot with PAP (Sigma-Aldrich) (1:2000) and peroxidase-conjugated secondary antibody (Nichirei Biosciences) (1:1000). We used a NuPAGE 4–12% Bis-Tris Gel (Invitrogen) for SDS-PAGE and an iBlot Transfer Stack PVDF membrane (Invitrogen) for Western blot. Chemiluminescence was induced by SuperSignal West Femto Maximum Sensitivity Substrate (Thermo Fisher Scientific) and detected on a LAS-4000 image analyzer (Fujifilm) using ImageQuant LAS 4000 (GE Healthcare).

Polysome profiling

Frozen yeast cells were mixed with frozen droplets of 600 µL lysis buffer (20 mM Tris–HCl (pH 7.5), 150 mM NaCl, 5 mM $MgCl_2$, 1 mM dithiothreitol, 100 µg/mL cycloheximide, and 1% Triton X-100) and lysed with Multi-beads Shocker (Yasui Kikai). Lysates were treated with 25 U of TURBO DNase (Thermo Fisher Scientific) and cleared by centrifugation at 20,000 g for 10 min at 4 °C. RNA concentration in the lysate was measured with a Qubit RNA BR Assay Kit (Thermo Fisher Scientific). Sucrose gradients (10–50% sucrose in lysis buffer without Triton X-100) were prepared in 14 × 95 mm open-top Polyclear centrifuge tubes (SETON) using a Gradient Station (BioComp). Lysates containing 20 µg RNA were loaded on top of the sucrose gradients and

centrifuged at 35,300 rpm for 2.5 h at 4 °C using a rotor P40ST (Hitachi Koki). After ultra-centrifugation, the absorbance at 254 nm was measured continuously on a Bio-mini UV monitor (ATTO).

Statistical analysis

Where appropriate, values are expressed as mean ± SD. Statistical analyses of RNA-seq date from three biological replicates were conducted using the Benjamini–Hochberg method, and a false discovery rate ≤0.05 was considered statically significant (*Controlling the False Discovery Rate: A Practical and Powerful Approach to Multiple Testing Yoav Benjamini*, n.d.). Statistical analyses with more than two groups were performed by Bonferroni correction. An adjusted p-value of ≤0.05 was considered statistically significant. All data are representative of multiple repeated experiments.

Chapter 3: Study on the nature of yeast gene groups for which overexpression is functionally adaptive

3.1 Introduction

Organisms have the ability to maintain growth, reproduction, and survival even under stressful environmental conditions (Hohmann and Mager 2003). This ability is achieved through evolutionarily-conserved intracellular systems such as signaling pathways, gene regulatory networks, and stress-induced proteins that play essential roles under stress (Tatebe and Shiozaki 2017; Genest, Wickner, and Doyle 2019; Widmann et al. 1999). For example, a protein kinase complex mTOR is known to be an evolutionarily conserved hub of signaling pathways for regulation of gene expression in changing environments(J. Kim and Guan 2019). Heat shock transcription factors are known to precisely regulate the expression of heat shock proteins, which are chaperone proteins for protecting cell function from proteotoxicity caused by protein misfolding (Gomez-Pastor, Burchfiel, and Thiele 2018). Thus, cell behavior in response to environmental stresses, such as gene expression levels, was thought to be programmed and optimized (Gasch et al. 2000; Zaslaver et al. 2004).

Mutations that increase gene expression levels independently of regulatory mechanisms (i.e., overexpression), such as single nucleotide polymorphisms (SNPs) and copy number variations (CNVs) can lead to adaptation to new environments. For example, overexpression of hypoxia-inducible factor was reported in several cancer types(Zhong et al. 1999), which could be caused by point mutations(“Correction for Sutter et al., Hypoxia-Inducible Factor 1α Protein Expression Is Controlled by Oxygen-Regulated Ubiquitination That Is Disrupted by Deletions and Missense Mutations” 2022). That was considered an adaptation to a low oxygen concentration (hypoxia)

environment(Zhong et al. 1999; L. C. Kim and Simon 2022). Peter et al. reported a CNV of ENA1 encoding a P-type ATPase sodium pump, associated with salt sensitivity, among over 1,000 isolations of *S. cerevisiae*(Peter et al. 2018; Haro, Garciadeblas, and Rodríguez-Navarro 1991).

However, it is poorly understood why and how overexpression can be adaptive despite well-established stress response systems. Overexpression often has detrimental consequences for the cell(Makanae et al. 2013; Sopko et al. 2006). An exceptional but well-studied example of adaptive overexpression is drug resistance. Cells and individuals acquire drug resistance when specific genes that interact with drugs are overexpressed(Palmer and Kishony 2014). For example, the glyphosate-resistant *Amaranthus palmeri* population from Georgia contained 5-160 copies of 5-enolpyruvylshikimate-3-phosphate synthase more than non-resistant polutation(Gaines et al. 2010). *Plasmodium falciparum*, a malaria-causing parasite, acquired resistance to the antimalarial drug Mefloquine through CNVs of *pfmdr1* (*Mefloquine Resistance in Plasmodium Falciparum and Increased Pfmdr1 Gene Copy Number*, n.d.). Overexpression experiments are often used to identify drug targets due to the role that gene overexpression can play in drug resistance (Rine et al. 1983). In contrast to drug resistance, the effects of overexpression on environmental stresses cannot be readily assumed because of the combined effects of many factors.

The adaptive effects of overexpression may vary depending on genetic background. Several studies have shown that differences in genetic background strongly affect the phenotype of mutations. For instance, the gene deletion phenotypes such as gene essentiality and the tolerance to gene overexpression due to gene amplification also depend on genetic background and environments (Galardini et al. 2019; D. Robinson et al. 2021). Similarly, adaptive mutations also depend on environments and genetic backgrounds, referred to as context-dependency (Brettner et

al. 2022; Eguchi, Bilolikar, and Geiler-Samerotte 2019). The adaptive effects of overexpression also may depend on genetic background and environmental differences. For example, under salt stress, several *Saccharomyces cerevisiae* genes such as *ENA1* and *HAL1-9,* named Halotolerance*,* were reported as their overexpression increased salt tolerance (Gaxiola et al. 1992; Gläser et al. 1993; Ferrando et al. 1995; Mulet et al. 1999; Mendizabal et al. 1998; Daran-Lapujade et al. 2009). However, these adaptive effects of overexpression may also vary between different genetic backgrounds of the same species.

Genes whose overexpression is functionally adaptive (GOFAs), to our knowledge, have not previously been identified using genome-wide approaches in the context of environmental stress and genetic backgrounds. While genome-wide overexpression approaches have been used to study adaptive effects, these studies have primarily focused on identifying drug targets and have used strains with the same genetic background(Arnoldo et al. 2014; Luesch et al. 2005; Ho et al. 2009; Beaupere et al. 2018). Recently, the negative effects of gene overexpression in different genetic backgrounds have been explored using a yeast genome-wide overexpression library(D. Robinson et al. 2021). Still, the adaptive effects of overexpression have not yet been investigated.

This study systematically isolated GOFAs to approach why and how overexpression can be adaptive under complex genetic background-environment interaction. I developed "overexpression profile" using the model eukaryote *Saccharomyces cerevisiae*. Then, I isolated GOFAs from about 5,500 yeast genes under high temperature, high salt, and oxidative stress. GOFAs suggested that gene overexpression can compensate for deficiencies to maximize fitness under stress.

I also identified GOFAs under salt stress using three different genetic-background strains of S. *cerevisiae*; BY4741, CEN.PK and DBVPG6765. BY4741 is one of the most used laboratory strains derived from S288C (Brachmann et al. 1998). This strain was utilized in many genome-wide studies such as a yeast knockout collection (Winzeler et al. 1999), a purification peptide ORFs collection (Ghaemmaghami et al. 2003), and a fluorescence protein clone collection (Huh et al. 2003). CEN.PK is another laboratory strain known as salt-sensitive (Daran-Lapujade et al. 2009). DBVPG6765 is the distantly related Wine/European strains (Yue et al. 2017). The identification of GOFAs suggested that whether gene overexpression is adaptive is highly dependent on genetic background and environmental factors. Moreover, I showed the "overexpression profile" is possible to determine the missing piece for cell growth in each genetic background and environment by examining GOFAs.

3.2 Results

3.2.1 GOFAs under stress are a unique set of genes

To systematically identify GOFA and to characterize cells from GOFAs, I set up an overexpression profile, as shown in Fig. 7A. The profile consists of four steps; 1) Construction of libraries pooling *S. cerevisiae* BY4741 cells that harbor a 2μ plasmid with each of the cloned 5,751 genes of the BY4741 genome. The initial version used two sets of gTOW6000 libraries (Makanae et al. 2013) to build Pool_a and Pool_b; 2) Competitive culture and passaging of the pooled libraries; 3) Long-read plasmid sequencing of plasmid inserts extracted from the culture pool library by the Oxford Nanopore Technologies MinION (Figure 8A); 4) Analysis of sequence data to calculate the frequencies of plasmid inserts and identification of GOFAs. I confirmed that Pool_a and Pool_b covered more than 93% of the 5,751 genes (Figure 8B).

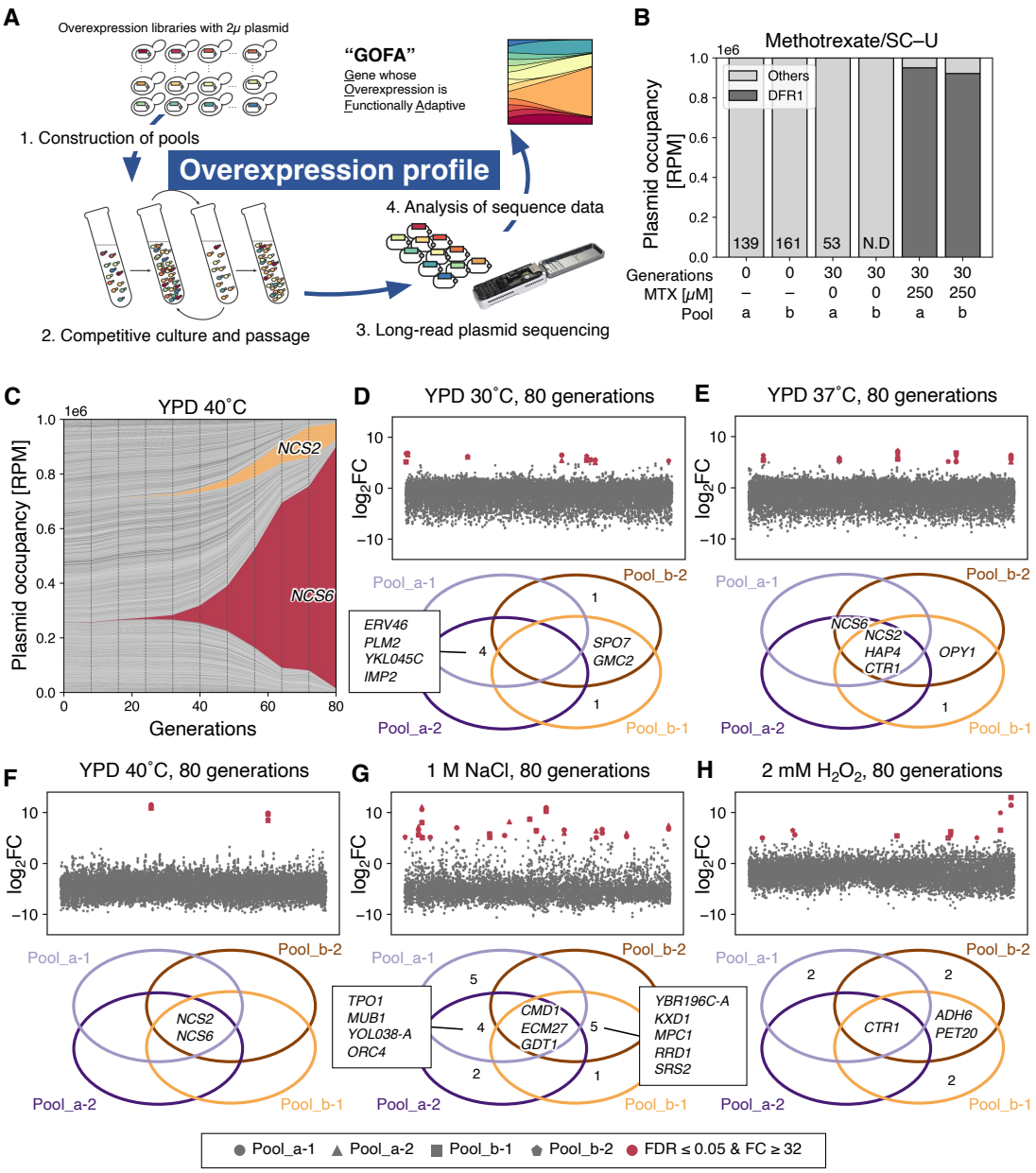
A
Overexpression libraries with 2μ plasmid
1. Construction of pools
"GOFA"
Gene whose
Overexpression is
Functionally Adaptive
Overexpression profile
4. Analysis of sequence data
2. Competitive culture and passage
3. Long-read plasmid sequencing
B
Methotrexate/SC–U
1e6
Others
DFR1
Plasmid occupancy [RPM]
139
161
53
N.D
Generations 0 0 30 30 30 30
MTX [μM] – – 0 0 250 250
Pool a b a b a b
C
YPD 40˚C
NCS2
NCS6
Plasmid occupancy [RPM]
Generations
D
YPD 30˚C, 80 generations
log2FC
Pool_a-1
Pool_b-2
Pool_a-2
Pool_b-1
ERV46
PLM2
YKL045C
IMP2
SPO7
GMC2
E
YPD 37˚C, 80 generations
NCS6
NCS2
HAP4
CTR1
OPY1
F
YPD 40˚C, 80 generations
NCS2
NCS6
G
1 M NaCl, 80 generations
TPO1
MUB1
YOL038-A
ORC4
CMD1
ECM27
GDT1
YBR196C-A
KXD1
MPC1
RRD1
SRS2
H
2 mM H2O2, 80 generations
CTR1
ADH6
PET20
Pool_a-1 Pool_a-2 Pool_b-1 Pool_b-2 FDR ≤ 0.05 & FC ≥ 32

Figure 7. GOFAs under well-studied stresses are a unique set of genes. A) The overexpression profile for identifying GOFAs developed in this study. The detail is explained in the text. **B)** A proof of concept for overexpression profile: identification of GOFA as a drug target (under 250 μM methotrexate). The bar plot and the numbers show occupancies of a plasmid harboring *DFR1* showing with reads per million (RPM) reads. **C)** The time course of plasmid occupancy under heat stress. One of the four replicates at 40˚C in YPD for 80 generations (samples were analyzed every eight generations). Occupancies of each plasmid are shown with reads per million (RPM) reads, and the orange and red areas correspond to the enriched genes *NCS2* and *NCS6*, respectively. **D-H)** Fold changes of plasmid occupancies after the cultivation (upper) and hit genes in each replicate under well-studied stresses (lower, FDR ≤ 0.05 and FC $\geq 2^5$); YPD at 30˚C (C, control), 37˚C (D) and 40˚C (E) as the heat stresses, 1 M NaCl (F) as the salt stress, 2 mM H_2O_2 (G) as the oxidative stress. Hit genes were shown as red-filled symbols. Genes identified as GOFAs are summarized in Table 4.

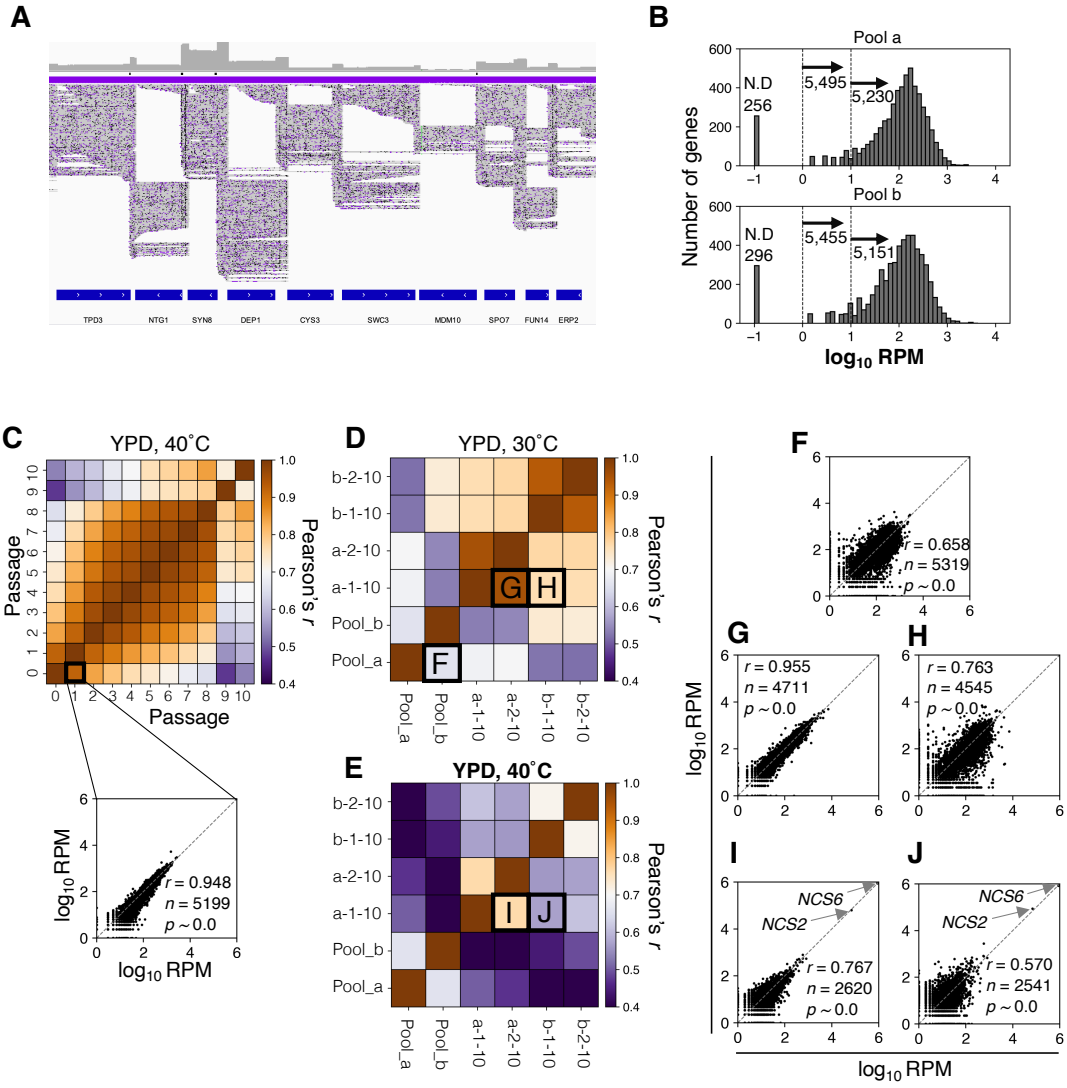
A
TPD3
NTG1
SYN8
DEP1
CYS3
SWC3
MDM10
SPO7
FUN14
ERP2
B
Pool a
N.D
256
5,495
5,230
Pool b
N.D
296
5,455
5,151
Number of genes
log10 RPM
C
YPD, 40˚C
Passage
Passage
Pearson's r
log10 RPM
log10 RPM
r = 0.948
n = 5199
p ~ 0.0
D
YPD, 30˚C
b-2-10
b-1-10
a-2-10
a-1-10
Pool_b
Pool_a
G
H
F
Pearson's r
E
YPD, 40˚C
I
J
F
r = 0.658
n = 5319
p ~ 0.0
G
r = 0.955
n = 4711
p ~ 0.0
H
r = 0.763
n = 4545
p ~ 0.0
I
NCS6
NCS2
r = 0.767
n = 2620
p ~ 0.0
J
NCS6
NCS2
r = 0.570
n = 2541
p ~ 0.0
log10 RPM
log10 RPM

Figure 8. A quality check of sequencing data by overexpression profile. A) An example of plasmid inserts sequencing result, visualized by a genome browser, IGV. **B)** Distribution of plasmid inserts (RPM) in pool_a (upper) and pool_b (lower). Those with an RPM of 0 are appended with 0.1 for convenience. Vertical dashed lines indicate RPM ≥1 or RPM ≥10. The mean, median, and SD of RPM in pool_a were 76.8, 120, and 6.42, respectively, and in pool-b were 70.6, 115, and 7.05. **C)** A heatmap showing Pearson's correlation among each passage in the identical replicate under 40˚C. A purple-to-orange presents low to high Pearson's correlations. The lower panel shows a scatter plot comparing RPM before and after 1st passage. **D-E)** RPM scores were quite reproducible between the replicates that originated the identical pool, while they had some differences when originated pools differed. Heatmaps showing Pearson's correlation among four replicates on the 10th passages under (D) 30˚C and (E) 40˚C. "a-" and "b-" in the four replicates originated from pool_a and pool_b responsively. F-J letters mean these correlations were shown in Extended Data Figure1F-J as scatter plots. **F-J)** Scatter plots comparing RPM. The comparisons are described in D and E. r, n, and p mean correlation coefficients, sample number, and p-values, respectively. "p ~ 0" indicate that the p-value is smaller than the value our computer can calculate.

Table 4 GOFAs under well-studied stress.

Systematic name	Standard name	YPD30	YPD37	YPD40	NaCl	H_2O_2
YKL109W	HAP4		GOFA			
YNL119W	NCS2		GOFA	GOFA		
YPR124W	CTR1		GOFA			GOFA
YGL211W	NCS6			GOFA		
YBR109C	CMD1				GOFA	
YBR187W	GDT1				GOFA	
YJR106W	ECM27				GOFA	

* Here I considered hits in all four replication as GOFAs.

As proof of concept for the overexpression profile, I screened for GOFA in the presence of 250 μM methotrexate (MTX)(Giaever et al. 2004), an antagonistic inhibitor of dihydrofolate reductase in yeast encoded by *DFR1*. As expected, 30 generations of competitive culture enriched the *DFR1* plasmid to more than 90% of the total (Fig. 7B). Next, I identified GOFAs under the most studied stresses in yeast (Fig. 9A), namely heat stress (37 ˚C and 40 ˚C), salt/osmotic stress (1 M NaCl) and oxidative stress (2 mM H_2O_2). The exact temperature and concentration of chemicals were determined to stress normal yeast growth (Fig. 9B-D). I performed the overexpression profile with four biological replications (two different original pools, each with two replicas.). There were higher correlations of plasmid occupancy between different time points and between replicates with the same origin pool than between replicates with different origin pools (Fig. 8C-J). Fig. 7C shows the time course of plasmid occupancy at 40˚C. *NCS2* and *NCS6* were found to be dramatically enriched during incubation.

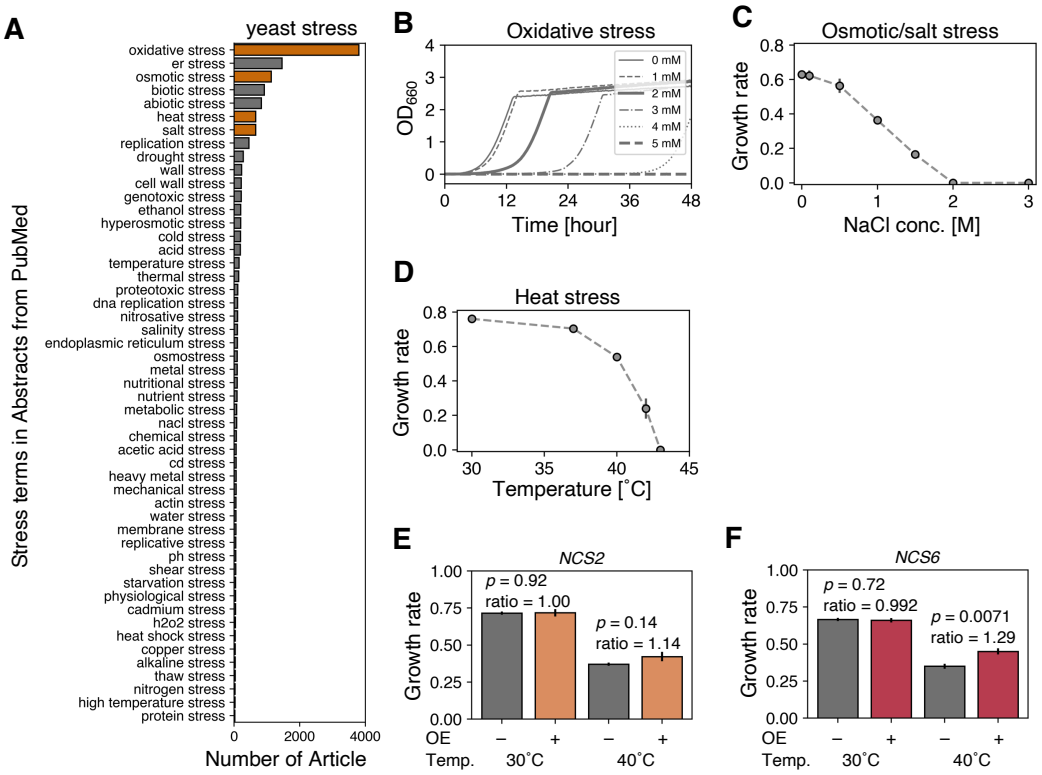

Figure 9. The well-studied stress in yeast. A) The number of articles in which "XXX stress" appears in the abstract of the articles obtained from PubMed search for "yeast stress". The orange bars indicate the stresses which we focused on in this study. **B)** Growth curves of BY4741 with various amounts of H_2O_2 in YPD. **C)** Growth rates of BY4741 with various amounts of NaCl in YPD. **D)** Growth rates of BY4741 in YPD under some temperatures. **E-F)** The growth rates of BY4741 cells overexpressing (*-oe*). (E) *NCS2-oe* and (F) *NCS6-oe* at 30˚C and 40˚C. The *p*-values are from two-tailed Welch's t-test (n = 3). Ratios were the average growth rate over the empty vector control. Error bars show SD (n = 3).

There was a negative correlation between insert length and the number of reads, suggesting some technical bias in reading inserts (Fig. 10A-C). To reduce these analysis biases, I calculated the fold change relevant to pools and defined genes with higher fold change than 32 and lower FDR then 0.05 as hits. Fig. 7D-H show the fold change of 5,751 genes and genes hit in each condition. The replicates with the same origin pool shared more hit genes than the pairs with different origin pools. There also were higher correlations of fold change between replication with the same pools than between different pools of origin (Fig. 10F-M). In YPD medium at 30˚C, no genes were hit in all four replicates even after 80 generations (Fig. 7C). Moreover, most dose-sensitive genes (Makanae et al. 2013) were shed from the culture as expected (Fig. 11A-C) (D. Robinson et al. 2021). At 37˚C, *NCS2*, *CTR1*, and *HAP4*; at 40˚C, *NCS2* and *NCS6* were hit (Fig. 7E and F); under 1 M NaCl, *CMD1*, ECM*27* and *GDT1*, were hit; under H_2O_2, *CTR1* was hit in all four replicates (Fig. 7G and H). I here considered genes hit in all replicates as true positives and as GOFAs.

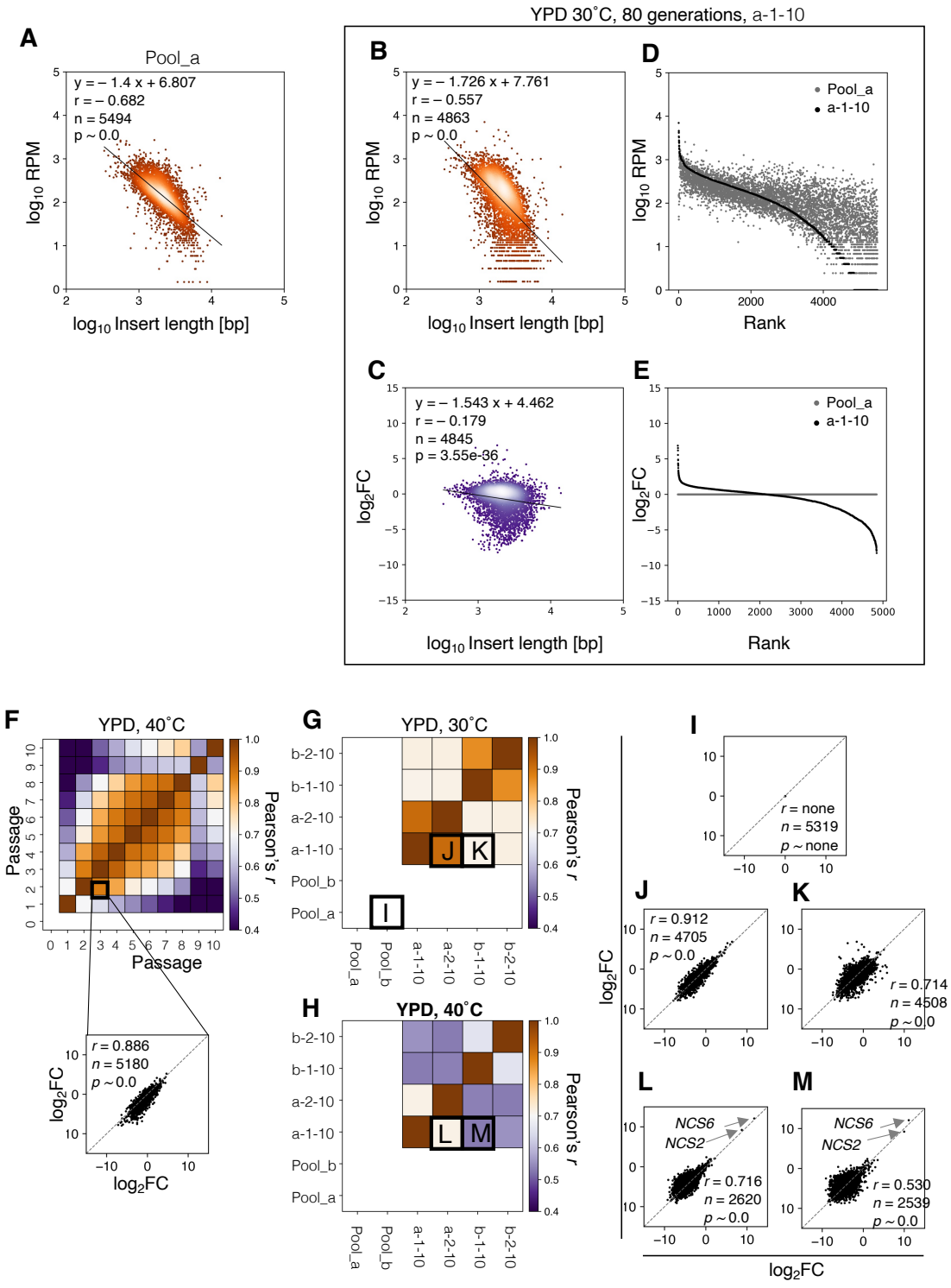
YPD 30˚C, 80 generations, a-1-10
A
Pool_a
y = – 1.4 x + 6.807
r = – 0.682
n = 5494
p ~ 0.0
log10 RPM
log10 Insert length [bp]
B
y = – 1.726 x + 7.761
r = – 0.557
n = 4863
p ~ 0.0
log10 RPM
log10 Insert length [bp]
D
Pool_a
a-1-10
log10 RPM
Rank
C
y = – 1.543 x + 4.462
r = – 0.179
n = 4845
p = 3.55e-36
log2FC
log10 Insert length [bp]
E
Pool_a
a-1-10
log2FC
Rank
F
YPD, 40˚C
Passage
Passage
Pearson's r
r = 0.886
n = 5180
p ~ 0.0
log2FC
log2FC
G
YPD, 30˚C
b-2-10
b-1-10
a-2-10
a-1-10
Pool_b
Pool_a
J
K
I
Pearson's r
H
YPD, 40˚C
L
M
Pearson's r
I
r = none
n = 5319
p ~ none
J
r = 0.912
n = 4705
p ~ 0.0
K
r = 0.714
n = 4508
p ~ 0.0
L
NCS6
NCS2
r = 0.716
n = 2620
p ~ 0.0
M
NCS6
NCS2
r = 0.530
n = 2539
p ~ 0.0
log2FC
log2FC

Figure 10. Calculating fold change to be corrected for insert frequency bias by inset length. **A-B)** Negative correlations between insert frequency (RPM) and insert length (bp) in (A) pool_a or (B) 10^{th} passage. The solid lines mean regression lines (regression equations are shown in the figure.). The shading of colors implies the density of the points, which are thinner with higher density. **C)** A scatter plot comparing fold change (FC) and inset length in the 10^{th} passage. The solid lines mean regression lines (regression equations are shown in the figure). The shading of colors implies the density of the points, which are thinner with higher density. **D-E)** Scatter plots show (E) RPM or (F) fold change (FC) in the initial pool (grey) and the 10^{th} passage (dark grey). These scores were sorted in descending order of RPM and fold change (FC) in the 10^{th} passage. **F)** A heatmap showing Pearson's correlation of FC among each passage in the identical replicate under 40˚C. A purple-to-orange presents low to high Pearson's correlations. The lower panel shows a scatter plot comparing RPM before and after 1^{st} passage. **G-H)** FC were quite reproducible between the replicates that originated the identical pool, while they had some differences when originated pools differed. Heatmaps showing Pearson's correlation among four replicates on the 10^{th} passages under (G) 30˚C and (H) 40˚C. "a-" and "b-" in the four replicates originated from pool_a and pool_b responsively. I-M letters mean these correlations were shown in Extended Data Figure3I-M as scatter plots. **I-M)** Scatter plots comparing RPM. The comparisons are described in G and H. r, n, and p mean correlation coefficients, sample number, and p-values, respectively. "p ~ 0" indicates that the p-value is smaller than our computer can calculate.

I initially expected that our overexpression profile would identify so-called "stress-responsive genes" induced under stress conditions. For example, overexpression of some heat shock-responsive genes might confer high-temperature tolerance. However, no above-mentioned GOFAs appear to be included in such categories. In fact, none of GOFAs matched stress-inducible genes such as "environmental stress-responsive genes" or "heat shock responsive genes" (Gasch et al. 2000; Solís et al. 2018). The original libraries contained those genes, but they dropped out during competitive culture (Figure 11). These results suggested that GOFAs identified by our overexpression profile are a unique set of genes, which means genes that are not induced under stress but whose overexpression is adaptive, that might be helpful for an understanding of unexplored cellular physiology under stress.

To obtain clues to the nature of the identified GOFAs, I focused on *NCS2* and *NCS6* at 40˚C (Fig. 7C and F). Overexpression of *NCS6* (*-oe*) significantly increased the growth rate by 1.29-fold, while *NCS2-oe* increased the growth rate by 1.14-fold, but not significantly (Figure 9E and 9F). *NCS2* and *NCS6* are involved in the thiolation of wobble uridine of tRNAs in the *URM1* pathway (Goehring, Rivers, and Sprague 2003), and the *URM1* pathway is known to have strain-dependent thermo−sensitivity (Tyagi and Pedrioli 2015; Alings et al. 2015). Since the BY4741 strain derived from S288C has a thermosensitive *URM1* pathway (Alings et al. 2015), I thought that *NCS2-oe* and *NCS6-oe* should compensate for their functions at high temperatures. Thus, I hypothesized that GOFAs generally function to compensate for cellular requirements in each environment.

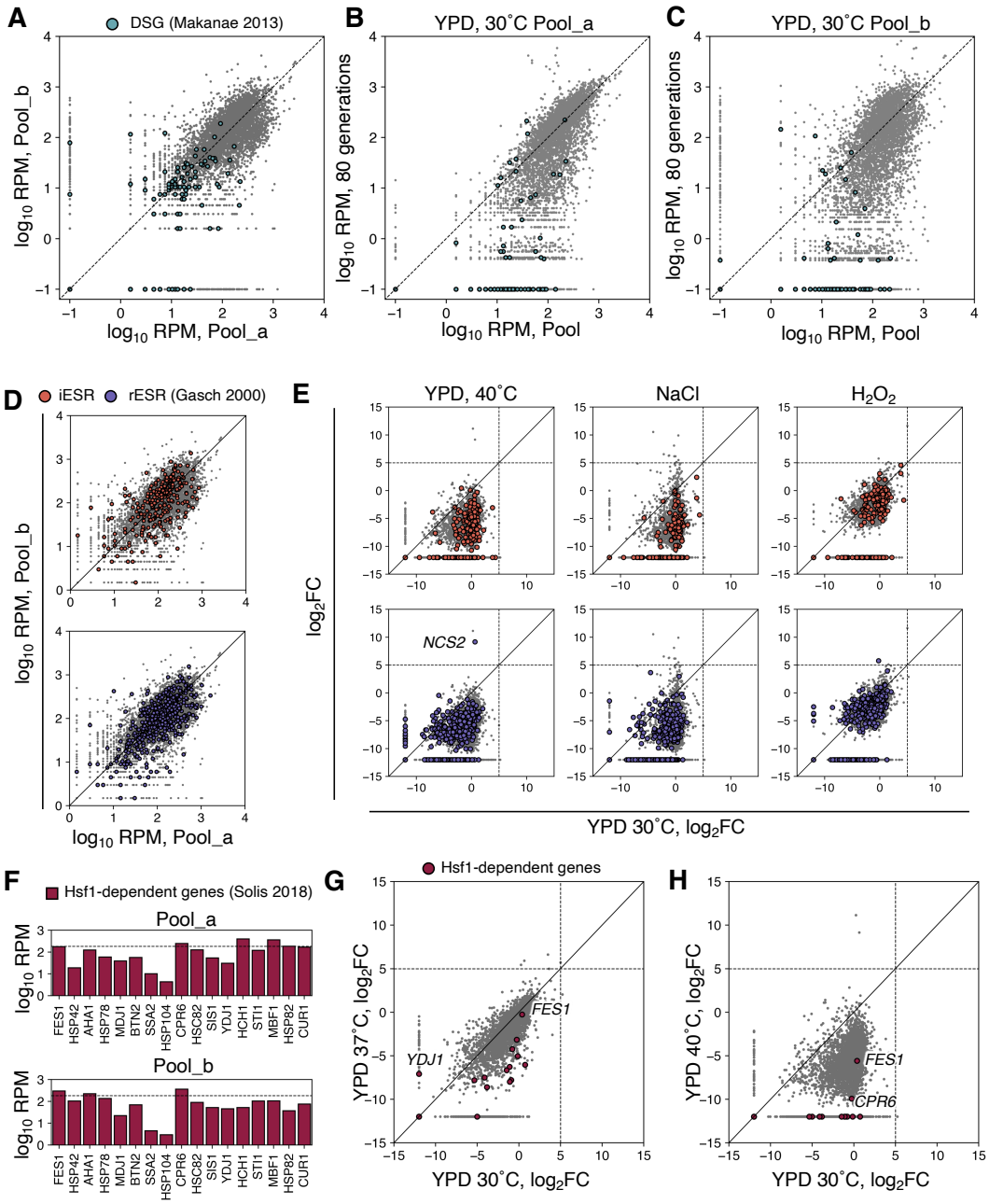
A
DSG (Makanae 2013)
log10 RPM, Pool_b
log10 RPM, Pool_a
B
YPD, 30˚C Pool_a
log10 RPM, 80 generations
log10 RPM, Pool
C
YPD, 30˚C Pool_b
log10 RPM, 80 generations
log10 RPM, Pool
D
iESR
rESR (Gasch 2000)
log10 RPM, Pool_b
log10 RPM, Pool_a
E
YPD, 40˚C
NaCl
H2O2
log2FC
NCS2
YPD 30˚C, log2FC
F
Hsf1-dependent genes (Solis 2018)
Pool_a
log10 RPM
Pool_b
FES1
HSP42
AHA1
HSP78
MDJ1
BTN2
SSA2
HSP104
CPR6
HSC82
SIS1
YDJ1
HCH1
STI1
MBF1
HSP82
CUR1
G
Hsf1-dependent genes
YPD 37˚C, log2FC
YPD 30˚C, log2FC
FES1
YDJ1
H
YPD 40˚C, log2FC
YPD 30˚C, log2FC
FES1
CPR6

Figure 11. Stress-induced genes were not enriched as GOFAs. A-C) RPM of dosage-sensitive genes(Makanae et al. 2013) (DSG, green circle) at (A) initial in pool_a and pool_b, and (B) after 80 generation cultivation under YPD 30˚C in pool_a, (C) and pool_b. **D)** Initial RPM of induced Environmental Stress Response genes(Gasch et al. 2000) (iESR, top and orange circle) and reduced ESR (rESR, bottom, and purple circle) in Pool_a and Pool_b. The grey circles mean other genes than ESR. **E)** The scatter plots show comparisons of fold change of iESR (top and orange circle) and rESR (bottom and purple circle) between 30˚C and other three conditions: 40˚C (left), 1 M NaCl (middle), and 2 mM H_2O_2 (right). The grey circles mean other genes than ESR. **F)** Initial RPM of heat shock response genes (Hsf1-dependent genes(Solís et al. 2018)) in Pool_a (top) and Pool_b (bottom). **G-H)** The scatter plots show comparisons of FC of Hsf1-dependent genes between 30˚C and (G) 37˚C or (H) 40˚C. The red and grey circles mean Hsf1-dependent genes and other genes responsively. All circles are the mean FC of four replicates. The horizontal and vertical dashed lines indicate the threshold of GOFAs ($FC \geq 2^5$). Genes with a FC of nan (undetected) have -15 added for convenience.

3.2.2 GOFAs enriched under salt stress propose Ca^{2+} limitation of the culture medium

To further ascertain the above hypothesis, I next focused on GOFAs enriched under salt stress (1 M NaCl, Fig. 7G). GOFAs enriched in all four replicates (*CMD1*, *GDT1*, and *ECM27*, Fig. 12A) were involved in intracellular calcium homeostasis (Fig. 12B). *CMD1* encodes calmodulin (Mortimer, Contopoulou, and King 1992), and *GDT1* and *ECM27* encode calcium transporters that localize to the Golgi and ER membranes, respectively (Colinet et al. 2016; Klukovich and Courchesne 2016). I confirmed that their overexpression significantly increased the growth rate under 1 M NaCl (Fig. 12C).

Genes hit only in replication of either origin pool were unsure whether false positive or true positive. I thence also focused on *YBR196C-A*, enriched in Pool_b-derived replicates (Fig. 12A), has been reported as an "emerging gene" and encodes an adaptive protein that localizes to the ER membrane (Fig. 12B) (Vakirlis et al. 2020) but its function has not been revealed yet. I also confirmed that *YBR196C-A-oe* significantly increased the growth rate under 1 M NaCl (Fig. 12C). This result indicates that genes that did not hit all replicate always do not mean false positive. However, I did not validate other genes anymore. In addition, I thought that *YBR196C-A* might also be related to calcium homeostasis.

I confirmed the enhancement of the "calcium pulse" (rapid increases in cytosolic Ca^{2+} concentration) upon salt/osmotic stress exposure under *GDT1-oe* and *ECM27-oe* (Fig. 12D)(Colinet et al. 2016; Klukovich and Courchesne 2016; Batiza, Schulz, and Masson 1996; Nakajima-Shimada et al. 1991). *YBR196C-A-oe* also enhanced the calcium pulse even stronger (Fig. 12D). Based on these results and our hypothesis, GOFAs compensated something, I speculated that GOFA under high salt might compensate for the calcium requirement under our

experimental conditions. Indeed, it was true, as the addition of Ca^{2+} (5 and 20 mM) to the 1M NaCl medium increased the growth rate of cells under salt stress (Fig. 2E). Furthermore, the increase in growth rate with some Ca^{2+} addition canceled out the advantage of GOFAs under salt stress (Fig. 2F), suggesting that GOFAs mimic Ca^{2+} addition.

During the competitive culture under salt stress, I unexpectedly observed that the control strain without libraries also adapted (or "evolved" to adapt) to the salt stress (lineage1 and lineage2 in Fig. 12G). The two evolved lineages after 10 passages (Ev) grew significantly faster than the ancestral strain (An) under 1 M NaCl (Fig. 2H and 2I). I performed genome pool sequencing of the An and Ev and found base substitutions in the genome that cause P393Q in Pma1 on the lineage1, G428D, and G824E in Pmr1on the lineage2 as mutations occurring in competitive cultures (Fig. 12J and Table 5). Since Pma1 and Pmr1 are also involved in calcium homeostasis (Withee, Sen, and Cyert 1998; Rudolph et al. 1989) (Fig. 12B), I speculated that cells may have also evolved to compensate for calcium deficiency under our conditions through these mutations. This idea also seemed correct since the increased growth rate due to the addition of Ca^{2+} under salt stress canceled out the advantage of the Ev strain (Fig. 12H and 12I, right).

The results so far indicate that the growth conditions used here lack sufficient Ca^{2+} for maximum salt tolerance of the yeast cells, resulting in the isolation of genes that may compensate for the Ca^{2+} requirement by overexpression (or mutation). Incidentally, the growth rate assay was performed by introducing plasmids into fresh strains that had not experienced salt stress (Fig.12C).

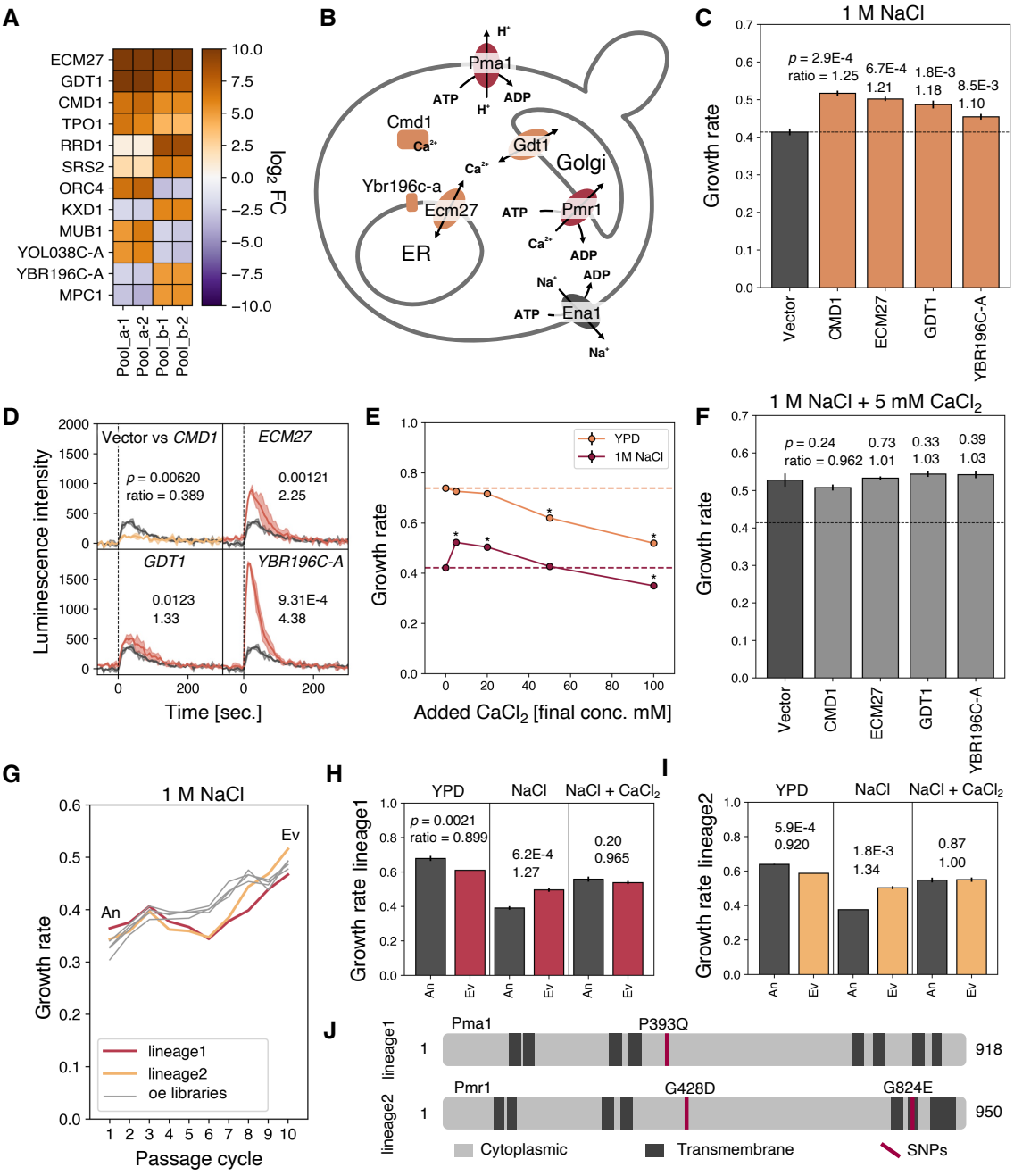
A
ECM27
GDT1
CMD1
TPO1
RRD1
SRS2
ORC4
KXD1
MUB1
YOL038C-A
YBR196C-A
MPC1
Pool_a-1
Pool_a-2
Pool_b-1
Pool_b-2
log2 FC
B
Pma1
ATP
ADP
Cmd1
Gdt1
Golgi
Ybr196c-a
Ecm27
ER
Pmr1
Ena1
C
1 M NaCl
Growth rate
p = 2.9E-4
ratio = 1.25
6.7E-4
1.21
1.8E-3
1.18
8.5E-3
1.10
Vector
CMD1
ECM27
GDT1
YBR196C-A
D
Vector vs CMD1
ECM27
p = 0.00620
ratio = 0.389
0.00121
2.25
GDT1
YBR196C-A
0.0123
1.33
9.31E-4
4.38
Luminescence intensity
Time [sec.]
E
YPD
1M NaCl
Growth rate
Added CaCl2 [final conc. mM]
F
1 M NaCl + 5 mM CaCl2
p = 0.24
ratio = 0.962
0.73
1.01
0.33
1.03
0.39
1.03
Growth rate
Vector
CMD1
ECM27
GDT1
YBR196C-A
G
1 M NaCl
Growth rate
An
Ev
lineage1
lineage2
oe libraries
Passage cycle
H
YPD
NaCl
NaCl + CaCl2
Growth rate lineage1
p = 0.0021
ratio = 0.899
6.2E-4
1.27
0.20
0.965
I
YPD
NaCl
NaCl + CaCl2
Growth rate lineage2
5.9E-4
0.920
1.8E-3
1.34
0.87
1.00
J
lineage1
Pma1
P393Q
1
918
lineage2
Pmr1
G428D
G824E
1
950
Cytoplasmic
Transmembrane
SNPs

Figure 12 GOFAs as well as adaptive mutants under salt stress, propose Ca^{2+} limitation in the culture medium. A) Genes whose DoE was ≥10,000 in at least one of four replicates under salt stress. Their DoE scores (log_{10} DoE) are shown with the darkness of the orange color. **B)** A cellular diagram illustrating protein functions in calcium homeostasis identified in this study. **C)** Growth rates of the cells overexpressing GOFAs under 1 M NaCl. **D)** The cytoplasmic Ca^{2+} pulses of the cells overexpressing GOFAs upon the salt stress measured by the aequorin luminescence assay. Grey lines show the empty vector as the control and orange lines show the target. The vertical dashed lines represent the timing of added NaCl. Each maximum value of luminescence intensity was used for Welch's t-test. **E)** The effect of $CaCl_2$ addition on growth rates of BY4741 with (red) or without 1 M NaCl (orange). The horizontal dashed lines show the growth rate of BY4741 in YPD (orange dash) or 1 M NaCl without adding $CaCl_2$ (red dash). Asterisks indicate significant differences. **F)** Growth rates of the cells overexpressing GOFAs under 1 M NaCl with 5 mM $CaCl_2$. The horizontal dashed line presents the empty vector control's growth rate without $CaCl_2$ addition (shown in C). **G)** Growth rates of overexpression libraries (oe libraries) and empty vector controls during the passages under salt stress. The linage1 (red) and linege2 (orange) of the vector controls and four replicates of overexpression libraries (grey) under 1 M NaCl are shown. For the vector control, the cells first inoculated were designated as "ancestor (An)" and the cells obtained after the 10th passage cycle as "evolved (Ev)". **H and I)** Growth rates of An and Ev cells of linege1 (H) and linege2 (I) under YPD (left), 1 M NaCl (middle), and 1 M NaCl with 5 mM $CaCl_2$ (right). **J)** Diagrams showing the amino acid substitutions in Pma1 and Pmr1 from the Ev lineage 1 and lineage 2. The dark grey areas indicate the transmembrane domains, and red bars indicate amino acid substitutions. The *p*-values are from Welch's t-test (n = 3). The significance was evaluated by the Bonferroni correction ($p \leq 0.05/4 = 0.0125$). Error bars or the filled areas indicate SD.

Table 5. Variants calling of lineage 1 and linage 2**.**

Lineage	#CHROM	POS	REF	ALT	Locus	Gene
lineage1	VII	481489	G	T	CDS	*PMA1*
lineage1	VI	11006	A	G	Intergenic DNA	
lineage2	VII	187995	C	T	CDS	*PMR1*
lineage2	VII	189183	C	T	CDS	*PMR1*
lineage2	VII	982396	A	G	Intergenic DNA	
lineage2	XI	589175	T	A	CDS	*TRZ1*

3.2.3 GOFAs reflect differences in yeast strains

I expected that previously reported genes such as *ENA1* and *HAL* genes were hit as GOFAs in the 1 M NaCl conditions. Still, these genes were not included in the hits I identified (Fig. 7G and 2A). Because *S. cerevisiae* varies greatly in salt tolerance among strains (Peter et al. 2018) (Fig. 13A), I speculated that strain–genetic background differences might reflect GOFAs.

To test this possibility, I analyzed the effect of Ca^{2+} on the salt tolerance of different *S. cerevisiae strains*; laboratory strains BY4741 (a derivative of S288C used so far), W303, and CEN.PK2-1C (CEN.PK) and a European wine strain, DBVP6765 (Fig. 14A). I also analyzed several other strains, as shown in Fig.13B. As reported, their salt tolerance without Ca^{2+} was quite different; under 1 M NaCl, DBVP6765 grew much slower than BY4741 and W303, and CEN.PK did not grow (Fig. 14A, 0 mM Ca^{2+}). Interestingly, adding Ca^{2+} dramatically improved the salt tolerance of DBVP6765 and CEN.PK; adding 5 mM Ca^{2+} nearly canceled the salt sensitivity of DBVP6765 compared to BY4741 and W303 (Fig. 14A) while adding up to 50 mM Ca^{2+} salt tolerance of CEN.PK increased gradually but significantly (Fig. 14A). Note that the addition of Ca^{2+} did not increase the growth rate of the strains without salt stress but decreased it (Fig. 13C-D). These results suggest that the differences in salt sensitivity of each strain may be explained by differences in Ca^{2+} requirements, which could potentially reflect differences in GOFAs. Therefore, I next attempted to identify the GOFAs of CEN.PK and DBVP6765 strains.

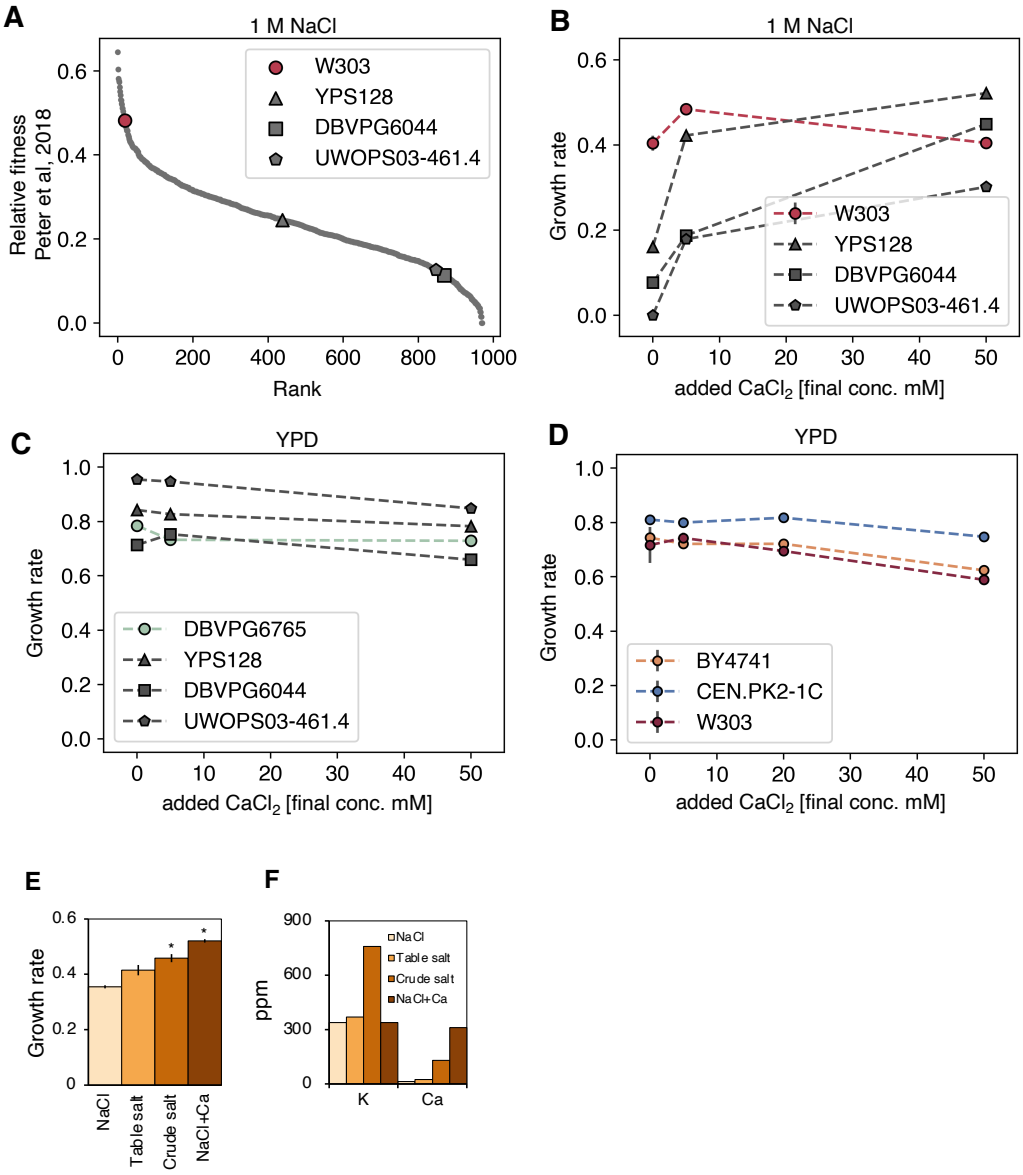
A
1 M NaCl
Relative fitness
Peter et al, 2018
Rank
W303
YPS128
DBVPG6044
UWOPS03-461.4
B
1 M NaCl
Growth rate
added CaCl2 [final conc. mM]
W303
YPS128
DBVPG6044
UWOPS03-461.4
C
YPD
Growth rate
added CaCl2 [final conc. mM]
DBVPG6765
YPS128
DBVPG6044
UWOPS03-461.4
D
YPD
Growth rate
added CaCl2 [final conc. mM]
BY4741
CEN.PK2-1C
W303
E
Growth rate
NaCl
Table salt
Crude salt
NaCl+Ca
F
ppm
NaCl
Table salt
Crude salt
NaCl+Ca
K
Ca

Figure 13. The addition of Ca^{2+} increased the growth rates of various strains under salt stress but did not without salt stress. A) Relative fitness of various strains; W303 (red, circle), YPD128 (triangle), DBVPG6044 (square), and UWOPS03-461.4 (pentagon), under 1M NaCl. The relative fitness data were from Peter et al. 2018. **B)** Relationship between the addition of $CaCl_2$ and growth rates of various strains under 1 M NaCl. The growth rate of UWOPS03-461.4 without $CaCl_2$ addition could not be defined but set to 0 for convenience. Three biological replicates were measured for W303. **C)** Relationship between the addition of $CaCl_2$ and growth rates of various strains under YPD. The green circles mean DBVPG6765's growth rates. **D)** Relationship between the addition of $CaCl_2$ and growth rates of various strains; BY4741 (orange), CEN.PK2-1C (blue), and W303 (red), under YPD. Error bars indicate SD (n = 3). There are no significant differences between adding Ca or not (Welch's t-test and Bonferroni correction ($p \leq 0.05/3$)).**E)** Growth rate of BY4741 under three salts: NaCl as an experiential reagent, a table salt, and a crude salt. NaCl+Ca means NaCl medium adding 5 mM $CaCl_2$. Asterisks indicate significant differences compared to NaCl (Welch's t-test and Bonferroni correction ($p \leq 0.05/3$)). **F)** K^+ and Ca^{2+} concentrations in the medium used in F. Na^+ concentrations in all mediums were adjusted to 23.0 g/l. Error bars indicate SD (n = 3).

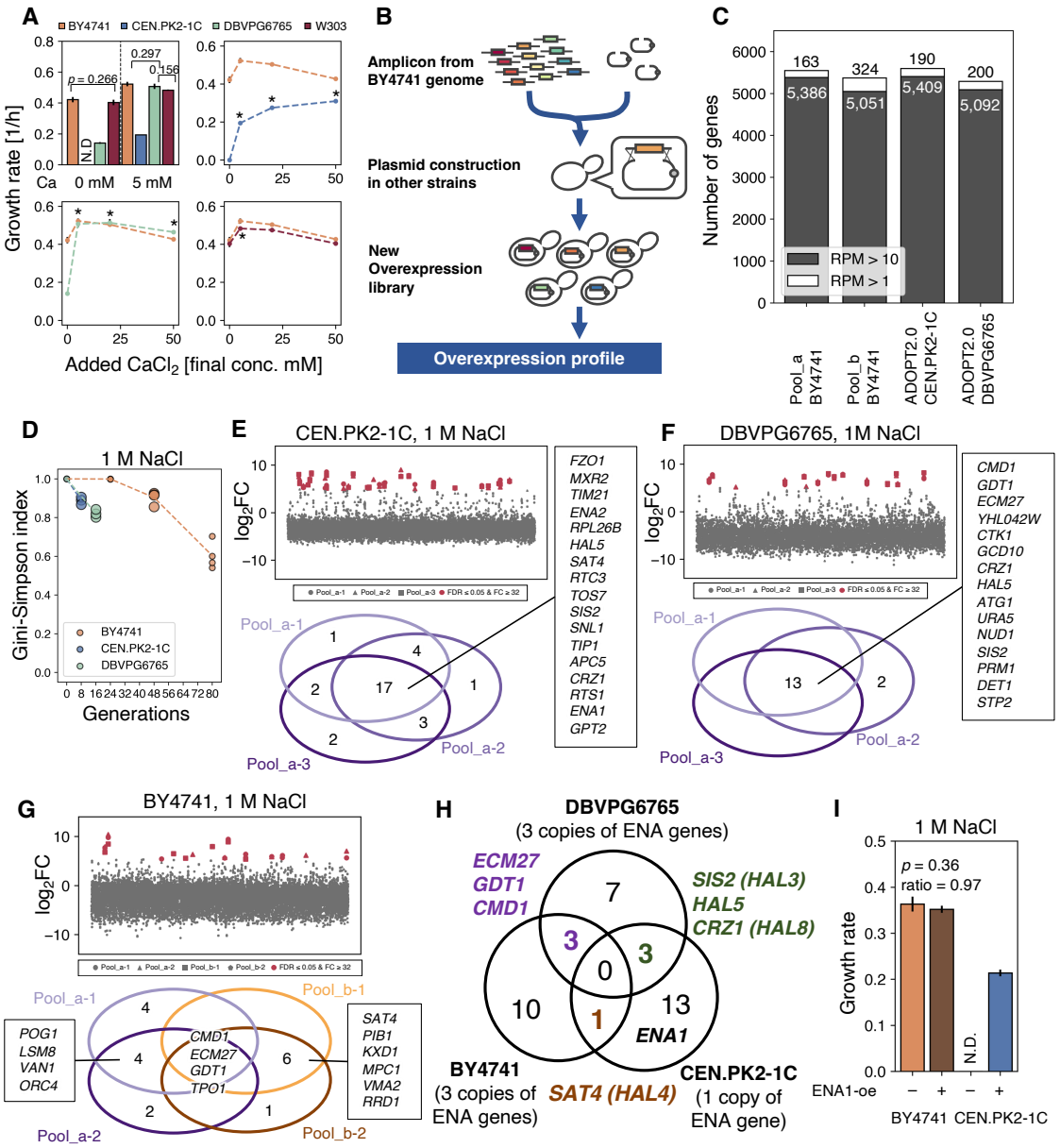
A
BY4741
CEN.PK2-1C
DBVPG6765
W303
Growth rate [1/h]
p = 0.266
0.297
0.156
N.D
Ca
0 mM
5 mM
Added CaCl2 [final conc. mM]
B
Amplicon from BY4741 genome
Plasmid construction in other strains
New Overexpression library
Overexpression profile
C
Number of genes
163
324
190
200
5,386
5,051
5,409
5,092
RPM > 10
RPM > 1
Pool_a BY4741
Pool_b BY4741
ADOPT2.0 CEN.PK2-1C
ADOPT2.0 DBVPG6765
D
1 M NaCl
Gini-Simpson index
BY4741
CEN.PK2-1C
DBVPG6765
Generations
E
CEN.PK2-1C, 1 M NaCl
log2FC
Pool_a-1
Pool_a-2
Pool_a-3
FDR ≤ 0.05 & FC ≥ 32
FZO1
MXR2
TIM21
ENA2
RPL26B
HAL5
SAT4
RTC3
TOS7
SIS2
SNL1
TIP1
APC5
CRZ1
RTS1
ENA1
GPT2
F
DBVPG6765, 1M NaCl
CMD1
GDT1
ECM27
YHL042W
CTK1
GCD10
CRZ1
HAL5
ATG1
URA5
NUD1
SIS2
PRM1
DET1
STP2
G
BY4741, 1 M NaCl
Pool_b-1
Pool_b-2
POG1
LSM8
VAN1
ORC4
CMD1
ECM27
GDT1
TPO1
SAT4
PIB1
KXD1
MPC1
VMA2
RRD1
H
DBVPG6765
(3 copies of ENA genes)
ECM27
GDT1
CMD1
SIS2 (HAL3)
HAL5
CRZ1 (HAL8)
BY4741
(3 copies of ENA genes)
SAT4 (HAL4)
CEN.PK2-1C
(1 copy of ENA gene)
ENA1
I
1 M NaCl
p = 0.36
ratio = 0.97
Growth rate
N.D.
ENA1-oe
BY4741
CEN.PK2-1C

Figure 14. GOFAs reflect differences in genetic backgrounds. A) Relationship between $CaCl_2$ addition and growth rates of various *S. cerevisiae* strains. Growth rates of BY4741 (orange), CEN.PK2-1C (blue), DBVPG6765 (green), and W303 (red), under 1M NaCl with added $CaCl_2$ are shown. The growth rate of CEN.PK2-1C without $CaCl_2$ addition could not be defined but set to 0 for convenience. The pairs without *p-value* indicate FDR ≤ 0,05 using by Welch's t-test and Benjamini-Hochberg method in the upper left panel. Asterisks mean significant difference against those without Ca^{2+} addition ($p \leq 0.05/4$). **B)** The new overexpression libraries constructed in this study. The detail is explained in the text. **C)** Coverages of the constructed libraries. The filled bars indicate RPM ≥ 10, and the unfilled bars indicate RPM ≥ 1. **D)** Decrease in the diversities of plasmids in the pooled libraries of CEN.PK2-1 (blue), DBVPG6756 (green), and BY4741 (orange), during the cultivation under salt stress. The diversity was evaluated as the Gini-Simpson index. The large circles indicate the data points used in H. **E-G)** Fold changes of plasmid occupancies after the cultivation (upper) and hit genes in each replicate 1 M NaCl (lower, FDR ≤ 0.05 and FC ≥ 2^5). Hit genes were shown as red-filled symbols. CEN.PK2-1C with 8 generations (E), DBVPG6765 with 16 generations (F), and BY4741 with 48 generations (G). The overexpression profiles of CEN.PK2-1C and DBVPG6765 were performed with three replicates originating from one pool, and BY4741 with four replicates. Hit Genes are summarized in Table S5. **H)** A Venn diagram showing overlaps of GOFAs in BY4741, DBVPG6765, and CEN.PK2-1C. Purpled genes are common to BY4741 and DBVPG6765, greened genes are common to CEN.PK2-1C and DBVPG6765, and browned gene, is common to BY4741 and CEN.PK2-1C. **I)** Growth rates of *ENA1-oe* in BY4741(oranges) and CEN.PK2-1C (blues) under salt stress. The *p*-values are from Welch's t-test (n = 3). Error bars represent SD (n = 3).

I then developed a scheme to transfer this plasmid library to other strains. I performed homologous recombination of a mixed PCR product containing the 5,803 genes of the BY4741 genome and 2μ plasmids in yeast cells (Fig. 14B). The constructed pooled libraries of CEN.PK and DBVPG6765 covered more than 5,000 genes (Fig. 14B and 14C). I performed the overexpression profiles of CEN.PK2-1C and DBVPG6765 with three replicates originating from one pool I newly constructed. Both of CEN.PK and DBVPG6765 pooled libraries grew faster and adapted more rapidly to salt stress than the vector control (Figure 15A). Because of faster growth than control, I considered some genes enriched and terminated the competitive culture after fewer generations than BY4741; CEN.PK2-1C was 8 generations and DBVPG6765 was 16 generations. Compared to BY4741, the diversity of the pool obtained by the Gini-Simpson index also decreased more quickly (Fig. 14D). I show hit genes in each strain in Fig. 14E-G. For a comparison of GOFAs across the strains, I considered genes hit in all three replicates as GOFAs in CEN.PK2-1C and DBVPG6765, and in two of four in BY4741, because of using two original pools. *SAT4* was one overlapping GOFA between BY4741 and CEN.PK (Fig. 14H, and Fig. 15B). CMD1, ECM27, and GDT1 overlapped between BY4741 and DBVPG6765. *HAL5, SIS2,* and *CRZ1*, which were previously reported as HAL genes, overlapped between CEN.PK2-1C and DBVPG6765. Particularly, *ENA1* was only identified as GOFAs in CEN.PK, and *ENA1-oe* in CEN.PK2-1C restored growth under 1 M NaCl but not in BY4741 (Fig. 14I). Thus, the differences in the genetic background could explain why these genes were not identified in the initial overexpression profile on BY4741. On the other hand, this overexpression profile with the construction of a new overexpression library could potentially reveal genetic background-dependent requirements.

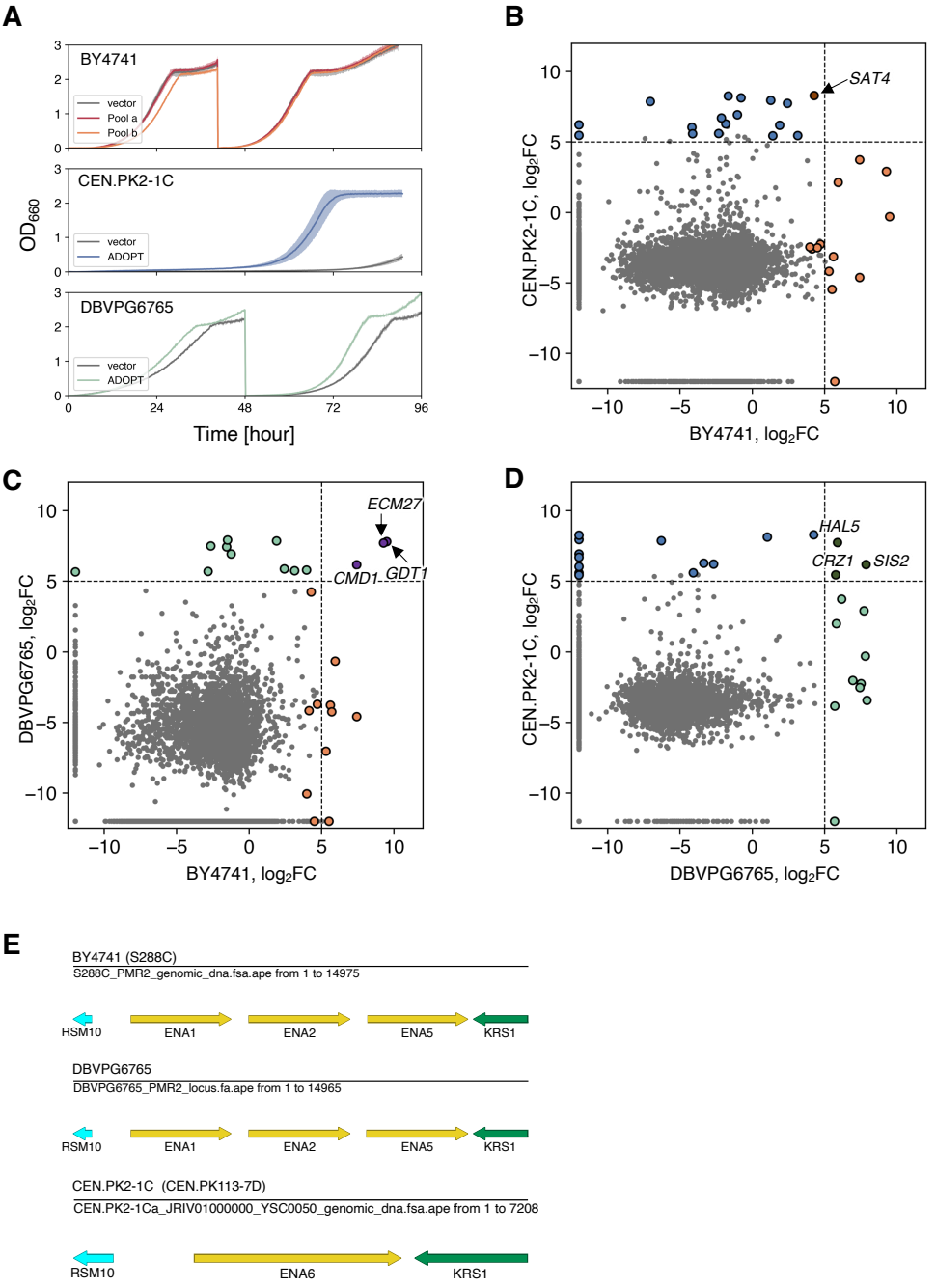
A
BY4741
vector
Pool a
Pool b
CEN.PK2-1C
vector
ADOPT
DBVPG6765
vector
ADOPT
OD660
Time [hour]
B
SAT4
CEN.PK2-1C, log2FC
BY4741, log2FC
C
ECM27
CMD1
GDT1
DBVPG6765, log2FC
BY4741, log2FC
D
HAL5
CRZ1
SIS2
CEN.PK2-1C, log2FC
DBVPG6765, log2FC
E
BY4741 (S288C)
S288C_PMR2_genomic_dna.fsa.ape from 1 to 14975
RSM10
ENA1
ENA2
ENA5
KRS1
DBVPG6765
DBVPG6765_PMR2_locus.fa.ape from 1 to 14965
RSM10
ENA1
ENA2
ENA5
KRS1
CEN.PK2-1C (CEN.PK113-7D)
CEN.PK2-1Ca_JRIV01000000_YSC0050_genomic_dna.fsa.ape from 1 to 7208
RSM10
ENA6
KRS1

Figure 15. Supplement to overexpression profiles of CEN.PK2-1C and DBVPG6765. A) Overexpresson libraries of CEN.PK2-1C (middle, blue) and DBVPG6765 (bottom, light green) grew faster than the vector controls and quickly adapted to the salt stress. The solid lines and the filled areas indicate the average of OD_{660} and the standard deviation (n = 3) responsively. The grey means the empty vector controls. The top panel shows the growth curves of overexpression libraries in BY4741 under salt stress. The red and orange correspond to replicates derived from Pool_a and Pool_b (each n = 2). **B-D)** Scatter plots show comparisons of the average FC; between (B) BY4741 and CEN.PK2-1C, (C) BY4741 and DBVPG6765, (D) DBVPG6765 and CEN.PK2-1C, under 1M NaCl. The orange, blue, and light green circles indicate GOFAs in BY4741, CEN.PK2-1C, and DBVPG6765, responsively. The brown, purple and green circles mean GOFAs in both BY4741 and CEN.PK2-1C, BY4741 and DBVPG6765, and CEN.PK2-1C and DBVPG6765. Genes with a FC of nan (undetected) have -15 added for convenience. The horizontal and vertical dashed lines indicate the threshold of GOFAs (FC $\geq 2^5$). **E)** Schematic diagram of PMR2 locus of BY4741, DBVPG6765, and CEN.PK2-1C.

3.2.4 GOFA reflects the factors that the strain requires in each environment

The salt sensitivity of CEN.PK has been explained by the weak expression of the *ENA* gene *ENA6* (Daran-Lapujade et al. 2009). BY4741 and DBVPG6765 have a cluster of three ENA genes, known as PMR2 locus(Wieland et al. 1995), but CEN.PK has only one ENA gene (Extended. Data. Fig. 6E, sequence data from(Yue et al. 2017; Engel et al. 2022; Song et al. 2015)). That may explain why *ENA1* was isolated as a GOFA (Fig. 14E and 14H). I examined how GOFAs are altered when sufficient *ENA* function is provided to CEN.PK by *ENA1-oe* since enhanced *ENA* function seems to be a primary genetic requirement for salt tolerance in CEN.PK. Therefore, I constructed a pooled library of diploid CEN.PK by crossing the pooled library of CEN.PK2-1C constructed in the *MATa* strain with the *ENA1*-overexpressing *MATα* strain (referred to as *ENA1-coe*) (see Fig. 16A and Figure. 17). I also constructed another co-overexpression library without *ENA1-oe* as a control (Figure. 17).

Fig. 16B shows the fold change of genes in the *ENA1-coe* pool after 16 generations under salt stress. Here, I considered genes hit in all three replicates as GOFAs. As expected, *ENA1-oe* altered GOFAs (Fig. 16C). *ENA1* itself, *CRZ1*, and *SIS2* were no longer GOFA, suggesting that their functions are directly related to *ENA* function. The calcium homeostasis gene, *ECM27*, became a GOFA, suggesting calcium is a secondary requirement for satisfactory *ENA* function. The most enriched GOFAs with and without *ENA1-oe* were *SAT4* and *HAL5*, which encode protein kinases that regulate K^+ importers (Mulet et al. 1999). Since these GOFAs were isolated independently from the enhanced *ENA* functions, I assumed that they proposed another requirement for CEN.PK other than *ENA1*, which should be potassium. To test this possibility, I analyzed salt tolerance by adding K^+ and found that CEN.PK could grow even under 1 M NaCl as previously reported(Illarionov, Lahtvee, and Kumar 2021) (Fig. 16D). The addition of K^+ also increased the

growth rate under *ENA1-oe*, and the addition of both K^+ and Ca^{2+} further increased the growth rate (Fig. 16D). These results confirm that K^+ is required for salt tolerance of CEN.PK, besides Ca^{2+} and enhanced *ENA* function.

These results strongly support the idea that GOFAs reflect factors that a given strain requires in each environment. Following this idea, the difference in salt-tolerant GOFAs between BY4741 (Fig. 7F and 14G) and CEN.PK (Fig. 14E and 16B) should reflect differences in Ca^{2+} and K^+ required for salt tolerance. Therefore, I measured the growth rates of BY4741 and CEN.PK under 1 M NaCl conditions at different Ca^{2+} and K^+ concentrations to illuminate their respective fitness landscapes. As expected, the fitness landscapes of BY4741 and CEN.PK were markedly different (Fig. 16E and 16F). Ca^{2+} requirements differed between BY4741 and CEN.PK (Fig. 16E and 16F); BY4741 grew maximally at 5 mM Ca^{2+}, while CEN.PK grew maximally at 50 mM Ca^{2+}. These requirements should be imitated by overexpression of *ECM27*, *GDT1*, and *CMD1* (imitating Ca^{2+} addition) in BY4741; *ENA1* and *ECM27* (imitating Ca^{2+} addition), *SAT4* and *HAL5* (imitating K^+ addition) in CEN.PK (Fig. 16G and Fig. 16H). I finally confirmed this idea for the Ca^{2+} requirement of CEN.PK; *ENA1-oe* and *ECN27-oe* additively conferred salt tolerance, but the effect was less pronounced when Ca^{2+} was added (Fig 16I and 16J).

Note that the Ca^{2+} and K^+ landscapes for salt tolerance may reflect the natural conditions of the yeast. That is, salts obtained from nature contain potassium and calcium, and when such salts were used, yeast growth was better than when pure NaCl was used (Fig. 13E and 13F). In other words, landscapes such as those in Figs. 16E and 16F are likely to be optimized for the salt composition of the living environment of each strain.

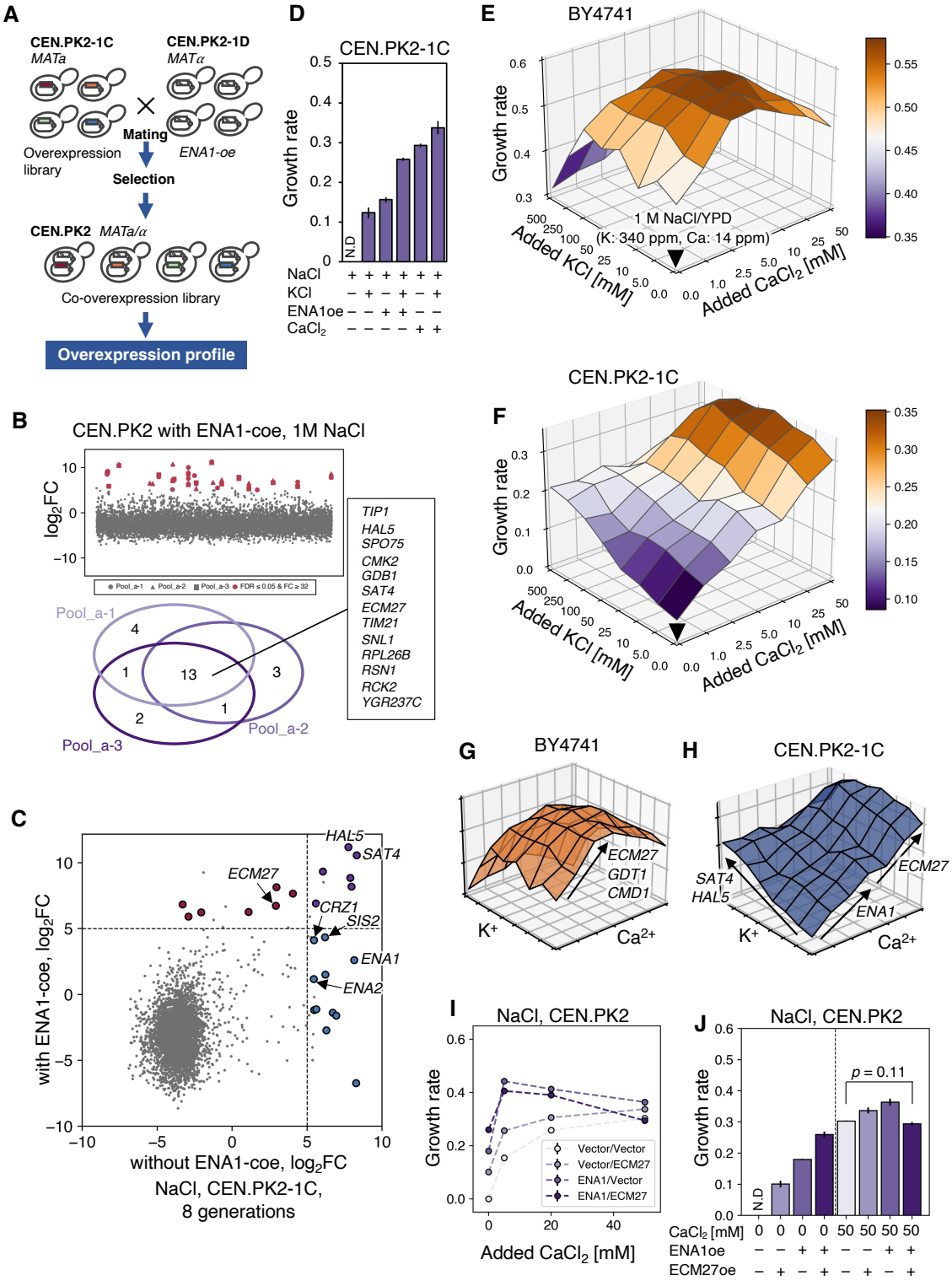

Figure 16. Strain-dependent requirements of calcium and potassium for the salt stress reflect strain-dependent GOFAs. A) Construction of the *ENA1* co-overexpression (*-coe*) library

by mating. The detail is explained in the text. **B)** Fold change of plasmid occupancy after the 16 generations in CEN.PK2 with *ENA1-oe* under 1 M NaCl (upper). Hit genes in each replicate under well-studied stresses (lower, FDR ≤ 0.05 and FC ≥ 2^5). These data are summarized in Table 6. **C)** A comparison of the Fold change of plasmid occupancy with and without *ENA1-coe* under 1 M NaCl. The colored circles indicate GOFAs: without *ENA1-coe* (blue), with *ENA1-coe* (red), and both (purple). The dash lines represent the threshold of GOFAs as FC ≥ 32. **D)** growth rates of CEN.PK2-1C under 1 M NaCl. N.D means not detected. Error bars indicate SD. All 15 pairs were significantly different (Welch's t-test and Benjamini-Hochberg correction), False Discovery Rate (*FDR* ≤ 0.05, n = 3). The value of N.D is set to 0 for the statistical test. **E-F)** Fitness landscapes of BY4741 (E) and CEN.PK2-1C (F) under 1 M NaCl with various KCl and $CaCl_2$ levels. The downward triangle points to 1 M NaCl/YPD, with increasing amounts of KCl or $CaCl_2$, added along the *x*- or *y*-axes. The growth rates at each KCl and $CaCl_2$ addition are represented as the *z*-axis and colored as a purple-to-orange heat map, corresponding to the relative growth rate. **G-H)** A diagram of the expected relationship between slopes on fitness landscapes and GOFAs in BY4741 (G) and CEN.PK2-C (H). Arrows indicate the correspondence between Ca^{2+} or K^+ requirement and each GOFA. **I and J)** Effects of $CaCl_2$ addition on the growth rates of CEN.PK cells overexpressing *ENA1* (*ENA1-oe*) and *ECM27* (*ECM27-oe*). *ENA1 and ECM27* were overexpressed using pTOW48036 and pRS423nz, respectively. The Vector/Vector cells without $CaCl_2$ addition did not grow but the growth rate was set to 0 for convenience in I and shown as N.D in J. Error bars indicate SD (n = 3). All 6 pairs with 0 mM $CaCl_2$ and 5 pairs with 50 mM $CaCl_2$ were significantly different (Welch's t-test and Benjamini-Hochberg correction), *FDR* ≤ 0.05, n = 3). A pair with no significance is shown in the figure. The value of N.D is set to 0 for the statistical test.

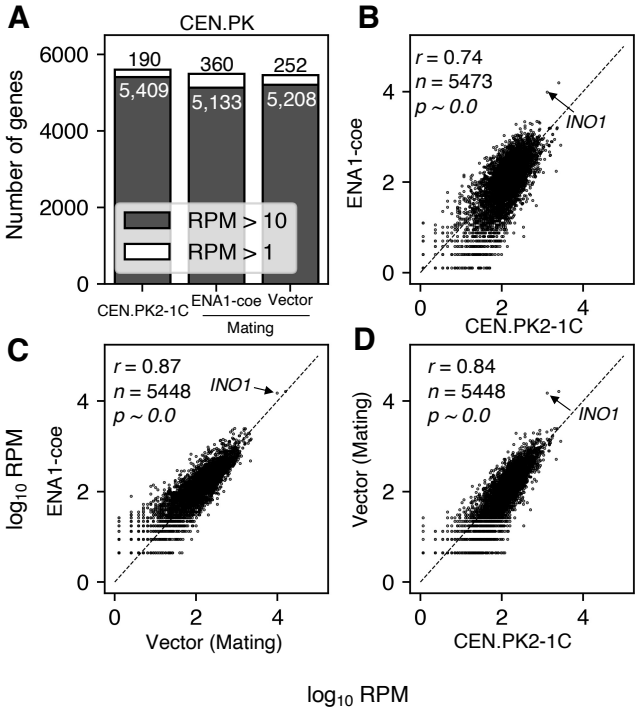

Figure 17. The quality check of the CEN.PK2-ENA1 co-overexpression library. A) CEN.PK2-ENA1 co-overexpression (-coe) libraries covered over 5,000 genes in CEN.PK. The filled and opened bars indicate RPM ≥ 10 and RPM ≥ 1. **B-C)** Scatter plots show comparisons of initial RPM between (B) CEN.PK2-1C and CEN.PK2-ENA1-coe, (C) CEN.PK2-ENA1-coe and Vector, and (D) CEN.PK2-1C and Vector. As an addendum, I found that *INO1* was enriched in these libraries during construction and might compensate for the lack of Inositol in the SC medium used in the selection (Hanscho et al. 2012).

Table 5 GOFAs in various strains under salt stress.

Systematic name	Standard name	BY4741	CEN.PK2-1C	DBVPG6765	CEN.PK+ENA1
YCR008W	SAT4	GOFA	GOFA		GOFA
YJR106W	ECM27	GOFA		GOFA	GOFA
YBR109C	CMD1	GOFA		GOFA	
YBR187W	GDT1	GOFA		GOFA	
YBR127C	VMA2	GOFA			
YDR313C	PIB1	GOFA			
YGL079W	KXD1	GOFA			
YGL080W	MPC1	GOFA			
YIL122W	POG1	GOFA			
YIL153W	RRD1	GOFA			
YJR022W	LSM8	GOFA			
YLL028W	TPO1	GOFA			
YML115C	VAN1	GOFA			
YPR162C	ORC4	GOFA			
YJL165C	HAL5		GOFA	GOFA	GOFA
YKR072C	SIS2		GOFA	GOFA	
YNL027W	CRZ1		GOFA	GOFA	
YBR067C	TIP1		GOFA		GOFA
YGR033C	TIM21		GOFA		GOFA
YGR034W	RPL26B		GOFA		GOFA
YIL016W	SNL1		GOFA		GOFA
YBR179C	FZO1		GOFA		
YCL033C	MXR2		GOFA		
YDR039C	ENA2		GOFA		
YDR040C	ENA1		GOFA		
YHR087W	RTC3		GOFA		
YOL019W	TOS7		GOFA		
YOR014W	RTS1		GOFA		
YOR249C	APC5		GOFA		
YKR067W	GPT2		GOFA		
YDR051C	DET1			GOFA	
YGL180W	ATG1			GOFA	
YHL042W	YHL042W			GOFA	
YKL139W	CTK1			GOFA	
YML106W	URA5			GOFA	
YNL062C	GCD10			GOFA	
YNL279W	PRM1			GOFA	
YOR373W	NUD1			GOFA	
YGR237C	YGR237C				GOFA
YLL005C	SPO75				GOFA
YLR248W	RCK2				GOFA
YMR266W	RSN1				GOFA
YOL016C	CMK2				GOFA
YPR184W	GDB1				GOFA

*I considered genes hit in all three replicates as GOFAs in CEN.PK2-1C and DBVPG6765, and in two of four in BY4741

3.2.5 Mitochondria appear to be the primary target for enhanced salt tolerance with calcium addition

Salt tolerance in *S. cerevisiae* has been explained as the induction of *ENA* genes by the calcium pulse (Cyert and Philpott 2013) (Fig.18A). However, in BY4741, Ca^{2+} addition did not enhance Ena1 protein level under 1 M NaCl (Fig. 19A); and *ENA1-oe* did not improve salt tolerance (Fig. 14I). Furthermore, Ca^{2+} addition restored growth retardation even after 15 hours of salt stress exposure (Fig. 18B-D). In contrast, prior Ca^{2+} addition did not improve growth (Fig. 18E). Even deletion mutants of *CNB1* and *CRZ1*, which are involved in the Ca-dependent *ENA1* induction pathway, recovered their growth rate upon Ca^{2+} addition (Fig. 18A and 18F). Therefore, the induction of the *ENA* gene by short-term calcium pulse itself does not fully explain the positive effect of Ca^{2+} addition on the salt tolerance of BY4741.

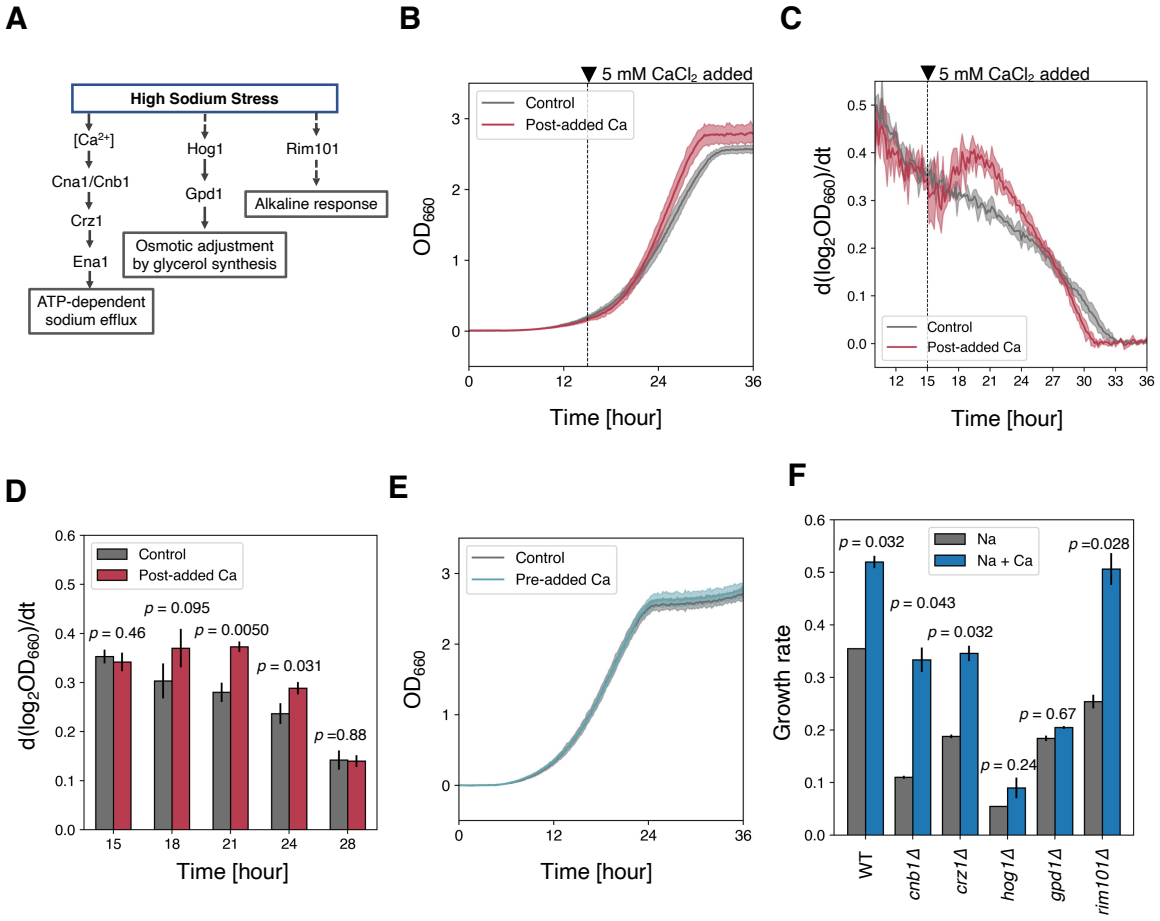

Figure 18. The effects of calcium addition alone cannot be explained by short-term stress response enhancement. A) A scheme of major responses to salt stress. B-D) Growth of BY4741 under salt stress with $CaCl_2$ added after salt stress exposure. **B-D)** The growth curves of BY4741 under 1 M NaCl (grey) and post-added 5 mM $CaCl_2$ at 15 hours later (red). (C) Instantaneous growth rates per hour and (D) their comparison at every 3 hours. The vertical dashed line means the timing of $CaCl_2$ addition. The filled areas and error bars indicate SD (n = 3). The *p*-values are from Welch's t-test. **E)** The growth curves of BY4741 under 1 M NaCl (grey) and pre-added 5 mM $CaCl_2$ at pre-cultivation (green). The filled areas indicate SD (n = 3). **F)** Growth rates of knockouts related to major responses to salt stress. The grey and blue bars indicate growth rates under 1 M NaCl with/without 5 mM $CaCal_2$ responsively. Error bars indicate SD (n = 2). The *p*-values are from two-tailed Welch's t-test (n = 2).

To elucidate the unknown Ca-induced salt tolerance mechanism, I used a complementary approach to overexpression profile: functional profiling of gene knockout mutants. The pooled knockout collection (Giaever et al. 2002) was competitively cultured and subjected to relative fitness analysis under three conditions (no salt, 1 M NaCl (Na), 1 M NaCl with 5 mM $CaCl_2$ (Na/Ca)) to systematically assess gene contribution (Fig. 19B). The salt tolerance of knockout mutants involved in the assumed Ca-dependent mechanism should not be enhanced even by Ca^{2+} addition; in other words, the relative fitness should be lower under Na/Ca conditions than in Na conditions (indicated by the blue dots in Fig. 19C). I isolated 296 genes with lower relative fitness in the Na/Ca environment compared to Na ($FDR \leq 0.05$, $\Delta Z \leq -1$) and found that they were enriched in the GO terms "mitochondria-related genes" and "ribosome" (Fig. 19D, Table 7).

I thus focused on the knockout strains of mitochondrial (Mito) genes. First, we examined the salt tolerance of the knockout mutants of the Mito genes and noticed their interesting behaviors; one group of Mito genes constituted a distinctly separated group with improved salt tolerance ($Z_{Na} - Z_{YPD} \geq 1$, Group I Mito. genes, Fig. 19E). They appear to be salt tolerant, but this is not the case. The reasons for this can be explained as follows: (1) Under non-stress conditions, these mutants have poor relative fitness (Z_{YPD}) due to their poorer proliferation than other mutants (Fig. 19F and Fig. 20A, YPD). (2) Conversely, under salt stress, these mutants do not change their proliferation (already impaired), while most other mutants proliferate poorly. Their relative fitness (Z_{Na}) is thus the same as the other mutations (Fig. 19F and Fig. 20A, YPD). (3) The change in relative fitness between Z_{Na} and Z_{YPD} makes these mutants appear salt tolerant (Fig 19E). Ca^{2+} addition reduced their relative fitness (Z_{NaCa}) because they did not respond to Ca^{2+}, whereas the other mutants did (Fig. 19F and Fig. 20A, Na/Ca, and 19H). In summary, the knockout mutants of the Groupe I Mito genes grow slowly under non-stress conditions, but their growth is unchanged under salt

stress, and they do not respond to Ca^{2+} addition. Therefore, their normal function should be attacked by salt stress and restored by Ca^{2+} addition. We also noticed that some mito genes ($Z_{Na} - Z_{YPD} \leq -1$, Group II Mito. genes) showed the opposite behavior to the Group I mito genes (Fig. 19E-H). Group II's growth is normal under non-stress conditions, but their growth is strongly attenuated under salt stress, and they normally respond to Ca^{2+} addition (Fig. 19F and Fig. 20A). Thus, their normal function should protect the cells from salt stress, but when Ca^{2+} is sufficient, their protective function is not necessary.

I next characterized the Group I and II Mito genes in detail. Interestingly, the molecular functions of the proteins encoded in Group I and II were clearly separated between complex II and ubiquinone (UQ) of the mitochondrial respiratory chain (Fig. 19I and J). From this, I speculated that salt stress causes respiratory chain dysfunction (perhaps a process later than UQ), which is restored by Ca^{2+} addition. I thus observed mitochondria with Tim50-Gfp as a mitochondrial localization tag and a staining reagent that reacts with reactive oxygen species (ROS) under salt stress with and without Ca2+ using by the fluorescence microscope **(**Fig. 19K**).** As a result, mitochondria were more developed and generated more ROS under salt stress, while the addition of Ca^{2+} maintained mitochondrial development but suppressed ROS generation. Taken together, I concluded that our assumed Ca^{2+}-dependent salt tolerance mechanism is related to mitochondrial function. Because of the high energy demand under salt stress (Olz et al. 1993), yeast cells probably need more productive mitochondrial function. As a result, high concentrations of ROS are generated, causing growth defects, which may be suppressed by the addition of Ca^{2+}.

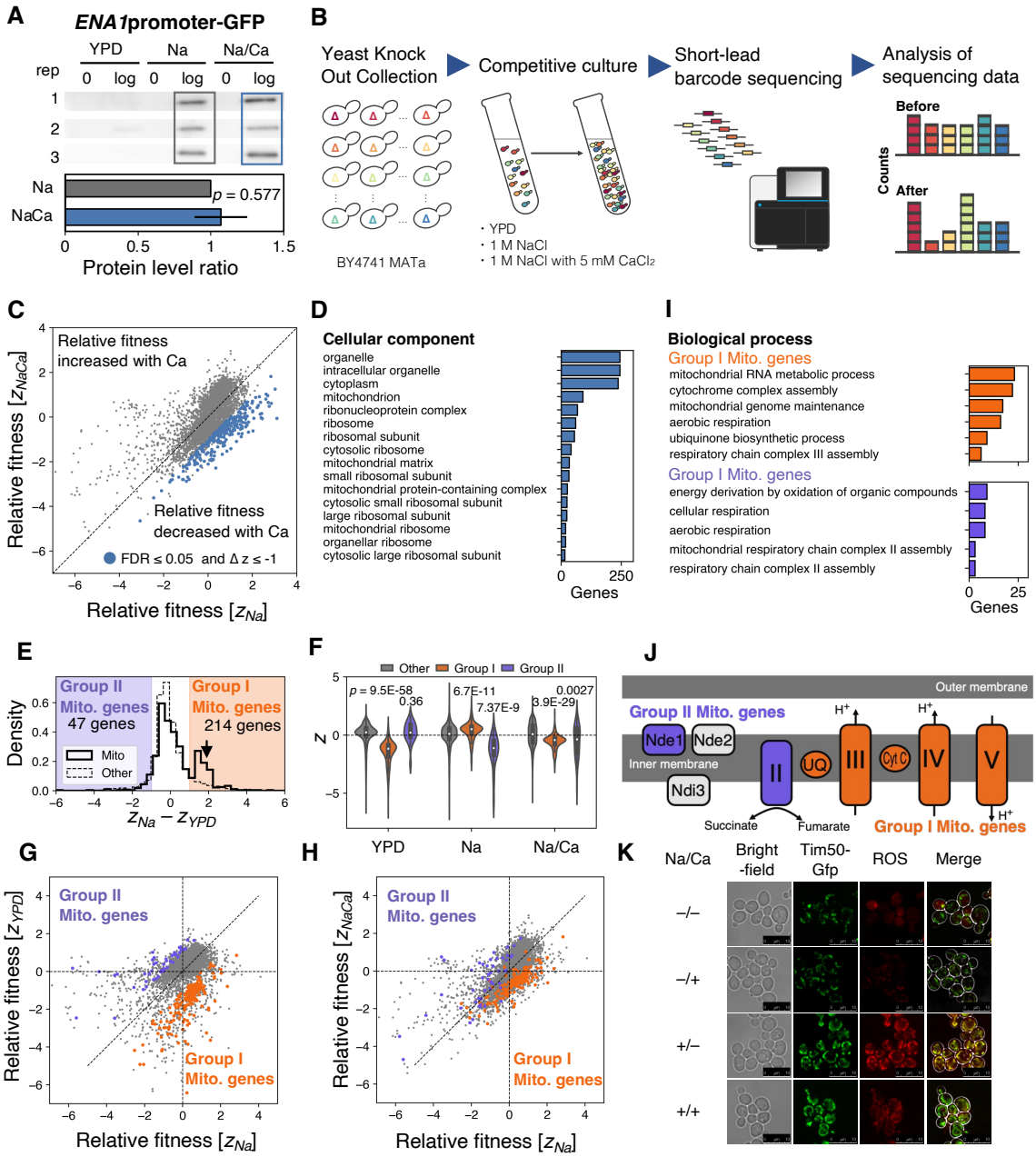
A
ENA1promoter-GFP
YPD
Na
Na/Ca
rep
0
log
0
log
0
log
1
2
3
Na
NaCa
p = 0.577
0
0.5
1
1.5
Protein level ratio
B
Yeast Knock Out Collection
Competitive culture
Short-lead barcode sequencing
Analysis of sequencing data
BY4741 MATa
YPD
1 M NaCl
1 M NaCl with 5 mM CaCl2
Before
After
Counts
C
Relative fitness increased with Ca
Relative fitness decreased with Ca
FDR ≤ 0.05 and Δ z ≤ -1
Relative fitness [zNaCa]
Relative fitness [zNa]
D
Cellular component
organelle
intracellular organelle
cytoplasm
mitochondrion
ribonucleoprotein complex
ribosome
ribosomal subunit
cytosolic ribosome
mitochondrial matrix
small ribosomal subunit
mitochondrial protein-containing complex
cytosolic small ribosomal subunit
large ribosomal subunit
mitochondrial ribosome
organellar ribosome
cytosolic large ribosomal subunit
0
250
Genes
I
Biological process
Group I Mito. genes
mitochondrial RNA metabolic process
cytochrome complex assembly
mitochondrial genome maintenance
aerobic respiration
ubiquinone biosynthetic process
respiratory chain complex III assembly
Group I Mito. genes
energy derivation by oxidation of organic compounds
cellular respiration
aerobic respiration
mitochondrial respiratory chain complex II assembly
respiratory chain complex II assembly
0
25
Genes
E
Group II Mito. genes
47 genes
Group I Mito. genes
214 genes
Mito
Other
Density
zNa − zYPD
F
Other
Group I
Group II
p = 9.5E-58
0.36
6.7E-11
7.37E-9
0.0027
3.9E-29
z
YPD
Na
Na/Ca
J
Outer membrane
Group II Mito. genes
Nde1
Nde2
Inner membrane
Ndi3
II
UQ
III
Cyt C
IV
V
H+
Succinate
Fumarate
Group I Mito. genes
G
Group II Mito. genes
Group I Mito. genes
Relative fitness [zYPD]
Relative fitness [zNa]
H
Group II Mito. genes
Group I Mito. genes
Relative fitness [zNaCa]
Relative fitness [zNa]
K
Na/Ca
Bright -field
Tim50-Gfp
ROS
Merge
−/−
−/+
+/−
+/+

Figure 19. Mitochondria seem to be a prime target of enhanced salt tolerance by adding calcium. A) Expression of *ENA1* under the salt stress was not enhanced by $CaCl_2$ addition. The *ENA1* promoter activity was detected by the Western blotting of EGFP under the control of the *ENA1* promoter under three conditions: YPD, 1 M NaCl (Na), and 1 M NaCl with 5 mM $CaCl_2$/YPD (Na/Ca). The lower panel shows the EGFP level in Na/Ca relative to Na during the logarithmic growth phase. The error bar indicates the SD of relative values (n = 3). The *p*-value was calculated using Welch's t-test. **B)** A scheme of systematic analysis for relative fitness of gene knockouts. The detail is explained in the text. **C)** Comparing relative knockouts' fitness (Z) between Na and Na/Ca. The blue cycles indicate knockouts with reduced fitness ($FDR \leq 0.05$ and $\Delta Z \leq 1$, Welch's t-test and the Benjamini-Hochberg correction), n = 3). **D)** Enriched gene ontology (GO) terms in "cellular component" in the 296 knockouts with reduced fitness under Na/Ca ($p \leq 0.05$, Holm-Bonferroni correction). The bar plot shows the number of genes with indicated GO terms. Other categories of enriched GO terms are shown in Table S6. **E)** The distribution of fitness was corrected by YPD ($Z_{Na} - Z_{YPD}$). The solid and the dashed line indicate mitochondria (Mito) genes and the other genes, respectively. The orange area represents Group I Mito. genes ($Z_{Na} - Z_{YPD} \geq 1$), and the purple area means Group II Mito. genes ($Z_{Na} - Z_{YPD} \leq -1$). **F)** The distribution of relative knockouts' fitness of Group I (orange), Group II (purple), and the others (grey, 4,052 genes) under each condition. The *p*-values are from Welch's t-test by comparison with Other. **G-H)** Comparisons of relative knockouts' fitness between Na versus YPD (G) and Na versus Na/Ca (H). The purple and the orange cycles indicate the knockouts belonging to Group I and Group II, respectively. The vertical and horizontal dashed line means $Z = 0$. **I)** Enriched GO terms in "biological function" of the knockouts belonging to Group I (upper, orange) and Group II (bottom, purple) ($p \leq 0.05$, Holm-Bonferroni correction). A complete set of enriched GO terms are shown in Table 8. **J)** The Group I and Group II Mito. genes have separated functions in the mitochondrial respiratory chain. The diagram shows the mitochondrial respiratory chain in which complexes or proteins within Group I and Group II Mito. genes were colored orange and purple, respectively. **K)** Microscopic images of the cells with the mitochondria and their reactive oxygen species (ROS) level under four conditions. Plus, or minus of "Na" indicate YPD with or without 1 M NaCl, and plus or minus of "Ca" indicates with or without 5 mM $CaCl_2$. The green color shows mitochondria inner membrane observed with Tim50-GFP. The red color indicates the mitochondrial ROS level stained by MitoTracker™ Red CM-H2Xros.

Table 7 GO terms enriched in relative fitness decreased KO strains with Ca

Biological process	*Holm-Bonferroni correction	
GO term	P-values	GOID
cytoplasmic translation	4.77E-12	GO:0002181
ribosomal small subunit biogenesis	3.29E-08	GO:0042274
peptide metabolic process	4.53E-08	GO:0006518
translational elongation	5.09E-08	GO:0006414
translation	8.33E-08	GO:0006412
peptide biosynthetic process	1.07E-07	GO:0043043
amide biosynthetic process	2.76E-07	GO:0043604
cellular macromolecule biosynthetic process	3.21E-07	GO:0034645
mitochondrial gene expression	3.32E-07	GO:0140053
cellular amide metabolic process	7.39E-07	GO:0043603
protein metabolic process	0.00000323	GO:0019538
mitochondrial translation	0.0000116	GO:0032543
organonitrogen compound biosynthetic process	0.0000541	GO:1901566
organonitrogen compound metabolic process	0.000187	GO:1901564
cellular macromolecule metabolic process	0.000411	GO:0044260
ribosomal small subunit assembly	0.000426	GO:0000028
ribosome biogenesis	0.004932	GO:0042254
gene expression	0.005703	GO:0010467
ribonucleoprotein complex biogenesis	0.008285	GO:0022613
maturation of SSU-rRNA	0.009097	GO:0030490
biosynthetic process	0.011366	GO:0009058
cellular metabolic process	0.011653	GO:0044237
cellular biosynthetic process	0.012496	GO:0044249
macromolecule biosynthetic process	0.017142	GO:0009059
organic substance biosynthetic process	0.024827	GO:1901576
ribosome assembly	0.047076	GO:0042255
Cellular component		
GO term	P-values	GOID
ribosome	2.64E-25	GO:0005840
ribosomal subunit	5.61E-23	GO:0044391
cytosolic ribosome	3.86E-18	GO:0022626
small ribosomal subunit	3.32E-17	GO:0015935
cytosolic small ribosomal subunit	2.07E-14	GO:0022627
ribonucleoprotein complex	4.23E-09	GO:1990904
mitochondrial matrix	0.00000223	GO:0005759
large ribosomal subunit	0.0000321	GO:0015934
intracellular organelle	0.000036	GO:0043229
organelle	0.0000383	GO:0043226
organellar ribosome	0.0000408	GO:0000313
mitochondrial ribosome	0.0000408	GO:0005761
mitochondrion	0.000111	GO:0005739
cytoplasm	0.001352	GO:0005737
mitochondrial protein-containing complex	0.004225	GO:0098798
cytosolic large ribosomal subunit	0.009552	GO:0022625
Molecular function		
GO term	P-values	GOID
structural constituent of ribosome	1.60E-22	GO:0003735
structural molecule activity	1.86E-15	GO:0005198

To confirm the adverse effects of salt stress on mitochondria, we investigated salt stress-induced transcriptome changes (RNA-seq) in the vector control and *CMD1-oe, ECM27-oe*, and *GDT1-oe*. The gene groups whose expression levels were significantly upregulated under salt stress conditions included "response oxidative stress (GO:0006979)", and "arginine biosynthetic process (GO:0006526)" (Fig. 20B). Under salt stress conditions, arginine uptake was significantly reduced by 20% (Fig. 20C). Since arginine synthesis is closely related to mitochondrial function (Vowinckel et al. 2021) (Fig. 20D), we speculated that the elevated expression of these genes might be due to mitochondrial dysfunction under salt stress, which results in a reduction in arginine synthesis. In fact, the expression of these groups of arginine synthesis genes was commonly suppressed by *CMD1-oe*, *ECM27-oe*, and *GDT1-oe* (Fig. 20E). These results are consistent with our idea that mitochondrial function is impaired under salt stress but is restored when calcium is supplied.

A

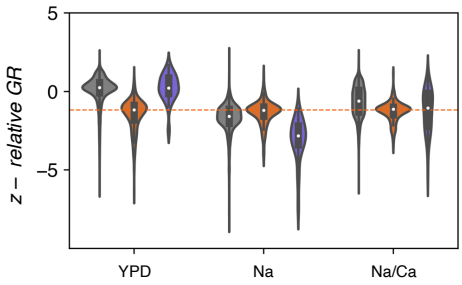

B

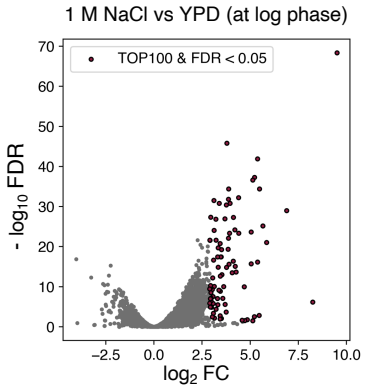

Biological process	GOID	Match
response to oxidative stress	GO:0006979	9/88
arginine biosynthetic process	GO:0006526	4/88
cellular response to chemical stress	GO:0062197	9/88
cellular response to oxidative stress	GO: 0034599	8/11
Cellular component	**GOID**	**Match**
-	-	-
Molecular function	**GOID**	**Match**
-	-	-

C

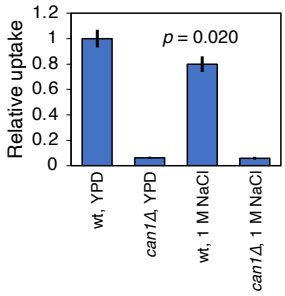

D

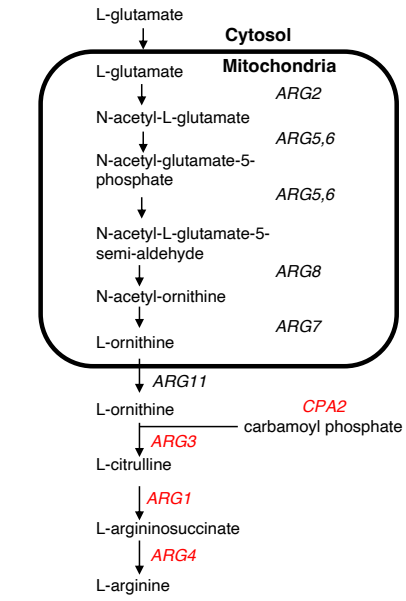

E

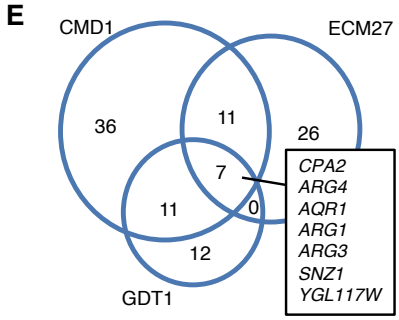

Figure 20. Transcriptome analysis of cells under salt stress obtained by RNAseq analysis. **A)** Relative fitness distribution when the growth rates in each condition were subtracted from Fig. 5F. **B)** Transcriptome changes in 1 M NaCl and YPD at log growth phase. ORFs with the top 100 most enormous fold changes and significant changes (*FDR* ≤ 0.05) compared with YPD are highlighted. Gene ontology terms enriched in highlighted ORFs are shown in the left table. **C)** Arginine intake assay under YPD and 1 M NaCl. The *p*-values are from Welch's t-test (n = 3). The error bars indicate SD. **D)** Scheme showing arginine synthesis pathway in *S. cerevisiae.* Red-colored genes were upregulated under 1 M NaCl and downregulated in GOFA's overexpression stains. **E)** Venn diagram showing downregulated genes (*FDR* ≤ 0.05) in GOFA's overexpression stains. These data are summarized in Table 9.

Table 8 GO terms enriched in Group I and II mito genes.

▪ **Group I mito genes**		
Biological process	*Holm-Bonferroni correction	
GO term	P-values	GOID
mitochondrial gene expression	5.46E-74	GO:0140053
mitochondrial translation	1.52E-61	GO:0032543
mitochondrion organization	7.92E-23	GO:0007005
peptide metabolic process	1.61E-20	GO:0006518
cellular amide metabolic process	1.55E-19	GO:0043603
translation	1.16E-18	GO:0006412
peptide biosynthetic process	1.65E-18	GO:0043043
amide biosynthetic process	4.82E-18	GO:0043604
mitochondrial RNA metabolic process	7.04E-18	GO:0000959
cytochrome complex assembly	2.88E-17	GO:0017004
mitochondrial respiratory chain complex assembly	4.53E-17	GO:0033108
cellular macromolecule biosynthetic process	1.53E-13	GO:0034645
translational elongation	1.76E-12	GO:0006414
organonitrogen compound biosynthetic process	3.12E-12	GO:1901566
mitochondrial genome maintenance	1.26E-09	GO:0000002
respiratory chain complex IV assembly	2.58E-09	GO:0008535
mitochondrial cytochrome c oxidase assembly	2.58E-09	GO:0033617
regulation of mitochondrial gene expression	1.77E-08	GO:0062125
regulation of mitochondrial translation	1.31E-07	GO:0070129
mitochondrial RNA processing	1.50E-07	GO:0000963
positive regulation of mitochondrial translation	9.52E-07	GO:0070131
gene expression	4.83305E-06	GO:0010467
ubiquinone metabolic process	5.09504E-06	GO:0006743
ubiquinone biosynthetic process	5.09504E-06	GO:0006744
ketone biosynthetic process	5.09504E-06	GO:0042181
quinone metabolic process	5.09504E-06	GO:1901661
quinone biosynthetic process	5.09504E-06	GO:1901663
amino acid activation	6.03399E-06	GO:0043038
tRNA aminoacylation	6.03399E-06	GO:0043039
tRNA aminoacylation for mitochondrial protein translation	3.87702E-05	GO:0070127
organic substance biosynthetic process	6.33634E-05	GO:1901576
protein metabolic process	6.64108E-05	GO:0019538
biosynthetic process	0.000100112	GO:0009058
organonitrogen compound metabolic process	0.00012399	GO:1901564
cellular biosynthetic process	0.000170538	GO:0044249
cellular nitrogen compound biosynthetic process	0.000567047	GO:0044271
mitochondrial protein processing	0.000619214	GO:0034982
aerobic respiration	0.001972006	GO:0009060
respiratory chain complex III assembly	0.002248328	GO:0017062
mitochondrial respiratory chain complex III assembly	0.002248328	GO:0034551
tRNA aminoacylation for protein translation	0.002856196	GO:0006418
cellular respiration	0.00482937	GO:0045333
cellular macromolecule metabolic process	0.006173706	GO:0044260
mitochondrial tRNA processing	0.009284164	GO:0090646
protein maturation	0.01078275	GO:0051604
cellular nitrogen compound metabolic process	0.020024756	GO:0034641
mitochondrial DNA replication	0.044811406	GO:0006264
mitochondrial tRNA 5'-end processing	0.044811406	GO:0097745
metabolic process	0.044811576	GO:0008152

Cellular component		
GO term	P-values	GOID
mitochondrion	2.97E-154	GO:0005739
mitochondrial matrix	3.30E-68	GO:0005759
mitochondrial protein-containing complex	6.20E-58	GO:0098798
organellar ribosome	8.28E-50	GO:0000313
mitochondrial ribosome	8.28E-50	GO:0005761
mitochondrial envelope	4.45E-48	GO:0005740
mitochondrial membrane	1.17E-46	GO:0031966
mitochondrial inner membrane	8.77E-46	GO:0005743
organelle inner membrane	1.37E-43	GO:0019866
organelle envelope	1.54E-37	GO:0031967
envelope	1.54E-37	GO:0031975
intracellular membrane-bounded organelle	6.40E-28	GO:0043231
membrane-bounded organelle	7.38E-28	GO:0043227
organellar large ribosomal subunit	1.15E-26	GO:0000315
mitochondrial large ribosomal subunit	1.15E-26	GO:0005762
ribosome	1.84E-25	GO:0005840
cytoplasm	1.26E-23	GO:0005737
ribosomal subunit	1.29E-22	GO:0044391
membrane-enclosed lumen	2.62E-22	GO:0031974
organelle lumen	2.62E-22	GO:0043233
intracellular organelle lumen	2.62E-22	GO:0070013
intracellular organelle	7.31E-22	GO:0043229
organelle	7.99E-22	GO:0043226
membrane	6.11E-20	GO:0016020
organellar small ribosomal subunit	5.70E-16	GO:0000314
mitochondrial small ribosomal subunit	5.70E-16	GO:0005763
extrinsic component of mitochondrial inner membrane	2.05E-15	GO:0031314
large ribosomal subunit	1.83E-11	GO:0015934
extrinsic component of organelle membrane	1.40E-10	GO:0031312
organelle membrane	1.82E-09	GO:0031090
small ribosomal subunit	1.02E-08	GO:0015935
intracellular anatomical structure	3.83E-07	GO:0005622
inner mitochondrial membrane protein complex	2.80982E-06	GO:0098800
extrinsic component of membrane	3.45359E-06	GO:0019898
intrinsic component of mitochondrial membrane	4.74523E-06	GO:0098573
ribonucleoprotein complex	1.96387E-05	GO:1990904
matrix side of mitochondrial inner membrane	4.33349E-05	GO:0099617
mitochondrial intermembrane space	5.22369E-05	GO:0005758
integral component of mitochondrial membrane	0.000110646	GO:0032592
organelle envelope lumen	0.000132286	GO:0031970
lumenal side of membrane	0.000251825	GO:0098576
cytochrome complex	0.002674004	GO:0070069
intrinsic component of mitochondrial inner membrane	0.002829441	GO:0031304
mitochondrial respiratory chain complex III	0.009428982	GO:0005750
respiratory chain complex III	0.009428982	GO:0045275
respiratory chain complex	0.016426413	GO:0098803
mitochondrial respirasome	0.020489734	GO:0005746
nucleoid	0.030162544	GO:0009295
mitochondrial nucleoid	0.030162544	GO:0042645
glutamyl-tRNA(Gln) amidotransferase complex	0.038383922	GO:0030956
mitochondrial inner membrane peptidase complex	0.038383922	GO:0042720

Molecular function		
GO term	P-values	GOID
structural constituent of ribosome	8.54E-21	GO:0003735
structural molecule activity	3.64E-12	GO:0005198
ligase activity	2.95415E-06	GO:0016874
aminoacyl-tRNA ligase activity	0.001976613	GO:0004812
ligase activity, forming carbon-oxygen bonds	0.001976613	GO:0016875
oxidoreduction-driven active transmembrane transporter act	0.012302113	GO:0015453
ubiquinol-cytochrome-c reductase activity	0.043420933	GO:0008121
oxidoreductase activity, acting on diphenols and related subs	0.043420933	GO:0016679
▪ **Group II mito genes**		
Biological process		
GO term	P-values	GOID
aerobic respiration	3.31E-03	GO:0009060
cellular respiration	1.30E-02	GO:0045333
energy derivation by oxidation of organic compounds	2.24E-02	GO:0015980
respiratory chain complex II assembly	2.29E-02	GO:0034552
mitochondrial respiratory chain complex II assembly	2.29E-02	GO:0034553
Cellular component		
GO term	P-values	GOID
mitochondrion	6.60E-31	GO:0005739
mitochondrial matrix	1.30E-05	GO:0005759
mitochondrial envelope	1.42E-05	GO:0005740
mitochondrial membrane	1.84E-04	GO:0031966
intracellular membrane-bounded organelle	3.08E-04	GO:0043231
membrane-bounded organelle	3.17E-04	GO:0043227
organelle envelope	9.93E-04	GO:0031967
envelope	9.93E-04	GO:0031975
cytoplasm	2.59E-03	GO:0005737
intracellular organelle	6.21E-03	GO:0043229
organelle	6.33E-03	GO:0043226
Molecular function		
GO term	P-values	GOID
-	-	

Table 9 DEGs in overexpression strains under salt stress.

Systematic name	Standard name	CMD1-oe	ECM27-oe	GDT1-oe	YBR196C-A-oe
YAL036C	RBG1		rDEGs		
YBR104W	YMC2		rDEGs		
YCL048W-A	YCL048W-A	rDEGs	iDEGs	rDEGs	
YER069W	ARG5,6	rDEGs			
YJL045W	YJL045W	rDEGs			
YOR203W	YOR203W	rDEGs			
YOR302W	YOR302W	rDEGs			
YGR130C	YGR130C	iDEGs		iDEGs	
YHR097C	YHR097C	iDEGs		iDEGs	
YBR109W-A	YBR109W-A	iDEGs			
YMR244W	YMR244W	iDEGs			
YBR115C	LYS2	rDEGs	rDEGs		
YCL036W	GFD2	rDEGs	rDEGs		
YCR072C	RSA4		rDEGs		
YDL182W	LYS20	rDEGs	rDEGs		
YDR035W	ARO3	rDEGs	rDEGs		
YDR158W	HOM2	rDEGs	rDEGs		
YGL234W	ADE5,7		iDEGs		
YBR056W-A	YBR056W-A		iDEGs		
YCR024C-B	YCR024C-B		iDEGs		
YFL052W	YFL052W		iDEGs		
YMR304C-A	YMR304C-A		iDEGs		
YDL114W	YDL114W			rDEGs	rDEGs
YLR177W	YLR177W			iDEGs	
YDR034W-B	YDR034W-B				rDEGs
YFL054C	YFL054C				rDEGs
YMR085W	YMR085W				rDEGs
YMR196W	YMR196W				rDEGs
YBR196C-A	YBR196C-A				iDEGs
YBR196C-B	YBR196C-B				iDEGs
YPR184W	GDB1				rDEGs
YPR160W	GPH1				rDEGs
YEL053W-A	YEL053W-A		rDEGs		
YPR010C	RPA135	rDEGs			
YPL223C	GRE1	rDEGs		rDEGs	
YER073W	ALD5	rDEGs	rDEGs		
YPL036W	PMA2	rDEGs	iDEGs		
YPL004C	LSP1				rDEGs
YOR374W	ALD4				rDEGs
YOR339C	UBC11	rDEGs			
YER175C	TMT1	rDEGs	rDEGs		
YOR306C	MCH5	rDEGs			
YOR303W	CPA1	rDEGs			
YOR273C	TPO4	iDEGs	iDEGs	iDEGs	
YOR255W	OSW1				rDEGs
YGL117W	YGL117W	rDEGs	rDEGs	rDEGs	
YOR173W	DCS2				rDEGs
YOR153W	PDR5			iDEGs	
YOR128C	ADE2		iDEGs		
YOL084W	PHM7		iDEGs		
YOL073C	DSC2	iDEGs			
YGL224C	SDT1		rDEGs		

YOL052C-A	DDR2			rDEGs	rDEGs
YGR050C	YGR050C		rDEGs		
YGR079W	YGR079W		rDEGs		
YNL160W	YGP1			rDEGs	
YNL112W	DBP2	rDEGs		rDEGs	
YNL104C	LEU4	rDEGs			
YNL091W	NST1			iDEGs	
YGR159C	NSR1	rDEGs	rDEGs		
YHR018C	ARG4	rDEGs	rDEGs	rDEGs	
YNCN0019C	snR191			rDEGs	
YNCL0023C	RDN58-2			rDEGs	
YNCL0014C	RDN58-1			rDEGs	
YHR029C	YHI9		rDEGs		
YNCJ0004C	snR190			rDEGs	
YNCD0010C	snR47		iDEGs		
YHR071W	PCL5		rDEGs		
YMR323W	ERR3	rDEGs			
YMR250W	GAD1				rDEGs
YMR175W	SIP18			rDEGs	
YMR169C	ALD3				rDEGs
YMR120C	ADE17		iDEGs		
YMR108W	ILV2	rDEGs			
YMR105C	PGM2	iDEGs		iDEGs	rDEGs
YHR214C-C	YHR214C-C		rDEGs		
YJL088W	ARG3	rDEGs	rDEGs	rDEGs	
YML128C	MSC1				rDEGs
YML123C	PHO84	rDEGs			
YML116W	ATR1	rDEGs			
YML100W	TSL1	iDEGs		iDEGs	
YJL194W	CDC6		rDEGs		
YLR359W	ADE13		iDEGs		
YLR258W	GSY2	iDEGs			
YLR237W	THI7	rDEGs			
YLR178C	TFS1				rDEGs
YLR134W	PDC5	rDEGs			
YLR058C	SHM2		iDEGs		
YKL221W	MCH2				rDEGs
YJL200C	ACO2		rDEGs		
YKL163W	PIR3	rDEGs		rDEGs	
YKL129C	MYO3	iDEGs		iDEGs	
YJR109C	CPA2	rDEGs	rDEGs	rDEGs	
YJR111C	YJR111C		rDEGs		
YKL029C	MAE1	rDEGs			
YJR158W	HXT16	rDEGs			
YKL078W	DHR2		rDEGs		
YJR106W	ECM27		iDEGs		
YJR059W	PTK2	iDEGs		iDEGs	
YJR016C	ILV3	rDEGs			
YKL120W	OAC1		rDEGs		
YKL211C	TRP3		rDEGs		
YJL116C	NCA3	rDEGs		rDEGs	
YLR413W	INA1		rDEGs		
YJL052W	TDH1	rDEGs		rDEGs	
YIR034C	LYS1	rDEGs			
YIR003W	AIM21	iDEGs			

YHR216W	IMD2	rDEGs			
YHR183W	GND1	rDEGs			
YHR104W	GRE3				rDEGs
YHR096C	HXT5		iDEGs		
YHR092C	HXT4		iDEGs		
YHR087W	RTC3	iDEGs			
YMR062C	ARG7	rDEGs	rDEGs		
YMR096W	SNZ1	rDEGs	rDEGs	rDEGs	
YMR325W	PAU19		rDEGs		
YHR016C	YSC84				rDEGs
YHR008C	SOD2				rDEGs
YHL040C	ARN1	rDEGs			
YHL021C	AIM17	iDEGs		iDEGs	
YGR256W	GND2	rDEGs		rDEGs	
YGR248W	SOL4				rDEGs
YNCK0002C	TRT2		rDEGs		
YGR088W	CTT1				rDEGs
YGR087C	PDC6	rDEGs	iDEGs	rDEGs	
YGR032W	GSC2		iDEGs		
YGL255W	ZRT1				iDEGs
YNCP0005C	snR17b		rDEGs		
YGL184C	STR3				rDEGs
YGL146C	RRT6				rDEGs
YGL121C	GPG1			rDEGs	
YGL037C	PNC1				rDEGs
YGL026C	TRP5	rDEGs			
YFR053C	HXK1				rDEGs
YFR015C	GSY1	iDEGs		iDEGs	
YFL059W	SNZ3			rDEGs	
YNL065W	AQR1	rDEGs	rDEGs	rDEGs	
YER091C	MET6				rDEGs
YNR067C	DSE4	iDEGs	rDEGs		
YER054C	GIP2	iDEGs			
YER052C	HOM3	rDEGs			
YEL011W	GLC3	iDEGs		iDEGs	
YEL007W	MIT1			iDEGs	
YDR536W	STL1		iDEGs		
YDR533C	HSP31	rDEGs		rDEGs	rDEGs
YDR345C	HXT3	rDEGs	iDEGs		
YDR343C	HXT6				rDEGs
YDR342C	HXT7				rDEGs
YNR069C	BSC5		rDEGs		
YDR127W	ARO1	rDEGs			
YDR074W	TPS2	iDEGs		iDEGs	
YDR070C	FMP16			rDEGs	rDEGs
YDR040C	ENA1			iDEGs	
YDR039C	ENA2			iDEGs	
YDR038C	ENA5			iDEGs	
YOL014W	YOL014W		rDEGs		
YDL245C	HXT15	rDEGs			
YDL223C	HBT1				rDEGs
YDL204W	RTN2				rDEGs
YOL058W	ARG1	rDEGs	rDEGs	rDEGs	
YDL110C	TMA17	iDEGs			

YDL039C	PRM7	rDEGs			
YDL022W	GPD1			iDEGs	
YCR106W	RDS1	rDEGs			
YOR202W	HIS3	rDEGs	rDEGs		
YCR057C	PWP2	rDEGs			
YCR005C	CIT2				iDEGs
YCL040W	GLK1				rDEGs
YOR337W	TEA1		rDEGs		
YCL030C	HIS4	rDEGs			
YBR296C	PHO89	iDEGs	iDEGs	iDEGs	
YBR249C	ARO4	rDEGs			
YBR230C	OM14				rDEGs
YBR214W	SDS24			iDEGs	
YBR203W	COS111		iDEGs	iDEGs	
YBR188C	NTC20			iDEGs	
YBR187W	GDT1			iDEGs	
YBR145W	ADH5	rDEGs			
YBR117C	TKL2			rDEGs	rDEGs
YPL111W	CAR1		rDEGs		
YBR109C	CMD1	iDEGs			
YBR108W	AIM3	iDEGs			
YBR105C	VID24	rDEGs		rDEGs	
YPL250C	ICY2	rDEGs	rDEGs		
YBR072W	HSP26	rDEGs		rDEGs	
YBR068C	BAP2	rDEGs			
YBL054W	TOD6	rDEGs			
YAR015W	ADE1		iDEGs		
YPR036W-A	SPO24		rDEGs		
YAL028W	FRT2	iDEGs			

*increased differential expression genes: iDGS (FDR≤0.05 and FC ≥ 1), decreased differential expression genes: rDGS (FDR≤0.05

and FC ≤ 1)

3.2.6 Enhanced mitochondrial function can confer salt tolerance only when sufficient calcium is supplied

If the enhanced mitochondrial function is necessary for salt tolerance in yeast, why have no mitochondria-related genes been identified as GOFAs? Perhaps sufficient Ca^{2+} is required to suppress "mitochondrial runaway" under salt stress, as shown in Fig. 19K. If this idea is correct, mitochondria-associated GOFAs should be isolated under Ca^{2+}-induced salt stress, which was the case (see below). I performed the overexpression profile under 1 M NaCl with 5 mM $CaCl_2$ (Fig. 21A). Upon Ca^{2+} addition, *CMD1*, *GDT1*, and *ECM27* did not become GOFAs, further supporting the idea that these GOFAs complement the Ca^{2+} requirement. On the other hand, a completely different group of genes (*CTR1*, *HAP4*, and *USV1*) were enriched as GOFAs (Fig. 21B and 21C). *HAP4* and *USV1* have been reported as transcription factors for mitochondrial respiratory genes (Forsburg and Guarente 1989; Hlynialuk et al. 2008). Of the 30 genes with genetic interactions with *HAP4* (Costanzo et al. 2016), 27 (PCC $\leq$ 0.2) belong to Group I Mito genes (Fig. 21E), strongly suggesting a functional relationship between mitochondrial respiration and *HAP4*.

I confirmed that *USV1-oe* and *HAP4-oe* promoted growth under salt stress only when Ca^{2+} was supplied (Fig. 21D). Interestingly, overexpression of these genes without Ca^{2+} delayed growth under salt stress (Fig. 21D), supporting the idea that enhanced mitochondrial function under salt stress without Ca^{2+} is detrimental. Knockout of Group I Mito. genes such as *COQ1* and *COX11* did not show a *HAP4-oe* advantage (Fig. 21E), possibly because of *HAP4* functions upstream of these genes. These results suggest that enhanced mitochondrial activity can confer salt tolerance only when sufficient calcium is supplied (Fig. 21F).

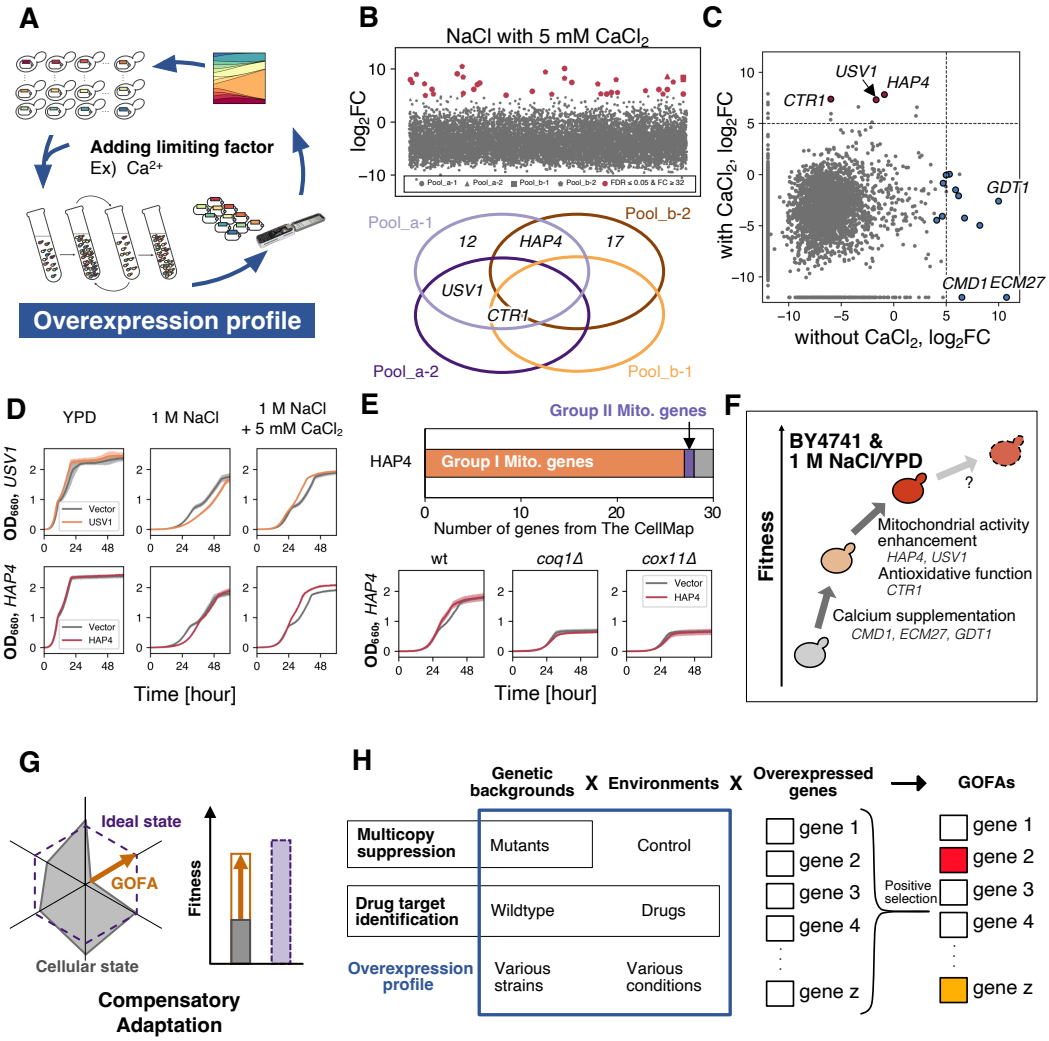
A
Adding limiting factor
Ex) Ca2+
Overexpression profile
B
NaCl with 5 mM CaCl2
log2FC
Pool_a-1
Pool_b-2
Pool_a-2
Pool_b-1
12
HAP4
17
USV1
CTR1
C
USV1
HAP4
CTR1
GDT1
CMD1
ECM27
with CaCl2, log2FC
without CaCl2, log2FC
D
YPD
1 M NaCl
1 M NaCl + 5 mM CaCl2
OD660, USV1
OD660, HAP4
Vector
USV1
HAP4
Time [hour]
E
Group II Mito. genes
HAP4
Group I Mito. genes
Number of genes from The CellMap
wt
coq1Δ
cox11Δ
OD660, HAP4
Time [hour]
F
BY4741 &
1 M NaCl/YPD
?
Mitochondrial activity enhancement
HAP4, USV1
Antioxidative function
CTR1
Calcium supplementation
CMD1, ECM27, GDT1
Fitness
G
Ideal state
GOFA
Cellular state
Fitness
Compensatory Adaptation
H
Genetic backgrounds
X
Environments
X
Overexpressed genes
GOFAs
Multicopy suppression
Mutants
Control
Drug target identification
Wildtype
Drugs
Overexpression profile
Various strains
Various conditions
gene 1
gene 2
gene 3
gene 4
gene z
Positive selection

Figure 21. Enhancing mitochondrial function can confer salt tolerance only when enough calcium is supplied. A) Repeated isolation of GOFAs after the addition of a limiting factor $CaCl_2$ under the salt stress. **B)** Fold change of plasmid occupancy after the 80 generations-cultivation of BY4741 overexpression library under 1 M NaCl with added 5 mM $CaCl_2$. (upper). Hit genes in each replicate under well-studied stresses (lower, FDR ≤ 0.05 and FC ≥ 2^5). **C)** A comparison of the fold changes of plasmid occupancies with and without $CaCl_2$ addition. The colored circles indicate GOFAs, with (red) and without $CaCl_2$ addition (blue). The dashed lines mean the threshold of GOFAs as fold change ≥ 2^5. No values were replaced by -15. **D)** Growth curves of *USV1-oe* (upper, orange) and *HAP4-oe* (lower, red) under three conditions: YPD, 1 M NaCl, 1 M NaCl with 5 mM $CaCl_2$. The grey line shows empty vector control. The filled areas indicate standard deviation (n = 3). **E)** The upper panel: Most genes harboring genetic interaction with *HAP4* belong to the Group I Mito. genes (PCC ≥ 0.2, data obtained from The CellMap (Costanzo et al. 2016). The lower panel: Growth curves of *HAP4-oe* in the deletion mutant of *COQ1* and *COX11*, the Group I Mito. genes harboring the genetic interaction with *HAP4*. The filled areas indicate SD (n = 3). **F)** An illustration showing the mechanism of fitness increase of BY4741 under 1 M NaCl/YPD by fulfilling its requirements by GOFAs. **G)** GOFAs manifest the potential for cellular stress tolerance (ideal state) due to compensating for cellular requirements. **H)** Overexpression profiling using overexpression profile. The detail is explained in the text.

Finally, I focused on *CTR1* (Fig. 21C). *CTR1*, encoding a copper importer (Dancis et al. 1994), was isolated as the major GOFA under oxidative stress (Fig. 7G). *CTR1-oe* or adding 1 mM $CuSO_4$ suppressed growth defects under oxidative stress (Fig. 22A and B). Furthermore, instead of *CTR1*, the catalase genes *CTT1* and *CTA1* became GOFAs under oxidative stress supplied with 1 mM $CuSO_4$ (Fig. 22B-D). These results suggest that copper is a major limiting factor for oxidative stress and that even supplying Ca^{2+} under salt stress requires sufficient antioxidative function (Fig. 22F).

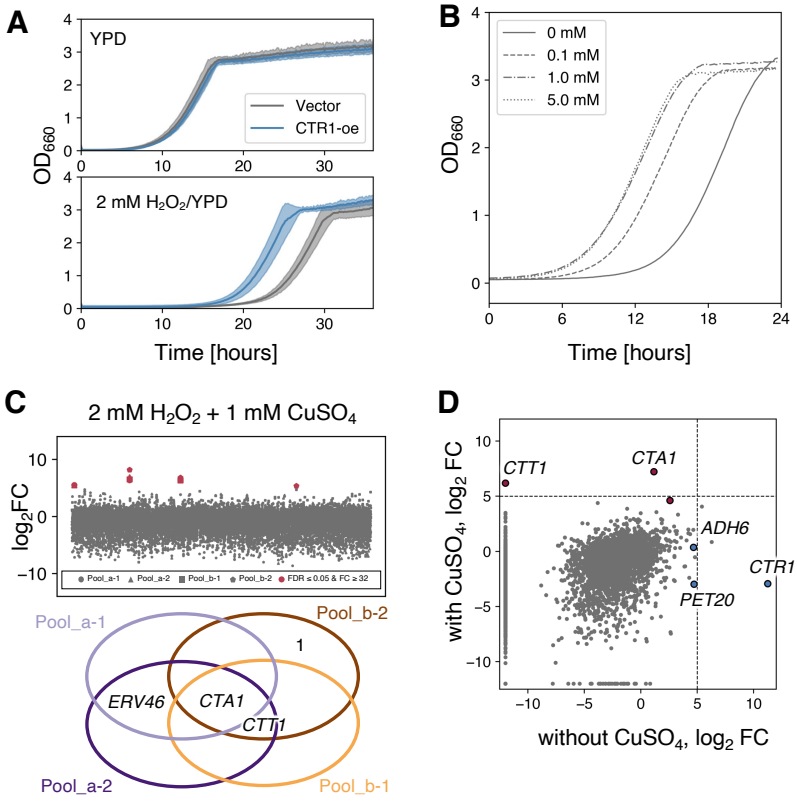

Figure 21. GOFAs enriched under oxidative stress propose Cu^{2+} limitation in the culture medium. A) CTR1-oe increased the growth of BY4741 under oxidative stress. Upper and lower panels indicate growth in YPD and 2 mM H_2O_2/YPD. The filled area shows SD (n = 3). **B)** The addition of $CuSO_4$ increased the growth of BY4741 under 2 mM H_2O_2. **C)** Fold change of plasmid occupancy after the 80 generations-cultivation of BY4741 overexpression library under 2 mM H_2O_2 with 1 mM $CuSO_4$. (upper). Hit genes in each replicate under well-studied stresses (lower, FDR ≤ 0.05 and FC $\geq 2^5$). **D)** A comparison of the fold changes of plasmid occupancies with and without $CuSO_4$ addition. The colored circles indicate GOFAs, with (red) and without $CaCl_2$ addition (blue). The dashed lines mean the threshold of GOFAs as fold change $\geq 2^5$. No values were replaced by -15.

3.3 Discussion

In this study, I aimed to understand the contribution of overexpression to overcoming stressful environments. Therefore, I developed a new experimental system to systematically isolate genes whose overexpression is functionally adaptive (GOFAs). I first examined the characteristics of genes that become GOFAs under environmental stress. The results revealed that GOFAs are genes that compensate for cellular deficiencies and that their adaptive function strongly depends on genetic background and environment. For example, GOFAs isolated under salt stress were associated with calcium homeostasis, and their adaptive function emerged from the lack of Ca^{2+} in the medium (Fig. 7 and 12). In fact, under Ca^{2+}-supplemented salt stress conditions, those adaptive functions were lost (Fig. 12), and GOFAs different from those without Ca^{2+} supplementation were isolated (Fig. 21). In CEN.PK, genes such as Na+ exporter *ENA1* and regulators of K^+ homeostasis, *SAT4,* and *HAL5*, were identified as GOFAs under salt stress, but not in BY4741 (Fig. 14). This difference in GOFAs can be explained by the difference in Ca^{2+} and K^+ requirements between BY4741 and CEN.PK. In fact, the adaptive effects of *ENA1-oe* and K^+ were more substantial in CEN.PK than in BY4741 (Fig. 14). Based on these facts, I propose that GOFAs compensate for the missing elements for cells to reach maximum stress tolerance ("ideal state" in Fig. 21G). In other words, examining GOFAs reveals the missing elements necessary to maximize cellular fitness within a given genetic background and environment.

One limitation of the overexpression profiling method developed in this study is that it is not always clear whether a hit gene identified in the screen is a true positive or a false positive. Indeed, as I indicated in Fig. 12G, a prolonged culture of the cells may enrich the plasmid for factors other than gene overexpression, which could result in false positives. Therefore, I should measure the growth rate individually to determine if the hit genes are GOFAs. In addition, whether a gene is

a hit depends on the initial pool as well as whether overexpression of that gene is adaptive (Figure 7D and G). It also depends on stochastic factors such as genetic drift. Therefore, the possibility of false positives and false negatives would be reduced if multiple initial pools could be prepared. The construction of an overexpression library using homologous recombination, as proposed in this study, will make that even easier to create multiple-initial libraries.

I believe that in the isolation of GOFAs, I observe a "compensatory adaptation/evolution" of cells to deficiency (Szamecz et al. 2014; Filteau et al. 2015). Besides screening for drug targets, genes that fall under GOFAs in this study are often explored as multicopy repressor genes, i.e., genes that suppress/compensate the deleterious phenotype of a mutant by multicopy plasmids (Ueguchi and Ito 1992; Prelich 2012). In addition, in deleterious mutants subject to intense selection pressure, aneuploidy and consequent overexpression often occur to suppress/compensate for the harmful effects (Szamecz et al. 2014; Puddu et al. 2019). On the other hand, the overexpression profile provided a new means of observing the complementary adaptation/evolution of various strains against potential defects under multiple environments (Fig. 21H).

I believe that GOFAs compensate for cellular deficiencies to achieve a potential cellular stress response. In other words, GOFAs merely augment the existing stress response system. This approach does not explain why cells have evolved sophisticated stress responses or how they acquire new stress responses. This study focused only on genes that could explain the adaptive mechanisms. In fact, among GOFAs, there are also genes whose adaptive mechanisms cannot be easily described and "emerging genes" (Van Oss and Carvunis 2019; Vakirlis et al. 2020) such as *YBR196C-A* in Fig.12. The mystery of the evolution of novel stress response mechanisms may be hidden in these genes. It may also be that the byproducts of compensatory adaptation to the

environment appear as functional novelties, like the morphological novelties that occur in the compensatory evolution of gene loss (Farkas et al. 2022).

Through the identification of GOFAs under salt stress by the overexpression profile, I found that calcium has a positive effect on long-lasting salt stress, distinct from the previously known short-time response of salt stress (Fig.12 and Extended Data Fig. 18). Furthermore, functional profiling of gene disruption mutants revealed that mitochondrial runaway might be subject to suppression by Ca^{2+} (Fig. 19). Overexpression of GOFAs (*HAP4* and *USV1*) identified under salt stress with supplied Ca^{2+} seem to enhance mitochondrial function, worked positively for salt stress tolerance only under calcium-supplying conditions, but rather negatively under calcium-limiting conditions (Fig. 21). This dictates that the primary function of calcium is to regulate mitochondrial activity under salt stress. As shown in this series of experiments, the advantage of the overexpression profile is its ability to rapidly and efficiently obtain GOFAs in various strains and environmental conditions (Fig. 21H). By using "overexpression profiling," we can uncover previously unexplored mechanisms of cellular adaptation.

3.4 Materials and Method

Strains and plasmids

The strains and plasmids used in this study are listed in Table 10.

Medium and yeast transformation

Yeast culture and transformation were performed as previously described (Amberg, Burke, and Strathern 2005). I used two types of mediums: YPD and Synthetic Complete (SC) medium. YPD included 10 g/L Bacto Yeast extract (BD, USA), 20g/L Bacto Peptone (Gibco, USA), and 20 g/L D-glucose. SC medium included 6.7g/L Yeast Nitrogen Base with Ammonium Sulfate (MP, USA), 0.65 g/L DO supplement-HisLeuUra (Clontech, USA), and 20g/L D-glucose or, where appropriate, 20mg/L Histidine, 8 mg/L Uracil, and 100 mg/L Leucine. D-glucose solution was added to the medium after autoclave. Milli-Q water (Merck, Germany) was used to condition the medium. In Fig. 6D and 6E, YPD and 1 M NaCl/YPD were diluted four times with sterile water or 1 M NaCl solution. I used Shio (Shiojigyo, Japan) and Setonohonjio (Ajinomoto, Japan) as the table salt and the crude salt representative.

Plasmid and strain construction

RNAseq was performed as described previously (Eguchi et al. 2018). The plasmids and strains were constructed by homologous recombination activity in yeast cells following previous report (Oldenburg et al. 1997), and their plasmid construction was verified by Sanger sequencing.

Exploring well-studied stress

Using the API on PubMed provided by NIH, efetch of E-utilities, I obtained 308,970 and 20,460 articles (as of 20th May 2022) searched for "yeast" and "yeast stress" (including authors. title, abstract, year of publication, and journal title), respectively. Using the TF-IDF method, I extracted the keywords with the highest scores up to 5th place from the abstract obtained for "yeast stress"(Rajaraman and Ullman 2011). Among all keywords, keywords including "stress" were extracted. Next, I determined whether or not each stress keyword appeared in the abstract of the articles obtained by "yeast stress. I used NLTK (3.6.7) for these analyses, a python library for natural language processing (Bird, Klein, and Loper 2009).

Growth rate assay

Target strains were inoculated into 4 ml of SC (–Ura or -HisUra) medium in test tubes and incubated overnight at 30˚C as pre-cultivation. Then, 25 µl of pre-cultured medium were inoculated into 6 ml of target medium in L-shaped tubes and cultured at 30˚C (excluding heat stress), recording optical density (OD) at 660 nm every 10 minutes with an ADVANTEC TVS062 (ADVANTEC, Japan) with shaking at 70 rpm. Growth rates [1/hour] were calculated from recorded OD data as the reciprocal of the mean doubling time, which was the slope of log base 2 of OD_{660} between 0.125 and 0.500 by linear approximation with scipy.optimize.curve_fit in the python library. If OD_{660} did not exceed 0.125 48 hours after inoculation, I designated not detected (N.D).

Overexpression profile

As the first step of the overexpression profile, the construction of overexpression library was following. In the case of the construction of BY4741-overexpression library, 5 µl of thawed gTOW6000 collection (Makanae et al. 2013) was inoculated into sixty 96-well plates with 200 µl of SC-Ura medium and incubated at 30˚C for 48 hours. All cultured mediums were then pooled in sterile flasks and divided into 50 ml tubes. Finally, pooled libraries were with the addition of final conc—7% v/v DMSO and stored at -80 ˚C.

The constructions of CEN.PK2-1C- and DBVPG6765-overexpression libraries were performed as follows. Each insert fragment of the gTOW6000 library was amplified by PCR using specific primer sets, as previously described(Makanae et al. 2013). The PCR reactions were performed in a 96-well format on a 50 µL scale using KODplus NEO (Toyobo) for 61 sets. All 96 reactions were pooled (4.8 mL) and mixed in equal volumes to create the mixed PCR products. the two plasmid fragments from pTOW40836 were amplified by PCR using two pairs of primers: 5'-GGATCCACTAGTTCTAGAGCGGCCG-3' and 5'- GCTCGTTACAGTCCGGTGCG -3', 5'-CTCGAGGGGGGGCCCGGTACCCAATTCGCCCTATA-3' and 5'-ACGAATGCACACGGTGTGGTGG -3'. The mixed PCR products of and introduced into the target strain. Transformation protocols were performed according to the previous report(Amberg, Burke, and Strathern 2005). To 6 ml of yeast with 1 OD_{660} unit, 60 µl of PCR mix, 30 µl of plasmid fragments, 1,440 µl of 50 w/v % polyethylene glycol 4,000, 216 µl of 1 M LiOH, and 144 µl of ssDNA were added and spread on 15 cm diameter SC-Ura agar medium. Incubated at 30˚C for 48 hours, scraped off the colonies on all agar templates, and added DMSO to final conc. 7 v/v%, and stored at -80˚C. Yeast cells were equivalent to 2 agar plates for DBVPG6765 and 5 agar plates for CEN.PK2-1C was transformed.

The CEN.PK2-ENA1 co-overexpression library was constructed following. The CEN.PK2-1C-overexpresson library and CEN.PK2-1D bearing pRS423nz2-ENA1 were mixed to be 1:1. Each used 2 OD units. Mixed strains were spread and cultured on an SC-HisUra agar plate (15 cm) for 48 hours at 30˚C. After incubation, to selectively reduce unmated yeasts, the colonies were scraped, and 2 OD units each were spread again on 5 plates of fresh SC-HisUra agar and incubated at 30˚C for 48 hours. Finally, the colonies were scraped off, and DMSO was added to reach the final conc. 7%, and stored at -80˚C.

As the second step of the overexpression profile, competitive culture and passage were followed. 1 ml of an overexpression library was inoculated into 5 ml of SC-Ura medium and incubated at 30°C overnight with shaking. Then, 24 µl (1:250 dilution) of the pre-cultured medium was inoculated into 6 ml of target medium in L-shaped tubes and cultured until stationary phase, measuring optical density with an ADVANTEC TVS062 (ADVANTEC, Japan). 24 µl (1/250 dilution) of the pre-cultured medium was passage into 6 ml of fresh medium in L-shaped tubes. The passage was repeated 1-10 times. For high stress, I used ADVANTEC TVS062 set temperatures at 37˚C or 40°C in a bio shaker BR-43FL (TITEC, Japan) set at 35°C. The all-cultured medium was transferred into a 5 ml tube, centrifuged at 15,000 rpm for 1 min, its supernatant was removed, and 1 ml of 10 v/v% DMSO water was added and suspended. The suspension was transferred to 1.5 ml tubes and stored at -80°C. For the methotrexate experiment, competitive cultures were made in 500 ml Erlenmeyer flasks with 150 ml of medium, and 4.5 µl (about 1:33,000 dilution) of the culture was inoculated and passaged.

As the third step of the overexpression profile, plasmid preparation from competitive cultured yeast and long-read sequencing was performed following. 500 µl of the thawed sample was transferred to a new 1.5 ml tube, and the remaining sample was re-stored at -80°C. The sample was centrifuged at 15,000 rpm for 1 min, and its supernatant was removed. The sample was resuspended with 250 µl of Solution 1 (1 M sorbitol, 0.1 M Na_2EDTA (pH 7.5), and 10 µg/ml RNase) and 5 µl of 10 units/µl Zymolyase–T100 (Nacalai tesque, Japan) and incubate for 30 minutes. 250 µl of Solution 2 (0.2 M NaOH and 1% w/v SDS) was added to the suspension and mixed. Then, 250 µl of Solution 3 (3 M potassium acetate and 2 M acetic acid) was added to the suspension and vortexed. The suspension was centrifuged for 10 minutes at 15,000 rpm to precipitate the insoluble material. The supernatant was added to a spin column (QIAprep Spin Miniprep Columns, Qiagen, Germany) and centrifuged at 13,000 rpm for 1 minute. After removing the column-through effluent, 750 µl of wash buffer (QIAprep Spin Miniprep Kit, Qiagen, Germany) was added and centrifuged for 1 minute. After removing the column-through effluent, the empty column was centrifuged at 13,000 rpm for 1 minute to dry the column. The column was set on a new 1.5 ml tube. The column on the tube was incubated with 50 µl of elution buffer (QIAprep Spin Miniprep Kit, Qiagen, Germany) and allowed to stand at room temperature for 2 minutes. And The column on the tube was centrifuged at 13,000 rpm for 1 minute to extract plasmids. Finally, 1 µl of the plasmid extracted solution was used to measure plasmid concentrations with a DNA staining reagent (Qubit 1X dsDNA HS Assay Kit, ThermoFisher, USA) and a Fluorometer (Qubit4, ThermoFisher, USA), the remaining solution was stored in -20˚C before subsequent usage.

Long-read sequencing for plasmid inserts was performed following. Sequencing library preparation was performed according to the manufacturer’s instructions, "Four-primer PCR

protocol", using SQK-PBK-004 (Oxford Nanopore Technologies, UK). 25 ng of purified plasmid was used as each sample, and PCR reactions were performed with half of the defined protocol and the own designed primers 5'-TTTCTGTTGGTGCTGATATTGCggcgaaaggggatgtgctg-3' and 5'-ACTTGCCTGTCGCTCTATCTTCggaaagcgggcagtgagcgc-3'. Libraries were sequenced using GridION or MinION and MinIT (Oxford Nanopore Technologies, UK) with the flow cell MinION R9.4.1. 6-12 samples per flow cell were analyzed in multiplexing. Base-calling and demultiplexing were performed using MinKNOW (Oxford Nanopore Technologies, UK) with guppy in high-throughput mode.

As the last step of overexpression profile, analysis of sequence data and identification of GOFAs were performing following. Sequence data (fastq format) was aligned to a reference genome sequence file (R64-1-1) of budding yeast S288C using minimap2 (2.24) (Heng Li 2018) to output an alignment file sam format). Next, the alignment file was reformatted and sorted using "view -Sb" and "sort" in Samtools (1.15) (Heng Li et al. 2009) to obtain a bam format file. Then, Bedtools (2.30.0) (Quinlan and Hall 2010) with "bamtobed" converted the bam format file to a bed format file. The aligned reads on gTOW6000 insert locus were extracted using "bedtools intersect" with an option "-F 0.5". The read counts on insert locus were counted by "bedtools coverage". Subsequent analyses were performed using python (3.8.12) with NumPy (1.21.2) and pandas (1.4.1), and visualized using IGV(J. T. Robinson et al. 2011). Reads for each insert were converted to reads per million (RPM). The fold change of plasmid occupancies was calculated according to the following equation,

$$FC_{n,i} = RPM_{n,i}/RPM_{0,i}$$

where $RPM_{0,i}$ is the ratio of insert i in the pool before competitive passages and $RPM_{n,i}$ is the ratio of insert i after n passages. In this study, genes with larger fold change than 32 (2^5) and FDR ≤

0.05 were considered as hits. Multiple hit genes were considered as GOFAs. FDR was calculated for each replicate by chi-square test and Benjamini-Hochberg method(Benjamini and Hochberg 1995). The chi-square test used the ratio of plasmid appearance before and after competitive culture, and the number of sequences reads as parameters. The diversity of plasmids was evaluated using the Gini-Simpson index, calculated following (Caso and Gil 1988; Jost 2006).

Aequorin assay

Plasmid pEVP11/AEQ-HIS3 was constructed by replacing *LEU2* of pEVP11/AEQ with *HIS3* (Batiza, Schulz, and Masson 1996). PCR amplified the fragments of *HIS3* with primers 5'-GGCCGAGCGGTCTAAGGCGCgtttcggtgatgacggtgaa-3' and 5'-GCGCTGGGTAAGGATGATGCgccgatttcggcctattggt-3' using pRS413 as a template. PCR amplified the fragments of pEVP11/AEQ without *LEU2* locus with primers 5'-ttcaccgtcatcaccgaaacGCGCCTTAGACCGCTCGGCC-3' and 5'-accaataggccgaaatcggcGCATCATCCTTACCCAGCGC-3' using pEVP11/AEQ as a template. pEVP11/AEQ-HIS3 was introduced into each overexpressing strain. I performed transformation protocols according to Amberg 2005. Target strains were inoculated into 4 ml of SC (–Ura or -HisUra) medium in test tubes and incubated overnight at 30˚C as pre-cultivation. Then, 200 µl of pre-cultured medium were inoculated into 5 ml YPD medium and cultured until OD_{660} reached 1.0. One OD_{660} unit was aliquoted into a 1.5 ml tube and centrifuged, and its supernatant was removed. The pellet was resuspended with 50 µl YPD, including 5 mM Coelenterazine H (Wako, Japan), and stood in the dark at room temperature for one hour. After centrifugation and removing the supernatant with Coelenterazine H, the pellet was washed with fresh YPD, suspended in 75 µl of YPD medium, and then applied to 96 well plates. Luminescence intensity was measured

using a microplate reader MTP-880Lab (COLONA, Japan). First, fluorescence intensity was measured for 50 seconds at 5-second intervals as a baseline. Then, 25 µl of 4 M NaCl solution was added to the well by the automatic dispenser DP-50N (COLONA, Japan). The plate was agitated for 5 seconds. The fluorescence intensity was measured every 5 seconds for 10 minutes.

Measurement of mineral concentration in the medium

Iused ionometers, LAQUAtwin (Na-11, K-11, Ca-11, HORIBA, Japan), to measure the mineral concentration in the medium I used in this study. I measured following the manufacturer's instructions. 500µl of each medium was spotted on the sensor of ionomers and measured.

Laboratory evolutionary experiment

The culture and passages followed the "overexpression profile" described above. 1 ml of BY4741 bearing pTOWug2836 as vector control was inoculated into 5 ml SC-Ura medium and incubated at 30°C overnight with shaking. Ten passages were cultured in YPD medium containing 1 M NaCl.

Genome preparation

The genome was extracted from pooled cultured strains according to the previous report(Amberg, Burke, and Strathern 2005) from 5 OD_{660}unit cultured yeast. 500 µl of Solution 1 (1 M sorbitol Solution 1 (1 M sorbitol, 0.1 M Na_2EDTA (pH 7.5) and 10 µg/ml RNase) and 5 µl of 10 units/µl Zymolyase solution were added to the pellet and suspended, incubated at 37°C for 30 minutes. After centrifugation and removal of the supernatant, add 250 µl buffer (20 mM Na_2EDTA and 50

mM Tris-Cl (pH 7.4)) and 25 µl 10% SDS was added and incubated at 65˚C for 30 minutes. 100 µl of 5 M potassium acetate was added to the sample and cooled on ice for 30 minutes. Then the sample was centrifuged, and its supernatant was transferred to a new 1.5 ml tube. 400 ml of isopropanol was added to the supernatant and placed at room temperature for 5 minutes. After Centrifuged again, the pellet was rinsed with 70 v/v% ethanol. 50 µl of sterile water was added to the pellet, extracting the genome. The extracted genome solution was stained with a DNA staining reagent (Qubit 1X dsDNA HS Assay Kit, ThermoFisher), and the plasmid concentration was measured with a Fluorometer (Qubit4, ThermoFisher).

Genome sequencing and variants calling

Genome quality check and resequencing were outsourced to Macrogen Japan (Japan). Library preparation was performed using TrueSeq DNA PCR Free Kit (Illumina, USA), and sequencing was performed using NovaSeq 6000 (Illumina, USA) under 150 bp paired-end conditions to obtain sequence data in fastq format files. Sequence data were aligned and mapped to a reference genome sequence file (R64-1-1) of budding yeast S288C using BWA (0.7.17) (Heng Li and Durbin 2009). Next, the alignment file (SAM format) was converted to a bam format file and sorted using Samtools (1.15). Variants for each sample were called performed using Bamtools (1.15) with "mpileup"(H. Li 2011) with "call" and filtered using vcfutils.pl varFilter (default parameters). Variants were annotated by snpEff (4.1) (H. Li 2011; Cingolani et al. 2012) using R64-1-1.86. Comparison of An and Ev variations was performed by bcftools isec. Called variants were checked manually using IGV (2.8.10) and validated by chi-square test for base composition between An and Ev.

The threshold for validation was set at an FDR of 0.05 or less, corrected by the Benjamini-Hochberg method(Benjamini and Hochberg 1995). The raw data were available in the DNA Data Bank of Japan (accession number: DRA014470).

GFP western blot analysis

GFP was detected by western blot as described previously (Ishikawa et al. 2017). ENA1-GFP cells were cultivated in YPD, 1 M NaCl/YPD and 1 M NaCl/YPD with 5 mM $CaCl_2$. One OD unit of the cells was harvested at the log phase (OD_{660} = 1.0). The cells were treated with 1 ml 0.2 mol/l NaOH and then 50 µl 1xNuPAGE LDS sample buffer (Invitrogen, USA) and heated at 70˚C for 10 mins. Protein lysate was labeled with Ezlabel FluoroNeo (ATTO, Japan) and separated by polyacrylamide gel electrophoresis on 4–12% on NuPAGE 4%–12% Bis-Tris Gel (Invitrogen, USA). The separated proteins were transferred onto a PVDF membrane (Invitrogen, USA) using the iBlot (Invitrogen, USA). GFP was probed by the anti-GFP antibody (Roche) (1: 1,000), peroxidase-conjugated secondary antibody (Nichirei Biosciences, Japan) (1: 1,000), and SuperSignal West Femto Maximum Sensitivity Substrate (Thermo Fisher Scientific, USA). In chemiluminescence detection mode, GFP was detected and measured using the LAS-4000 image analyzer (Fujifilm, Japan). Quantification of the band intensity was carried out using ImageJ (1.53k).

Genetic profiling using yeast gene knockout collection

96-well plates were dispensed with 200 µl of YPD, inoculated with 5 µl of thawed Yeast Knockout Out Haploid MAT-a Collection (Winzeler et al. 1999), and incubated at 30˚C for 48 hours. All culture strains were mixed in sterile flasks, divided into 50 ml tubes, and added final

conc. 7 % v/v DMSO, and stored at -80 ˚C. One ml of Pooled KO library was inoculated into 5 ml of YPD medium and incubated at 30°C overnight with shaking. Next, 6 ml of medium was dispensed into an L-shaped tube, and 24 µl (1/250 dilution) of the pre-culture was inoculated and incubated for a fixed time until steady-state while measuring optical density with an ADVANTEC TVS062. After a particular time, 6 ml of fresh medium was dispensed into another L-shaped tube, and the culture was passaged 24 µl (1/250dilution) of the culture. The passage was repeated two times. The genome of harvested cells was extracted (see Laboratory evolutionary experiment). Strain-specific DNA barcodes were amplified using multiplex primers and a common U2 primer. PCR conditions were set as follows: 5 min at 98˚C for initial denaturation, 30 cycles of 30 sec at 98˚C, 30 sec at 55˚C, 45 sec at 72˚C, and a final extension time of 10 min at 72˚C. PCR products were purified from 2% agarose gels using a Geneclean III kit (Qbiogene, USA), quantified using a Kapa qPCR kit (Sigma-Aldrich, USA), and sequenced with an Illumina HiSeq 2500 machine. Sequence analysis was performed on the second passages and the pre-culture pool. Each experiment was performed in biological triplicates performed for all conditions. We denoted relative fitness in terms of *Z*-scores, which was the standard normalized distribution of fold change between RPM of barcodes before and after cultivation. The false discovery rate (*FDR*) for the *Z*-score between conditions was calculated using Welch's t-test (Welch 1938) and the Benjamini-Hochberg correction (Benjamini and Hochberg 1995). GO enrichment analysis was performed using the Gene Lists function on the SGD website (www.yeastgenome.org/).

Microscopic observation of mitochondria

Microscopic observation was performed as described previously (Horiuchi et al. 2022). TIM50-GFP(Huh et al. 2003) were cultured in YPD, YPD with 5 mM $CaCl_2$, 1 M NaCl/YPD, and 1 M

NaCl/YPD with 5 mM $CaCl_2$. Cells were harvested at the log phase (OD_{660} = 1.0), and 1 µl of the suspension cell was mixed with 2 µl of YPD on a glass slide. Images were obtained and processed using the DMI6000 B microscope and Leica Application Suite X software (Leica Microsystems, Germany). The GFP fluorescence was observed using the GFP filter cube (Leica cat. # 11513899). Mitochondria were stained with 100 nM of MitoTracker Red CM-H2Xros (M7513, Thermo Fisher Scientific, USA) for 30 min and then washed with 0.5 ml of YPD. The cells were then observed using RFP filter cubes (Leica cat. # 11513894).

RNAseq

RNAseq was performed as described previously (Namba et al. 2022). The four strains: *CMD1-oe*, *ECM27-oe*, *GDT1-oe*, and vector control, were pre-cultured in SC-Ura at 30˚C overnight and cultured in YPD or YPD with 1M NaCl medium and harvested at the log growth phase (OD_{660} = 1.0). Purified RNA was quality-checked by BioAnalyzer (Agilent, USA) or MultiNA (Shimazu, Japan), and concentration was measured by Qubit (Thermo Fisher Scientific, USA). Purified RNA was stored at -80°C until subsequent experiments. cDNA library was prepared using the TrueSeq Stranded Total RNA kit (Illumina, USA) and half the protocol of the TrueSeq RNA library prep kit. 4 µg of the library was prepared by adding 1 µl of 142.8x diluted ERCC RNA Spike-in mix (ThermoFisher, USA) to 4 µg of total RNA. Libraries were quality checked on an Agilent 2100 BioAnalyzer (Agilent, USA), concentrations were measured on a Real-TIme PCR system (ThermoFisher, USA), and libraries were pooled. cDNA library Sequencing was performed by pair-end sequencing on an Illumina NextSeq 550 (Illumina, USA). Three biological duplications were analyzed for all strains. The sequences were checked for sequence quality by FastP (Chen et al. 2018) and then aligned using Hisat2 (D. Kim et al. 2019). The aligned data

were formatted into bam files by Samtools (Heng Li et al. 2009). Finally, expression level variation analysis was performed by EdgeR (Heng Li et al. 2009; M. D. Robinson, McCarthy, and Smyth 2010). The raw data were available in the DNA Data Bank of Japan (accession number: DRA014472). GO enrichment analysis was performed using the Gene Lists function on the SGD website (www.yeastgenome.org/).

Arginine uptake assay

BY4741 wild-type and *can1*Δ cells were cultured in YPD or YPD with 1 M NaCl medium and harvested at the log growth phase (OD_{660} = 1.0) and suspended in 4 ml of YPD or YPD with 1 M NaCl medium at a density of 2.5×10^8 cells/ml, respectively. The arginine uptake reaction was initiated by the addition of 1.0 ml YPD or YPD with 1 M NaCl medium containing [U-^{14}C]arginine at final radioactivity level of 0.518 kBq/ml, respectively. Immediately after addition (defined as 0 min), and after incubation for 60 min at 30˚C, 0.5 ml aliquots of cell suspension were withdrawn, and filtered on cellulose acetate membrane filters (0.45 μm; ADVANTEC, Japan), and washed with cold 10 mM HEPES (pH6.4). The radioactivities of recovered cells were measured using a liquid scintillation counter. Arginine uptake was calculated by subtracting the radioactivity of 0 min from that of 60 min. For the normalization of arginine uptake, protein contents in cells mixed with YPD not containing radiolabeled arginine and collected at 0 min and 60 min were measured by Lowry method.

Quantification and Statistical Analysis

Information on statistical analysis and biological replicates is included in figure legends. The significance level was set at 0.05.

Table 10 The used strains and plasmids in this chapter.

Reagent type (species) or resource	Designation	Source or reference
strain, strain background (*Saccharomyces cerevisiae*)	BY4741 (his3Δ1 leu2Δ0 ura3Δ0 met15Δ0 LYS)	Brachmann 1998
strain, strain background (*Saccharomyces cerevisiae*)	CEN.PK2 (MAT a/alpha his3Δ1/his3Δ1 leu2-3_112/leu2-3_112 ura3-52/ura3-52 trp1-289/trp1-289 MAL2-8c/MAL2-8c SUC2/SUC2)	Entian 2007
strain, strain background (*Saccharomyces cerevisiae*)	CEN.PK2-1C (MATa his3Δ1 leu2-3_112 ura3-52 trp1-289 MAL2-8c SUC2)	Entian 2007
strain, strain background (*Saccharomyces cerevisiae*)	CEN.PK2-1D (MAT alpha his3Δ1 leu2-3_112 ura3-52 trp1-289 MAL2-8c SUC2)	Entian 2007
strain, strain background (*Saccharomyces cerevisiae*)	DBVPG6765 (Mat a/alpha, ura3Δ0/ura3Δ0, leu2Δ0/leu2Δ0, lys2Δ0/LYS2, met15Δ0/MET15)	Louvel 2014
strain, strain background (*Saccharomyces cerevisiae*)	DBVPG6044 (Mat a/alpha, ura3Δ0/ura3Δ0, leu2Δ0/leu2Δ0, lys2Δ0/LYS2, met15Δ0/MET15)	Louvel 2014
strain, strain background (*Saccharomyces cerevisiae*)	YPS128 (Mat a/alpha, ura3Δ0/ura3Δ0, leu2Δ0/leu2Δ0, lys2Δ0/LYS2, met15Δ0/MET15)	Louvel 2014
strain, strain background (*Saccharomyces cerevisiae*)	UWOPS03-461.4 (Mat a/alpha, ura3Δ0/ura3Δ0, leu2Δ0/leu2Δ0, lys2Δ0/LYS2, met15Δ0/MET15)	Louvel 2014
strain, strain background (*Saccharomyces cerevisiae*)	W303 (MATa/alpha, leu2-3,112/ leu2-3,112, trp1-1/trp1-1, can1-100/can1-100, ura3-1/ura3-1, ade2-1/ade2-1, his3-11,15/ his3-11,15)	Voth 2005
strain, strain background (*Saccharomyces cerevisiae*)	fcy1::ENA1pro-moxGFP-sphi5MX	This study
strain, strain background (*Saccharomyces cerevisiae*)	TIM50-GFP	Huh 2003
strain, strain background (*Saccharomyces cerevisiae*)	cnb1::KanMX	Winzeler 1999
strain, strain background (*Saccharomyces cerevisiae*)	crz1::KanMX	Winzeler 1999
strain, strain background (*Saccharomyces cerevisiae*)	hog1::KanMX	Winzeler 1999
strain, strain background (*Saccharomyces cerevisiae*)	gpd::KanMX	Winzeler 1999
strain, strain background (*Saccharomyces cerevisiae*)	rim101::KanMX	Winzeler 1999
strain, strain background (*Saccharomyces cerevisiae*)	coq1::KanMX	Winzeler 1999
strain, strain background (*Saccharomyces cerevisiae*)	cox11::KanMX	Winzeler 1999
strain, strain background (*Saccharomyces cerevisiae*)	can1::KanMX	Winzeler 1999
strain, strain background (*Saccharomyces cerevisiae*)	ADOPT1.0 library	Makanae 2013
strain, strain background (*Saccharomyces cerevisiae*)	ADOPT2.0 library (CEN.PK2-1C)	This study
strain, strain background (*Saccharomyces cerevisiae*)	ADOPT2.0 library (DBVPG6765)	This study
strain, strain background (*Saccharomyces cerevisiae*)	ADOPT2.1 library (CEN.PK2, ENA1-coe)	This study
strain, strain background (*Saccharomyces cerevisiae*)	Pooled knockout library	Winzeler 1999
gene (*S. cerevisiae*)	NCS2	NA
gene (*S. cerevisiae*)	NCS6	NA
gene (*S. cerevisiae*)	CMD1	NA
gene (*S. cerevisiae*)	ECM27	NA
gene (*S. cerevisiae*)	GDT1	NA
gene (*S. cerevisiae*)	YBR196C-A	NA
gene (*S. cerevisiae*)	ENA1	NA
gene (*S. cerevisiae*)	CTR1	NA
gene (*S. cerevisiae*)	HAP4	NA
gene (*S. cerevisiae*)	USV1	NA
genetic reagent (*S. cerevisiae*)	moxGFP	Costantini 2015
recombinant DNA reagent	pTOWug2836	Moriya 2006
recombinant DNA reagent	pTOW40836	Moriya 2012
recombinant DNA reagent	pRS423	Sikorski 1989
recombinant DNA reagent	pRS423nz2	This study
recombinant DNA reagent	pTOWug2836-NCS2	Makanae2013
recombinant DNA reagent	pTOWug2836-NCS6	Makanae2013
recombinant DNA reagent	pTOWug2836-CMD1	Makanae2013
recombinant DNA reagent	pTOWug2836-ECM27	Makanae2013
recombinant DNA reagent	pTOWug2836-GDT1	Makanae2013
recombinant DNA reagent	pTOWug2836-YBR196C-A	Makanae2013
recombinant DNA reagent	pTOWug2836-ENA1	Makanae2013
recombinant DNA reagent	pTOWug2836-CTR1	Makanae2013
recombinant DNA reagent	pTOWug2836-HAP4	Makanae2013
recombinant DNA reagent	pTOWug2836-USV1	Makanae2013
recombinant DNA reagent	pRS423nz-ENA1	This study

In Chapter 2, it was shown that deletion of the gene *YJL175W*, which is a misannotated ORF, led to a partial loss of function of the protein Swi3 (*swi3ΔN*) and reduced the growth defects caused by overexpression of GFP (GFP-op), a condition linked to the protein burden effect. The phenotype of the *YJL175W* deletion is likely due to the truncation of Swi3 caused by the deletion. Results showed that there was a significant reduction in transcription, specifically in the transcripts encoding highly expressed, secreted proteins (Fig. 5). This also led to a reduction in total protein translation (Fig. 6A and B). These results can explain the cellular conditions created by the *YJL175W* deletion. Figures 6C and D present conceptual pie chart models to illustrate these conditions. In normal conditions, ribosomes are used to translate both necessary and unnecessary proteins for growth (Fig. 6C, WT). In *yjl175w*Δ cells, there are fewer transcripts encoding unnecessary proteins and thus, more ribosomes are available for other translations (Fig. 6C, *yjl175w*Δ). In GFP-op, many ribosomes are used to translate GFP, resulting in fewer ribosomes for necessary proteins and growth defects (Fig. 6D, WT). The additional ribosomes created by *yjl175w*Δ allows for more translation of necessary proteins, avoiding a reduction in their translation and thereby mitigating the growth defects (Fig. 6D, *yjl175w*Δ).

In Chapter 3, the focus was on understanding the role of overexpression in adapting to stressful environments. To do this, a new experimental system was developed to systematically identify genes whose overexpression is functionally adaptive (GOFAs). The characteristics of genes that become GOFAs under environmental stress were examined. The results showed that GOFAs are genes that compensate for cellular deficiencies and that their adaptive function depends on genetic background and environment. For instance, GOFAs isolated under salt stress were found to be associated with calcium homeostasis, and their adaptive function was observed in the lack of Ca^{2+}

in the medium (Fig. 7 and 12). However, when Ca^{2+} was added to the salt stress conditions, the adaptive function of these GOFAs was lost (Fig. 12) and different GOFAs were isolated (Fig. 21). In one strain, CEN.PK, genes such as ENA1, which is a Na^{+} exporter, and regulators of K^{+} homeostasis, *SAT4* and *HAL5*, were identified as GOFAs under salt stress but not in another strain, BY4741 (Fig. 14). This difference can be explained by the difference in Ca^{2+} and K^{+} requirements between the two strains. In fact, the adaptive effects of *ENA1* overexpression and K^{+} were more significant in CEN.PK than in BY4741 (Fig. 14). Therefore, it is proposed that GOFAs compensate for the missing elements necessary for cells to reach the maximum stress tolerance or "ideal state" (Fig. 21G). In other words, the examination of GOFAs reveals the essential elements needed to maximize cellular fitness within a specific genetic background and environment.

In this theme, I aimed to get at the relationship between overexpression and cellular adaptation, focusing on the effects of overexpression on cells, especially the positive effects. This study systematically identified gene group whose overexpression is functionally adaptive by developing an “overexpression profiling method”. These gene groups shed light on the relationship between environmental and genetic backgrounds, which is not yet fully understood. Overexpression profiling is also helpful in identifying essential but missing factors in specific environments and genetic backgrounds.

However, even though genes can be identified from this method, it is not clear why and how they function adaptively. It is increasingly apparent that cellular systems are highly complex, with a multitude of factors that influence their behavior, such as genetic background, epigenetics, and environmental conditions. To fully understand living organisms, there is a pressing need for a

framework that can integrate theoretical and computational approaches to simplify and clarify these complex systems. In the future, I aim to contribute to the development of such a framework, which can help us to better understand the intricacies of cellular systems and ultimately improve our ability to predict and manipulate their behavior.

Acknowledgments

I thank all members of the Moriya Laboratory for their helpful discussions. Japan Society of Promoting Science and Okayama University, OHOMOTO IKUEIKAI provided financial support for my doctoral dissertation research.

During my PhD term, a serious pandemic hit the world. I would like to express my gratitude to all the health care providers and their associates who have helped us. Thanks to these people, whose names I do not even know, I have completed my doctorate without retiring.

Special thanks to Dr. Hisao Moriya, he is the supervisor of this theme. I appreciate creating and keeping good environment for research and giving me many opportunities.

Finally, I would like to thank my families for their support.

Reference

Alings, Fiona, L. Peter Sarin, Christian Fufezan, Hannes C. A. Drexler, and Sebastian A. Leidel. 2015. “An Evolutionary Approach Uncovers a Diverse Response of TRNA 2-Thiolation to Elevated Temperatures in Yeast.” *RNA* 21 (2): 202–12.

Amberg, David C., Dan Burke, and Jeffrey N. Strathern. 2005. *Methods in Yeast Genetics: A Cold Spring Harbor Laboratory Course Manual*. CSHL Press.

Arnoldo, Anthony, Saranya Kittanakom, Lawrence E. Heisler, Anthony B. Mak, Andrey I. Shukalyuk, Dax Torti, Jason Moffat, Guri Giaever, and Corey Nislow. 2014. “A Genome Scale Overexpression Screen to Reveal Drug Activity in Human Cells.” *Genome Medicine* 6 (4): 32.

Batiza, A. F., T. Schulz, and P. H. Masson. 1996. “Yeast Respond to Hypotonic Shock with a Calcium Pulse.” *The Journal of Biological Chemistry* 271 (38): 23357–62.

Beadle, G. W., and E. L. Tatum. 1941. “Genetic Control of Biochemical Reactions in Neurospora.” *Proceedings of the National Academy of Sciences of the United States of America* 27 (11): 499–506.

Beaupere, Carine, Leticia Dinatto, Brian M. Wasko, Rosalyn B. Chen, Lauren VanValkenburg, Michael G. Kiflezghi, Mitchell B. Lee, et al. 2018. “Genetic Screen Identifies Adaptive Aneuploidy as a Key Mediator of ER Stress Resistance in Yeast.” *Proceedings of the National Academy of Sciences of the United States of America* 115 (38): 9586–91.

Ben-David, Uri, and Angelika Amon. 2020. “Context Is Everything: Aneuploidy in Cancer.” *Nature Reviews. Genetics* 21 (1): 44–62.

Benjamini, Yoav, and Yosef Hochberg. 1995. “Controlling the False Discovery Rate: A Practical and Powerful Approach to Multiple Testing.” *Journal of the Royal Statistical Society: Series B (Methodological)*. https://doi.org/10.1111/j.2517-

6161.1995.tb02031.x.

Bird, Steven, Ewan Klein, and Edward Loper. 2009. *Natural Language Processing with Python: Analyzing Text with the Natural Language Toolkit*. "O'Reilly Media, Inc."

Blaiseau, P. L., A. D. Isnard, Y. Surdin-Kerjan, and D. Thomas. 1997. "Met31p and Met32p, Two Related Zinc Finger Proteins, Are Involved in Transcriptional Regulation of Yeast Sulfur Amino Acid Metabolism." *Molecular and Cellular Biology* 17 (7): 3640–48.

Boyer, Laurie A., Michael R. Langer, Kimberly A. Crowley, Song Tan, John M. Denu, and Craig L. Peterson. 2002. "Essential Role for the SANT Domain in the Functioning of Multiple Chromatin Remodeling Enzymes." *Molecular Cell* 10 (4): 935–42.

Brachmann, C. B., A. Davies, G. J. Cost, E. Caputo, J. Li, P. Hieter, and J. D. Boeke. 1998. "Designer Deletion Strains Derived from Saccharomyces Cerevisiae S288C: A Useful Set of Strains and Plasmids for PCR-Mediated Gene Disruption and Other Applications." *Yeast (Chichester, England)* 14 (2): 115–32.

Brettner, Leandra, Wei-Chin Ho, Kara Schmidlin, Sam Apodaca, Rachel Eder, and Kerry Geiler-Samerotte. 2022. "Challenges and Potential Solutions for Studying the Genetic and Phenotypic Architecture of Adaptation in Microbes." *Current Opinion in Genetics & Development* 75 (101951): 101951.

Caso, Covadonga, and Maria Angeles Gil. 1988. "The Gini-Simpson Index of Diversity: Estimation in the Stratified Sampling." *Communications in Statistics - Theory and Methods*. https://doi.org/10.1080/03610928808829784.

Chen, Shifu, Yanqing Zhou, Yaru Chen, and Jia Gu. 2018. "Fastp: An Ultra-Fast All-in-One FASTQ Preprocessor." *Bioinformatics* 34 (17): i884–90.

Cingolani, Pablo, Adrian Platts, Le Lily Wang, Melissa Coon, Tung Nguyen, Luan Wang, Susan J. Land, Xiangyi Lu, and Douglas M. Ruden. 2012. "A Program for Annotating

and Predicting the Effects of Single Nucleotide Polymorphisms, SnpEff: SNPs in the Genome of Drosophila Melanogaster Strain W1118; Iso-2; Iso-3." *Fly* 6 (2): 80–92.

Colinet, Anne-Sophie, Palanivelu Sengottaiyan, Antoine Deschamps, Marie-Lise Colsoul, Louise Thines, Didier Demaegd, Marie-Clémence Duchêne, François Foulquier, Pascal Hols, and Pierre Morsomme. 2016. "Yeast Gdt1 Is a Golgi-Localized Calcium Transporter Required for Stress-Induced Calcium Signaling and Protein Glycosylation." *Scientific Reports* 6 (April): 24282.

Controlling the False Discovery Rate: A Practical and Powerful Approach to Multiple Testing Yoav Benjamini. n.d.

"Correction for Sutter et al., Hypoxia-Inducible Factor 1α Protein Expression Is Controlled by Oxygen-Regulated Ubiquitination That Is Disrupted by Deletions and Missense Mutations." 2022. *Proceedings of the National Academy of Sciences of the United States of America* 119 (38): e2210922119.

Costa, Elizabeth A., Kelly Subramanian, Jodi Nunnari, and Jonathan S. Weissman. 2018. "Defining the Physiological Role of SRP in Protein-Targeting Efficiency and Specificity." *Science (New York, N.Y.)* 359 (6376): 689–92.

Costanzo, Michael, Benjamin VanderSluis, Elizabeth N. Koch, Anastasia Baryshnikova, Carles Pons, Guihong Tan, Wen Wang, et al. 2016. "A Global Genetic Interaction Network Maps a Wiring Diagram of Cellular Function." *Science* 353 (6306). https://doi.org/10.1126/science.aaf1420.

Cyert, Martha S., and Caroline C. Philpott. 2013. "Regulation of Cation Balance in Saccharomyces Cerevisiae." *Genetics* 193 (3): 677–713.

Da, Guoping, Jeffrey Lenkart, Kehao Zhao, Ramin Shiekhattar, Bradley R. Cairns, and Ronen Marmorstein. 2006. "Structure and Function of the SWIRM Domain, a Conserved

Protein Module Found in Chromatin Regulatory Complexes." *Proceedings of the National Academy of Sciences of the United States of America* 103 (7): 2057–62.

Dancis, A., D. S. Yuan, D. Haile, C. Askwith, D. Eide, C. Moehle, J. Kaplan, and R. D. Klausner. 1994. "Molecular Characterization of a Copper Transport Protein in S. Cerevisiae: An Unexpected Role for Copper in Iron Transport." *Cell* 76 (2): 393–402.

Daran-Lapujade, Pascale, Jean-Marc Daran, Marijke A. H. Luttik, Marinka J. H. Almering, Jack T. Pronk, and Peter Kötter. 2009. "An Atypical PMR2 Locus Is Responsible for Hypersensitivity to Sodium and Lithium Cations in the Laboratory Strain Saccharomyces Cerevisiae CEN.PK113-7D." *FEMS Yeast Research* 9 (5): 789–92.

DelBove, Jessica, Gary Rosson, Matthew Strobeck, Jianguang Chen, Trevor K. Archer, Weidong Wang, Erik S. Knudsen, and Bernard E. Weissman. 2011. "Identification of a Core Member of the SWI/SNF Complex, BAF155/SMARCC1, as a Human Tumor Suppressor Gene." *Epigenetics: Official Journal of the DNA Methylation Society* 6 (12): 1444–53.

Dutta, Arnob, Mihaela Sardiu, Madelaine Gogol, Joshua Gilmore, Daoyong Zhang, Laurence Florens, Susan M. Abmayr, Michael P. Washburn, and Jerry L. Workman. 2017. "Composition and Function of Mutant Swi/Snf Complexes." *Cell Reports* 18 (9): 2124–34.

Eguchi, Yuichi, Gaurav Bilolikar, and Kerry Geiler-Samerotte. 2019. "Why and How to Study Genetic Changes with Context-Dependent Effects." *Current Opinion in Genetics & Development* 58–59 (October): 95–102.

Eguchi, Yuichi, Koji Makanae, Tomohisa Hasunuma, Yuko Ishibashi, Keiji Kito, and Hisao Moriya. 2018. "Estimating the Protein Burden Limit of Yeast Cells by Measuring the Expression Limits of Glycolytic Proteins." *ELife* 7 (August).

https://doi.org/10.7554/eLife.34595.

Engel, Stacia R., Edith D. Wong, Robert S. Nash, Suzi Aleksander, Micheal Alexander, Eric Douglass, Kalpana Karra, et al. 2022. “New Data and Collaborations at the Saccharomyces Genome Database: Updated Reference Genome, Alleles, and the Alliance of Genome Resources.” *Genetics* 220 (4). https://doi.org/10.1093/genetics/iyab224.

Farkas, Zoltán, Dorottya Kalapis, Zoltán Bódi, Béla Szamecz, Andreea Daraba, Karola Almási, Károly Kovács, et al. 2018. “Hsp70-Associated Chaperones Have a Critical Role in Buffering Protein Production Costs.” *ELife* 7 (January). https://doi.org/10.7554/elife.29845.

Farkas, Zoltán, Károly Kovács, Zsuzsa Sarkadi, Dorottya Kalapis, Gergely Fekete, Fanni Birtyik, Ferhan Ayaydin, et al. 2022. “Gene Loss and Compensatory Evolution Promotes the Emergence of Morphological Novelties in Budding Yeast.” *Nature Ecology & Evolution* 6 (6): 763–73.

Ferrando, A., S. J. Kron, G. Rios, G. R. Fink, and R. Serrano. 1995. “Regulation of Cation Transport in Saccharomyces Cerevisiae by the Salt Tolerance Gene HAL3.” *Molecular and Cellular Biology* 15 (10): 5470–81.

Filteau, Marie, Véronique Hamel, Marie-Christine Pouliot, Isabelle Gagnon-Arsenault, Alexandre K. Dubé, and Christian R. Landry. 2015. “Evolutionary Rescue by Compensatory Mutations Is Constrained by Genomic and Environmental Backgrounds.” *Molecular Systems Biology* 11 (10): 832.

Forsburg, S. L., and L. Guarente. 1989. “Identification and Characterization of HAP4: A Third Component of the CCAAT-Bound HAP2/HAP3 Heteromer.” *Genes & Development* 3 (8): 1166–78.

Gaines, Todd A., Wenli Zhang, Dafu Wang, Bekir Bukun, Stephen T. Chisholm, Dale L. Shaner, Scott J. Nissen, et al. 2010. “Gene Amplification Confers Glyphosate Resistance in Amaranthus Palmeri.” *Proceedings of the National Academy of Sciences of the United States of America* 107 (3): 1029–34.

Galardini, Marco, Bede P. Busby, Cristina Vieitez, Alistair S. Dunham, Athanasios Typas, and Pedro Beltrao. 2019. “The Impact of the Genetic Background on Gene Deletion Phenotypes in Saccharomyces Cerevisiae.” *Molecular Systems Biology* 15 (12): e8831.

Gasch, A. P., P. T. Spellman, C. M. Kao, O. Carmel-Harel, M. B. Eisen, G. Storz, D. Botstein, and P. O. Brown. 2000. “Genomic Expression Programs in the Response of Yeast Cells to Environmental Changes.” *Molecular Biology of the Cell* 11 (12): 4241–57.

Gaxiola, R., I. F. de Larrinoa, J. M. Villalba, and R. Serrano. 1992. “A Novel and Conserved Salt-Induced Protein Is an Important Determinant of Salt Tolerance in Yeast.” *The EMBO Journal* 11 (9): 3157–64.

Genest, Olivier, Sue Wickner, and Shannon M. Doyle. 2019. “Hsp90 and Hsp70 Chaperones: Collaborators in Protein Remodeling.” *The Journal of Biological Chemistry* 294 (6): 2109–20.

Ghaemmaghami, Sina, Won-Ki Huh, Kiowa Bower, Russell W. Howson, Archana Belle, Noah Dephoure, Erin K. O’Shea, and Jonathan S. Weissman. 2003. “Global Analysis of Protein Expression in Yeast.” *Nature* 425 (6959): 737–41.

Giaever, Guri, Angela M. Chu, Li Ni, Carla Connelly, Linda Riles, Steeve Véronneau, Sally Dow, et al. 2002. “Functional Profiling of the Saccharomyces Cerevisiae Genome.” *Nature* 418 (6896): 387–91.

Giaever, Guri, Patrick Flaherty, Jochen Kumm, Michael Proctor, Corey Nislow, Daniel F. Jaramillo, Angela M. Chu, Michael I. Jordan, Adam P. Arkin, and Ronald W. Davis.

2004. “Chemogenomic Profiling: Identifying the Functional Interactions of Small Molecules in Yeast.” *Proceedings of the National Academy of Sciences of the United States of America* 101 (3): 793–98.

Gläser, H. U., D. Thomas, R. Gaxiola, F. Montrichard, Y. Surdin-Kerjan, and R. Serrano. 1993. “Salt Tolerance and Methionine Biosynthesis in Saccharomyces Cerevisiae Involve a Putative Phosphatase Gene.” *The EMBO Journal* 12 (8): 3105–10.

Goehring, April S., David M. Rivers, and George F. Sprague Jr. 2003. “Urmylation: A Ubiquitin-like Pathway That Functions during Invasive Growth and Budding in Yeast.” *Molecular Biology of the Cell* 14 (11): 4329–41.

Gomez-Pastor, Rocio, Eileen T. Burchfiel, and Dennis J. Thiele. 2018. “Regulation of Heat Shock Transcription Factors and Their Roles in Physiology and Disease.” *Nature Reviews Molecular Cell Biology*. https://doi.org/10.1038/nrm.2017.73.

Hanscho, Michael, David E. Ruckerbauer, Neha Chauhan, Harald F. Hofbauer, Stefan Krahulec, Bernd Nidetzky, Sepp D. Kohlwein, Juergen Zanghellini, and Klaus Natter. 2012. “Nutritional Requirements of the BY Series of Saccharomyces Cerevisiae Strains for Optimum Growth.” *FEMS Yeast Research* 12 (7): 796–808.

Haro, R., B. Garciadeblas, and A. Rodríguez-Navarro. 1991. “A Novel P-Type ATPase from Yeast Involved in Sodium Transport.” *FEBS Letters* 291 (2): 189–91.

Helming, Katherine C., Xiaofeng Wang, and Charles W. M. Roberts. 2014. “Vulnerabilities of Mutant SWI/SNF Complexes in Cancer.” *Cancer Cell* 26 (3): 309–17.

Hlynialuk, Chris, Ryan Schierholtz, Amanda Vernooy, and George van der Merwe. 2008. “Nsf1/Ypl230w Participates in Transcriptional Activation during Non-Fermentative Growth and in Response to Salt Stress in Saccharomyces Cerevisiae.” *Microbiology* 154 (Pt 8): 2482–91.

Ho, Cheuk Hei, Leslie Magtanong, Sarah L. Barker, David Gresham, Shinichi Nishimura, Paramasivam Natarajan, Judice L. Y. Koh, et al. 2009. “A Molecular Barcoded Yeast ORF Library Enables Mode-of-Action Analysis of Bioactive Compounds.” *Nature Biotechnology* 27 (4): 369–77.

Hohmann, Stefan, and Willem H. Mager. 2003. “Introduction.” *Yeast Stress Responses*, 1–9.

Horiuchi, Satoshi, Shotaro Namba, Nozomu Saeki, Ayano Satoh, and Hisao Moriya. 2022. “Identification of Uncharacterized Proteins Potentially Localized to Mitochondria (UPMs) in Saccharomyces Cerevisiae Using a Fluorescent Protein Unstable in the Cytoplasm.” *Yeast* 39 (5): 303–11.

Huh, Won-Ki, James V. Falvo, Luke C. Gerke, Adam S. Carroll, Russell W. Howson, Jonathan S. Weissman, and Erin K. O’Shea. 2003. “Global Analysis of Protein Localization in Budding Yeast.” *Nature*. https://doi.org/10.1038/nature02026.

Illarionov, Aleksandr, Petri-Jaan Lahtvee, and Rahul Kumar. 2021. “Potassium and Sodium Salt Stress Characterization in the Yeasts Saccharomyces Cerevisiae, Kluyveromyces Marxianus, and Rhodotorula Toruloides.” *Applied and Environmental Microbiology* 87 (13): e0310020.

Ishikawa, Koji, Koji Makanae, Shintaro Iwasaki, Nicholas T. Ingolia, and Hisao Moriya. 2017. “Post-Translational Dosage Compensation Buffers Genetic Perturbations to Stoichiometry of Protein Complexes.” *PLoS Genetics* 13 (1): e1006554.

Jacob, François, and Jacques Monod. 1961. “Genetic Regulatory Mechanisms in the Synthesis of Proteins.” *Journal of Molecular Biology* 3 (3): 318–56.

Jost, Lou. 2006. “*Entropy and Diversity*.” *Oikos*. https://doi.org/10.1111/j.2006.0030-1299.14714.x.

Kadoch, Cigall, Diana C. Hargreaves, Courtney Hodges, Laura Elias, Lena Ho, Jeff Ranish, and

Gerald R. Crabtree. 2013. “Proteomic and Bioinformatic Analysis of Mammalian SWI/SNF Complexes Identifies Extensive Roles in Human Malignancy.” *Nature Genetics* 45 (6): 592–601.

Kafri, Moshe, Eyal Metzl-Raz, Ghil Jona, and Naama Barkai. 2016. “The Cost of Protein Production.” *Cell Reports* 14 (1): 22–31.

Kassabov, Stefan R., Bei Zhang, Jim Persinger, and Blaine Bartholomew. 2003. “SWI/SNF Unwraps, Slides, and Rewraps the Nucleosome.” *Molecular Cell* 11 (2): 391–403.

Kim, Daehwan, Joseph M. Paggi, Chanhee Park, Christopher Bennett, and Steven L. Salzberg. 2019. “Graph-Based Genome Alignment and Genotyping with HISAT2 and HISAT-Genotype.” *Nature Biotechnology* 37 (8): 907–15.

Kim, Joungmok, and Kun-Liang Guan. 2019. “MTOR as a Central Hub of Nutrient Signalling and Cell Growth.” *Nature Cell Biology* 21 (1): 63–71.

Kim, Laura C., and M. Celeste Simon. 2022. “Hypoxia-Inducible Factors in Cancer.” *Cancer Research*. American Association for Cancer Research (AACR).

Kintaka, Reiko, Koji Makanae, and Hisao Moriya. 2016. “Cellular Growth Defects Triggered by an Overload of Protein Localization Processes.” *Scientific Reports* 6 (August): 31774.

Kintaka, Reiko, Koji Makanae, Shotaro Namba, Hisaaki Kato, Keiji Kito, Shinsuke Ohnuki, Yoshikazu Ohya, Brenda J. Andrews, Charles Boone, and Hisao Moriya. 2020. “Genetic Profiling of Protein Burden and Nuclear Export Overload.” *ELife* 9 (November). https://doi.org/10.7554/eLife.54080.

Kitano, Hiroaki. 2004. “Biological Robustness.” *Nature Reviews. Genetics* 5 (11): 826–37.

Klukovich, Rachel, and William E. Courchesne. 2016. “Functions of Saccharomyces Cerevisiae Ecm27p, a Putative Na(+)/Ca(2+) Exchanger, in Calcium Homeostasis, Carbohydrate

Storage and Cell Cycle Reentry from the Quiescent Phase." *Microbiological Research* 186–187 (May): 81–89.

Kuras, L., H. Cherest, Y. Surdin-Kerjan, and D. Thomas. 1996. "A Heteromeric Complex Containing the Centromere Binding Factor 1 and Two Basic Leucine Zipper Factors, Met4 and Met28, Mediates the Transcription Activation of Yeast Sulfur Metabolism." *The EMBO Journal* 15 (10): 2519–29.

Kurland, C. G., and H. Dong. 1996. "Bacterial Growth Inhibition by Overexpression of Protein." *Molecular Microbiology* 21 (1): 1–4.

Laloux, I., E. Dubois, M. Dewerchin, and E. Jacobs. 1990. "TEC1, a Gene Involved in the Activation of Ty1 and Ty1-Mediated Gene Expression in Saccharomyces Cerevisiae: Cloning and Molecular Analysis." *Molecular and Cellular Biology* 10 (7): 3541–50.

Li, Bo, Victor Ruotti, Ron M. Stewart, James A. Thomson, and Colin N. Dewey. 2010. "RNA-Seq Gene Expression Estimation with Read Mapping Uncertainty." *Bioinformatics (Oxford, England)* 26 (4): 493–500.

Li, H. 2011. "A Statistical Framework for SNP Calling, Mutation Discovery, Association Mapping and Population Genetical Parameter Estimation from Sequencing Data." *Bioinformatics*. https://doi.org/10.1093/bioinformatics/btr509.

Li, Heng. 2018. "Minimap2: Pairwise Alignment for Nucleotide Sequences." *Bioinformatics* 34 (18): 3094–3100.

Li, Heng, and Richard Durbin. 2009. "Fast and Accurate Short Read Alignment with Burrows-Wheeler Transform." *Bioinformatics* 25 (14): 1754–60.

Li, Heng, Bob Handsaker, Alec Wysoker, Tim Fennell, Jue Ruan, Nils Homer, Gabor Marth, Goncalo Abecasis, Richard Durbin, and 1000 Genome Project Data Processing Subgroup. 2009. "The Sequence Alignment/Map Format and SAMtools."

Bioinformatics 25 (16): 2078–79.

Luesch, Hendrik, Tom Y. H. Wu, Pingda Ren, Nathanael S. Gray, Peter G. Schultz, and Frantisek Supek. 2005. "A Genome-Wide Overexpression Screen in Yeast for Small-Molecule Target Identification." *Chemistry & Biology* 12 (1): 55–63.

Makanae, Koji, Reiko Kintaka, Takashi Makino, Hiroaki Kitano, and Hisao Moriya. 2013. "Identification of Dosage-Sensitive Genes in Saccharomyces Cerevisiae Using the Genetic Tug-of-War Method." *Genome Research* 23 (2): 300–311.

Mefloquine Resistance in Plasmodium Falciparum and Increased Pfmdr1 Gene Copy Number. n.d.

Mendizabal, I., G. Rios, J. M. Mulet, R. Serrano, and I. F. de Larrinoa. 1998. "Yeast Putative Transcription Factors Involved in Salt Tolerance." *FEBS Letters* 425 (2): 323–28.

Moriya, Hisao. 2015. "Quantitative Nature of Overexpression Experiments." *Molecular Biology of the Cell* 26 (22): 3932–39.

Moriya, Hisao, Yuki Shimizu-Yoshida, and Hiroaki Kitano. 2006. "In Vivo Robustness Analysis of Cell Division Cycle Genes in Saccharomyces Cerevisiae." *PLoS Genetics* 2 (7): e111.

Mortimer, R. K., C. R. Contopoulou, and J. S. King. 1992. "Genetic and Physical Maps of Saccharomyces Cerevisiae, Edition 11." *Yeast* 8 (10): 817–902.

Mulet, J. M., M. P. Leube, S. J. Kron, G. Rios, G. R. Fink, and R. Serrano. 1999. "A Novel Mechanism of Ion Homeostasis and Salt Tolerance in Yeast: The Hal4 and Hal5 Protein Kinases Modulate the Trk1-Trk2 Potassium Transporter." *Molecular and Cellular Biology* 19 (5): 3328–37.

Nakajima-Shimada, J., H. Iida, F. I. Tsuji, and Y. Anraku. 1991. "Monitoring of Intracellular Calcium in Saccharomyces Cerevisiae with an Apoaequorin CDNA Expression

System." *Proceedings of the National Academy of Sciences of the United States of America* 88 (15): 6878–82.

Namba, Shotaro, Hisaaki Kato, Shuji Shigenobu, Takashi Makino, and Hisao Moriya. 2022. "Massive Expression of Cysteine-Containing Proteins Causes Abnormal Elongation of Yeast Cells by Perturbing the Proteasome." *G3* 12 (6). https://doi.org/10.1093/g3journal/jkac106.

Oldenburg, K. R., K. T. Vo, S. Michaelis, and C. Paddon. 1997. "Recombination-Mediated PCR-Directed Plasmid Construction in Vivo in Yeast." *Nucleic Acids Research* 25 (2): 451–52.

Olz, R., K. Larsson, L. Adler, and L. Gustafsson. 1993. "Energy Flux and Osmoregulation of Saccharomyces Cerevisiae Grown in Chemostats under NaCl Stress." *Journal of Bacteriology* 175 (8): 2205–13.

Palmer, Adam C., and Roy Kishony. 2014. "Opposing Effects of Target Overexpression Reveal Drug Mechanisms." *Nature Communications* 5 (1): 4296.

Peter, Jackson, Matteo De Chiara, Anne Friedrich, Jia-Xing Yue, David Pflieger, Anders Bergström, Anastasie Sigwalt, et al. 2018. "Genome Evolution across 1,011 Saccharomyces Cerevisiae Isolates." *Nature* 556 (7701): 339–44.

Peterson, C. L., and I. Herskowitz. 1992. "Characterization of the Yeast SWI1, SWI2, and SWI3 Genes, Which Encode a Global Activator of Transcription." *Cell* 68 (3): 573–83.

Phelan, M. L., S. Sif, G. J. Narlikar, and R. E. Kingston. 1999. "Reconstitution of a Core Chromatin Remodeling Complex from SWI/SNF Subunits." *Molecular Cell* 3 (2): 247–53.

Prelich, Gregory. 2012. "Gene Overexpression: Uses, Mechanisms, and Interpretation." *Genetics* 190 (3): 841–54.

Puddu, Fabio, Mareike Herzog, Alexandra Selivanova, Siyue Wang, Jin Zhu, Shir Klein-Lavi, Molly Gordon, et al. 2019. “Genome Architecture and Stability in the Saccharomyces Cerevisiae Knockout Collection.” *Nature* 573 (7774): 416–20.

Quinlan, Aaron R., and Ira M. Hall. 2010. “BEDTools: A Flexible Suite of Utilities for Comparing Genomic Features.” *Bioinformatics* 26 (6): 841–42.

Rajaraman, Anand, and Jeffrey David Ullman. 2011. “Data Mining.” In *Mining of Massive Datasets*, 1–17. Cambridge University Press.

Rine, J., W. Hansen, E. Hardeman, and R. W. Davis. 1983. “Targeted Selection of Recombinant Clones through Gene Dosage Effects.” *Proceedings of the National Academy of Sciences of the United States of America* 80 (22): 6750–54.

Robinson, Deelegant, Michael Place, James Hose, Adam Jochem, and Audrey P. Gasch. 2021. “Natural Variation in the Consequences of Gene Overexpression and Its Implications for Evolutionary Trajectories.” *ELife* 10 (August). https://doi.org/10.7554/eLife.70564.

Robinson, James T., Helga Thorvaldsdóttir, Wendy Winckler, Mitchell Guttman, Eric S. Lander, Gad Getz, and Jill P. Mesirov. 2011. “Integrative Genomics Viewer.” *Nature Biotechnology* 29 (1): 24–26.

Robinson, Mark D., Davis J. McCarthy, and Gordon K. Smyth. 2010. “EdgeR: A Bioconductor Package for Differential Expression Analysis of Digital Gene Expression Data.” *Bioinformatics* 26 (1): 139–40.

Rudolph, H. K., A. Antebi, G. R. Fink, C. M. Buckley, T. E. Dorman, J. LeVitre, L. S. Davidow, J. I. Mao, and D. T. Moir. 1989. “The Yeast Secretory Pathway Is Perturbed by Mutations in PMR1, a Member of a Ca2+ ATPase Family.” *Cell* 58 (1): 133–45.

Servant, Géraldine, Benoit Pinson, Aurélie Tchalikian-Cosson, Fanny Coulpier, Sophie Lemoine, Carole Pennetier, Antoine Bridier-Nahmias, et al. 2012. “Tye7 Regulates

Yeast Ty1 Retrotransposon Sense and Antisense Transcription in Response to Adenylic Nucleotides Stress." *Nucleic Acids Research* 40 (12): 5271–82.

Shain, A. Hunter, and Jonathan R. Pollack. 2013. "The Spectrum of SWI/SNF Mutations, Ubiquitous in Human Cancers." *PloS One* 8 (1): e55119.

Snoep, J. L., L. P. Yomano, H. V. Westerhoff, and L. O. Ingram. 1995. "Protein Burden in Zymomonas Mobilis: Negative Flux and Growth Control Due to Overexpression of Glycolytic Enzymes." *Microbiology (Reading, England)* 141 (9): 2329–37.

Solís, Eric J., Jai P. Pandey, Xu Zheng, Dexter X. Jin, Piyush B. Gupta, Edoardo M. Airoldi, David Pincus, and Vladimir Denic. 2018. "Defining the Essential Function of Yeast Hsf1 Reveals a Compact Transcriptional Program for Maintaining Eukaryotic Proteostasis." *Molecular Cell* 69 (3): 534.

Song, Giltae, Benjamin J. A. Dickins, Janos Demeter, Stacia Engel, Jennifer Gallagher, Kisurb Choe, Barbara Dunn, Michael Snyder, and J. Michael Cherry. 2015. "AGAPE (Automated Genome Analysis PipelinE) for Pan-Genome Analysis of Saccharomyces Cerevisiae." *PloS One* 10 (3): e0120671.

Sopko, Richelle, Dongqing Huang, Nicolle Preston, Gordon Chua, Balázs Papp, Kimberly Kafadar, Mike Snyder, et al. 2006. "Mapping Pathways and Phenotypes by Systematic Gene Overexpression." *Molecular Cell* 21 (3): 319–30.

Szamecz, Béla, Gábor Boross, Dorottya Kalapis, Károly Kovács, Gergely Fekete, Zoltán Farkas, Viktória Lázár, et al. 2014. "The Genomic Landscape of Compensatory Evolution." *PLoS Biology* 12 (8): e1001935.

Takasaki, Kazuto, Takamasa Miura, Manabu Kanno, Hideyuki Tamaki, Satoshi Hanada, Yoichi Kamagata, and Nobutada Kimura. 2013. "Discovery of Glycoside Hydrolase Enzymes in an Avicel-Adapted Forest Soil Fungal Community by a Metatranscriptomic

Approach." *PloS One* 8 (2): e55485.

Tang, Yun-Chi, and Angelika Amon. 2013. "Gene Copy-Number Alterations: A Cost-Benefit Analysis." *Cell* 152 (3): 394–405.

Tatebe, Hisashi, and Kazuhiro Shiozaki. 2017. "Evolutionary Conservation of the Components in the TOR Signaling Pathways." *Biomolecules* 7 (4). https://doi.org/10.3390/biom7040077.

Tyagi, Kshitiz, and Patrick G. A. Pedrioli. 2015. "Protein Degradation and Dynamic TRNA Thiolation Fine-Tune Translation at Elevated Temperatures." *Nucleic Acids Research* 43 (9): 4701–12.

Ueguchi, C., and K. Ito. 1992. "Multicopy Suppression: An Approach to Understanding Intracellular Functioning of the Protein Export System." *Journal of Bacteriology* 174 (5): 1454–61.

Vakirlis, Nikolaos, Omer Acar, Brian Hsu, Nelson Castilho Coelho, S. Branden Van Oss, Aaron Wacholder, Kate Medetgul-Ernar, et al. 2020. "De Novo Emergence of Adaptive Membrane Proteins from Thymine-Rich Genomic Sequences." *Nature Communications* 11 (1): 781.

Van Oss, Stephen Branden, and Anne-Ruxandra Carvunis. 2019. "De Novo Gene Birth." *PLoS Genetics* 15 (5): e1008160.

Vowinckel, Jakob, Johannes Hartl, Hans Marx, Martin Kerick, Kathrin Runggatscher, Markus A. Keller, Michael Mülleder, et al. 2021. "The Metabolic Growth Limitations of Petite Cells Lacking the Mitochondrial Genome." *Nature Metabolism* 3 (11): 1521–35.

Welch, B. L. 1938. "The Significance of the Difference Between Two Means When the Population Variances Are Unequal." *Biometrika*. https://doi.org/10.2307/2332010.

Widmann, C., S. Gibson, M. B. Jarpe, and G. L. Johnson. 1999. "Mitogen-Activated Protein

Kinase: Conservation of a Three-Kinase Module from Yeast to Human." *Physiological Reviews* 79 (1): 143–80.

Wieland, J., A. M. Nitsche, J. Strayle, H. Steiner, and H. K. Rudolph. 1995. "The PMR2 Gene Cluster Encodes Functionally Distinct Isoforms of a Putative Na+ Pump in the Yeast Plasma Membrane." *The EMBO Journal* 14 (16): 3870–82.

Wilson, Boris G., and Charles W. M. Roberts. 2011. "SWI/SNF Nucleosome Remodellers and Cancer." *Nature Reviews. Cancer* 11 (7): 481–92.

Winzeler, E. A., D. D. Shoemaker, A. Astromoff, H. Liang, K. Anderson, B. Andre, R. Bangham, et al. 1999. "Functional Characterization of the S. Cerevisiae Genome by Gene Deletion and Parallel Analysis." *Science* 285 (5429): 901–6.

Withee, J. L., R. Sen, and M. S. Cyert. 1998. "Ion Tolerance of Saccharomyces Cerevisiae Lacking the Ca2+/CaM-Dependent Phosphatase (Calcineurin) Is Improved by Mutations in URE2 or PMA1." *Genetics* 149 (2): 865–78.

Yue, Jia-Xing, Jing Li, Louise Aigrain, Johan Hallin, Karl Persson, Karen Oliver, Anders Bergström, et al. 2017. "Contrasting Evolutionary Genome Dynamics between Domesticated and Wild Yeasts." *Nature Genetics* 49 (6): 913–24.

Zaslaver, Alon, Avi E. Mayo, Revital Rosenberg, Pnina Bashkin, Hila Sberro, Miri Tsalyuk, Michael G. Surette, and Uri Alon. 2004. "Just-in-Time Transcription Program in Metabolic Pathways." *Nature Genetics* 36 (5): 486–91.

Zhong, H., A. M. De Marzo, E. Laughner, M. Lim, D. A. Hilton, D. Zagzag, P. Buechler, W. B. Isaacs, G. L. Semenza, and J. W. Simons. 1999. "Overexpression of Hypoxia-Inducible Factor 1alpha in Common Human Cancers and Their Metastases." *Cancer Research* 59 (22): 5830–35.